




Universitat Autònoma de Barcelona

**ADVERTIMENT.** L'accés als continguts d'aquesta tesi queda condicionat a l'acceptació de les condicions d'ús establertes per la següent llicència Creative Commons:  [http://cat.creativecommons.org/?page\\_id=184](http://cat.creativecommons.org/?page_id=184)

**ADVERTENCIA.** El acceso a los contenidos de esta tesis queda condicionado a la aceptación de las condiciones de uso establecidas por la siguiente licencia Creative Commons:  <http://es.creativecommons.org/blog/licencias/>

**WARNING.** The access to the contents of this doctoral thesis it is limited to the acceptance of the use conditions set by the following Creative Commons license:  <https://creativecommons.org/licenses/?lang=en>

# **FUNCTIONALIZATION OF CARBON NANOSTRUCUTRES BY INORGANIC NANOCRYSTALS AND POTENTIAL APPLICATIONS**

Jana Oliveras i Solà

March 2022

*Directors:* Prof. Víctor Punes i Dr. Neus Bastús

Programa de Doctorat de Ciència de Materials, Universitat Autònoma de Barcelona

Institut Català de Nanociència i Nanotecnologia



*“That you are here — that life exists, and identity; that the powerful play goes on and you may contribute a verse. **That the powerful play goes on and you may contribute a verse.** What will your verse be?” — John Keating, *Dead Poets Society**



## ACKNOWLEDGEMENTS

I would like to thank my supervisors Prof. Dr. Víctor Puentes and Dr. Neus G. Bastús for the opportunity they gave me on conducting this thesis in the Inorganic Nanoparticles Group. They have been a true team in uncountable discussion meetings, brainstorming sessions, result dissection and on both soothing and pushing me as well. Thank you for your trust.

I would like to thank our collaborators from the Artificial Photosynthesis Group at ICIQ, Dr. Antoni Llobet, Dr. Carolina Gimbert-Suriñach and Dr. Marta Ventosa for the multidisciplinary project described in CHAPTER 2 of the thesis. This project was, chronologically, the beginning of this journey and because of their interest, insights and testing we started universalizing the synthesis method. I acknowledge the technical help of Dr. Jordi Arbiol and Dr. Maria Chiara Spadaro for the microscopy described in CHAPTER 1, Dr. Guillaume Sautier for the XPS analysis showed in CHAPTER 1, Dr. Belén Ballesteros, Marcos Rosado and Francisco Belarre from the Microscopy Division of ICN2 for their help and assessment on several microscopy challenges I've found thorough this thesis and their EDX measurements described in CHAPTER 2, Dr. Núria Clos for the SQUID measurements described in CHAPTER 3, Dr. Gerard Boix for conducting the thermogravimetric analysis shown in CHAPTER 3, and Dr. Jessica Padilla for her help and instruction on XRD analysis.

I also acknowledge the financial support of GENE-SUR and FSE for the FI-AGAUR fellowship program (FI-2019) and the Autonomous University of Barcelona (UAB)

Now the difficult part comes in. How to explain and recall all the people who has been there in the last crazy years? The people who have pushed and worked hard, taking my hand through a PhD and a global pandemic. Where to start?

I owe all of the members of the Inorganic Nanoparticles Group a huge thank you. The past ones: Francesco, Lorenzo, Jordi, Javi, Xavier, Cristiane, the guidance of whom sparked me on starting this adventure. The present ones: Oscar, Karen, Carmen, Liza, Markus, from whom I am inspired every day, thank you for your support, your help, your presence. The future ones: for whom I hope this work to be useful. A special mention should be addressed in this regard to Javier Patarroyo, who has been many things to this thesis, from the beginning to the end he has shown up to me and the present work, and I will never forget it. Do you know we have a sibling group at the Vall d'Hebron Hospital? I thank them too, for kindly being in the group meetings every Friday, sharing their point of view and making this experience unavoidably multidisciplinary: Muriel, Lena, Joana, Martí, Ramón, Michele, Laura..., meeting you has been a blast. I would also like to mention my deepest appreciation to Emma Gómez, who has helped me through the bureaucracy of this journey, which started by filling my fellowship *in extremis*, you got me here. Also, I want to comment on the people of the Marketing and Communication Department, who has counted on me in numerous occasions regarding dissemination activities and made the Art Meets Nano contest – which was dreamed by a small group of scientific staff – possible.

I cannot stop thinking on how lucky I am for meeting insanely good people in this building. Smaller or bigger the conversations, your nods on the corridors, your smiles through the office door, your kindness on holding the elevator for me... it is easy to feel like home at ICN2, a weird and highly functional home, to all of you, thank you for your humanity: from the maintenance crew to the workshop, from the inspiring post-docs to the reception staff, when I think about this adventure, I think of all of you.

Thank you Andrés and Ainhoa for the 0 floor friendship, Cèlia for the vulnerability, Thais for helping finding my adult self, Enric for an everlasting friendship, Roque for the best motivational talks, Ruslan for the coffee, Sara for the creativity, Chiara for role modeling, Noemí for being my gym partner, Oscar for being my Colombian brother, Karen for being a supporting friend both inside and outside of the laboratory, Carmen for the good and the not-so-good times, Muriel for being the best belayer ever, Lena for the peace.

My life would not be my life without my boys, I thank you for keeping me there, for making me laugh, for being the anchor to this town. Thank you Cañete for your sweetness, Saba for your beautiful heart, Alberto for your easiness, Marc for the music, for your support and consideration, Moisés for all of the evenings at the climbing gym, the other Moisés for his old soul and peaceful manners. Speaking of friends, my dear girlfriends: Jackie, Cristina, Patty, Inés, Berta, Poonam, Judit... thank you for creating a safe space for me to thrive, for the endless conversations on woman independence and self-love, for never letting me go; your validation has been key for me to do this and I will be forever thankful for every second we share.

Thank you to the people who has been taking me climbing these last months, I don't really think writing a thesis was a feasible thing for me to do without all of the



lessons this habit of us provided me. Thank you because you encourage me when I fight, catch me when I fall and celebrate me when I rise. In the same way, I need to acknowledge Dr. Carla Pedreño for her hard work and professional help regarding my mental health.

Gràcies a la meva família pels valors. Als meus avis, tiets, cosins... per donar-me tant d'amor i tant gratuït. Als meus pares dels qui des de petita he après la bellesa i la duresa que comporta tenir un projecte propi i estimar-lo. Gràcies mare per tanta dolcesa, gràcies per les abraçades, pel teu support incondicional. Al Rex i a l'Anut i al meu germà Guim, el meu millor amic, sempre a peu de via.

I gràcies a la Canelita, etern company de moixaines.

# TABLE OF CONTENTS

<b>LIST OF ABBREVIATIONS.....</b>	<b>11</b>
<b>0. INTRODUCTION.....</b>	<b>13</b>
0.1. Nanocrystals: synthesis, challenges and characteristics .....	16
0.2. Strategies for the synthesis of carbon nanostructure – nanoparticle hybrids.....	19
0.3. Motivation .....	21
0.4. REFERENCES.....	22
<b>1. TOWARDS A GENERAL STRATEGY FOR THE FUNCTIONALIZATION OF CARBON NANOSTRUCTURES BY INORGANIC NANOCRYSTALS.....</b>	<b>29</b>
1.1. MATERIALS AND METHODS .....	32
1.1.1. Synthesis of semiconductor and metal nanocrystals .....	32
1.1.2. Post-synthesis procedure: preparation of the hybrid .....	37
1.1.3. Dynamic characterization experiments .....	38
1.2. CHARACTERIZATION TECHNIQUES.....	39
1.3. RESULTS AND DISCUSSION .....	39
1.3.1. Method validation and characterization .....	39
1.3.2. Assessment of the reproducibility, robustness and scalability of the decoration method.....	42
1.3.3. Advanced characterization of the hybrids .....	47
1.4. CONCLUSIONS .....	51
1.5. REFERENCES.....	51
<b>2. HYBRID MOLECULAR-NANOPARTICLE MATERIALS FOR LIGHT INDUCED WATER SPLITTING .....</b>	<b>57</b>
2.1. MATERIALS AND METHODS .....	62

2.1.1. Synthesis of Ru-tda/SWCNT/TiO <sub>2</sub> -NCs.....	62
2.1.2. Photocatalytic experiments .....	63
2.2. CHARACTERIZATION TECHNIQUES .....	63
2.3. RESULTS AND DISCUSSION .....	64
2.3.1. Synthesis of Ru-tda/SWCNT/TiO <sub>2</sub> -NCs and characterization.....	64
2.3.2. Electrochemical characterization of the sample.....	67
2.4. CONCLUSIONS AND PERSPECTIVES .....	71
2.5. REFERENCES .....	73
<b>3. SYNTHESIS AND APPLICATION STUDY OF Fe<sub>3</sub>O<sub>4</sub>/GRAPHENE HYBRID FOR WATER REMEDIATION .....</b>	<b>77</b>
3.1. MATERIALS AND METHODS.....	80
3.1.1. Synthesis of Fe <sub>3</sub> O <sub>4</sub> /Graphene and Fe <sub>3</sub> O <sub>4</sub> -TiO <sub>2</sub> /Graphene hybrids .....	81
3.2. CHARACTERIZATION TECHNIQUES .....	83
3.3. RESULTS AND DISCUSSION .....	83
3.3.1. Synthesis and characterization of Fe <sub>3</sub> O <sub>4</sub> /Graphene and Fe <sub>3</sub> O <sub>4</sub> -TiO <sub>2</sub> /Graphene hybrids.....	83
3.3.2. Fe <sub>3</sub> O <sub>4</sub> /Graphene hybrids as an adsorbent for pharmaceutical wastewater .....	86
3.3.3. Fe <sub>3</sub> O <sub>4</sub> /Graphene oxide hybrids as an adsorbent for pharmaceutical wastewater ...	90
3.3.4. Fe <sub>3</sub> O <sub>4</sub> -TiO <sub>2</sub> /Graphene hybrids for the recyclability of the remediation system.....	92
3.4. CONCLUSIONS AND PERSPECTIVES .....	94
3.5. REFERENCES .....	94
<b>4. GENERAL CONCLUSIONS.....</b>	<b>101</b>
<b>APPENDIX I. CHARACTERIZATION TECHNIQUES.....</b>	<b>I</b>
<b>APPENDIX II. LIST OF CONTRIBUTIONS .....</b>	<b>III</b>
Scientific articles.....	iii
Oral contributions .....	iii
Poster contributions .....	iv
Scientific dissemination and other contibutions .....	iv

# LIST OF ABBREVIATIONS

1-ODE: Octadecene

1-ODOL: 1-octadecanol

AQY: Apparent Quantum Yield

CNS: Carbon Nanostructure

CNT: Carbon Nanotube

CTAB: Hexadecyltrimethylammonium bromide

DCF: Diclofenac

G: Graphene

GA: Gallic acid

GO: Graphene Oxide

IBP: Ibuprofen

MUA: 11-mercaptoundecanoic acid

NC: Nanocrystal

NHE: Normal Hydrogen Electrode

NP: Nanoparticle

NSAID: Nonsteroidal Anti-Inflammatory Drugs

ODPA: Octadecylphosphonic acid

OEC: Oxygen Evolution Catalyst

OER: Oxygen Evolution Reaction

OIAc: Oleic acid

OIAm: Oleylamine

PRR: Proton Reduction Reaction

QD: Quantum Dot

RuIV(O)-tda: [RuIV(O)(tda)(pypyr)<sub>2</sub>]

Ru-tda: [Ru(tda)(pypyr)<sub>2</sub>], where tda<sup>2-</sup> = [2,2':6',2''-terpyridine]-6,6''-dicarboxylato and pypyr = 4-(pyren-1-yl)-N-(pyridin-4-ylmethyl)butanamide

SC: Trisodium citrate

SEA: Sacrificial Electron Acceptor

SWCNT: Single-Walled Carbon Nanotube

TA: Tannic acid

TMAOH: Tetramethylammonium hydroxide

TON: Turnover Number

TOPO: Trioctylphosphine oxide

WOC: Water Oxidation Catalyst

WOR: Water Oxidation Reaction

WS: Water Splitting

## 0. INTRODUCTION

Colloidal assembly of nanostructures is a promising tool of fabrication of more complex materials, enhancing their properties and expanding their applicability. [1] Inspired by biology, self-assembly explores the way the spatial arrangement of functional building-block materials translates into sophisticated properties. Building blocks of nanostructures are the atoms and molecules that conform them. In particular structures and conformations, these assembled structures (particles, macrostructures, etc.), can now become the building blocks of more complex materials hierarchically constructed spanning to different length scales, which expands the array of possibilities and the complexity of the final product.[2] The principle of self-assembly is to provide the constituents –or building blocks - the adequate characteristics for them to spontaneously form the desired structure in a fashion that will minimize the total energy of the system and thus be stable.[3] The colloidal-assembly of nanosized building blocks has been focused on developing a new generation of high-end technology devices for fields such as photonics, electronics, environmental and biomedical applications.[1]

Carbon-based nanomaterials have been of growing interest (**Figure 1**) in various scientific areas due to their structural features and mechanical, thermal optical and

chemical properties. Such materials include carbon nanotubes (CNTs), fullerenes, graphene (G) and its derivatives among others.

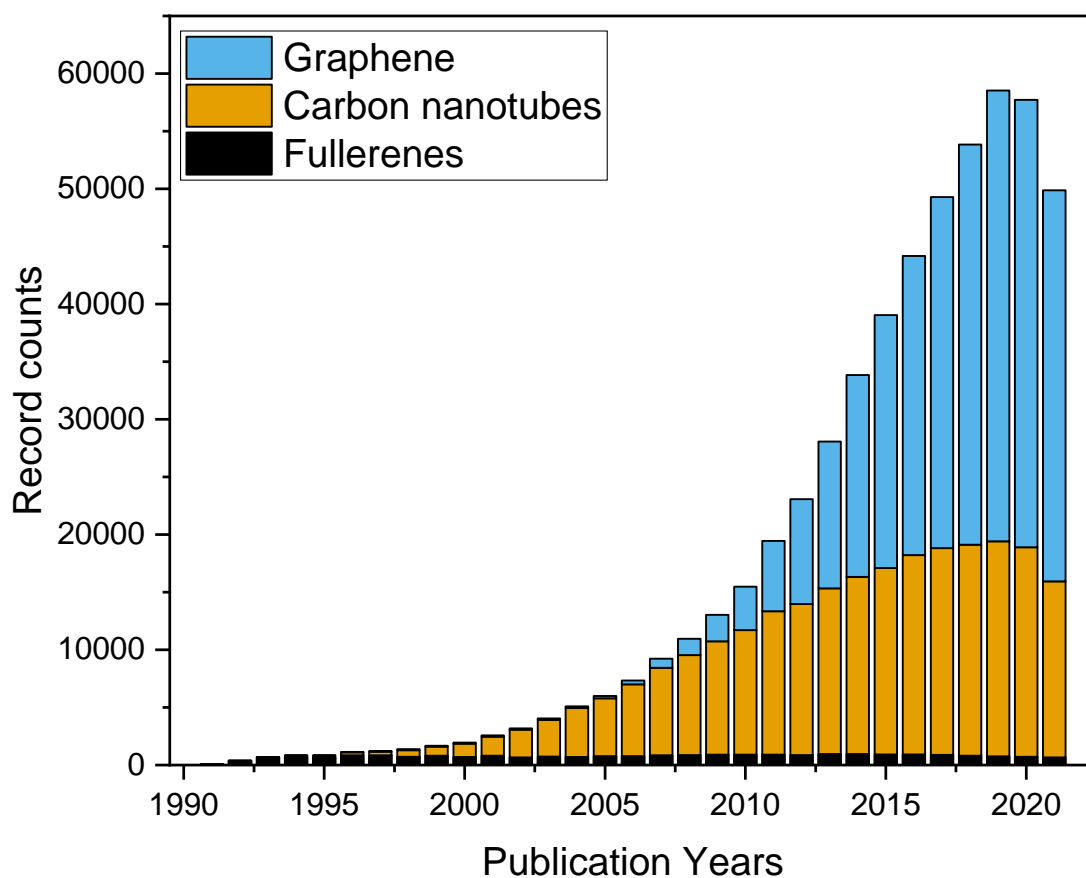


**Figure 1.** Number of publications per year in the last 25 years in the areas carbon nanostructures, graphene, carbon nanotubes and fullerenes. Data extracted from the Web of Knowledge (Science Citation Index) when searching for the key words ‘Graphene’, ‘Carbon nanotubes’, ‘Fullerene’.

Historically, we could say the carbon nanostructures (CNSs) research field started in 1970 with the prediction of fullerenes although they were discovered in a serendipitous manner almost fifteen years later in 1985[4]. The field continued in growing and CNTs were synthesised in 1991.[5] CNTs are rolled monolayers of graphite the mechanic, thermic and electronic properties of which depend exclusively on their rotation style.[6] Later on, the discovery of graphene – which was recognised with a Nobel Prize in physics in 2010 - as a one-atom thick layer of carbon with astonishingly relevant intrinsic carrier mobility ( $200\,000\text{ cm}^2\text{ V}^{-1}\text{ s}^{-1}$ ), thermal

conductivity ( $\sim 5000 \text{ W m}^{-1}\text{K}^{-1}$ ), Young's modulus ( $\sim 1.0 \text{ TPa}$ ), and optical transmittance ( $\sim 97.7\%$ ) has put carbon nanostructures in the spotlight of material science (**Figure 2**).[7]–[10]

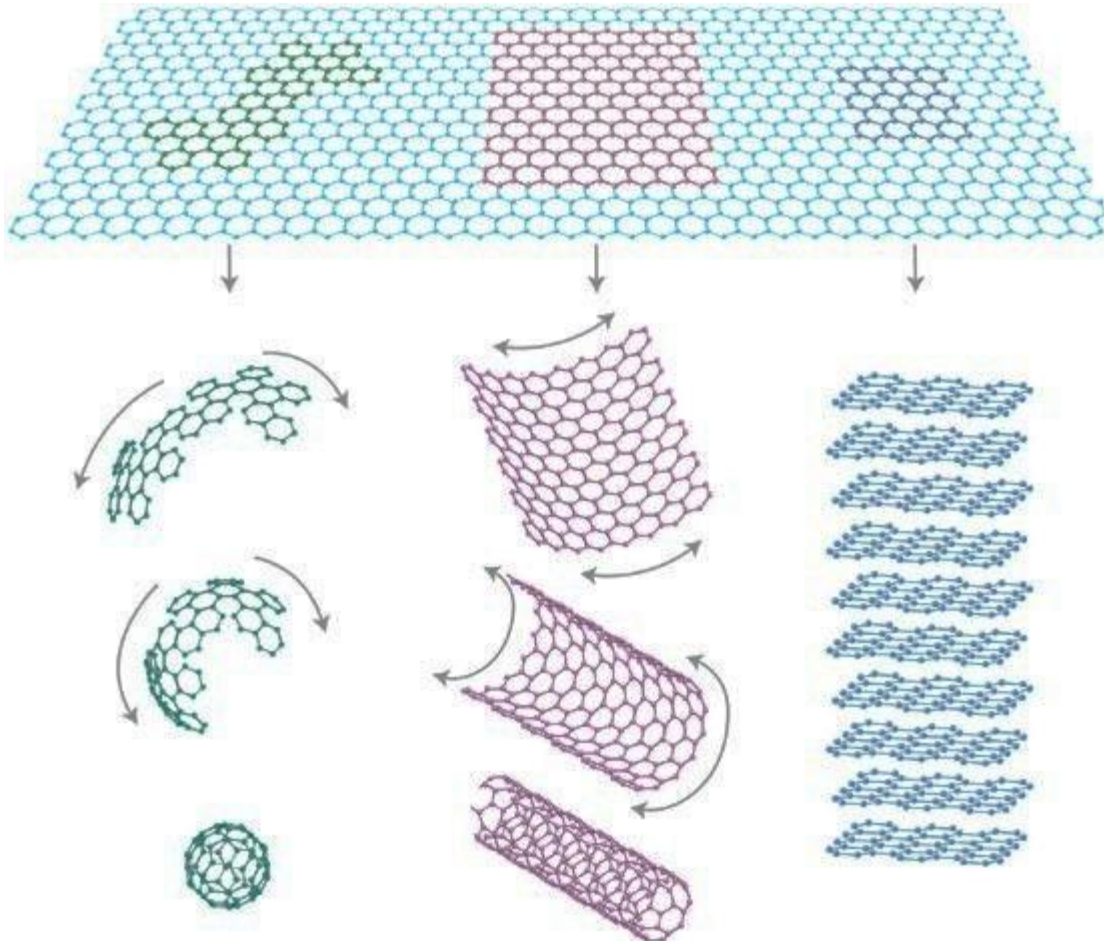


**Figure 2.** Graphene (baby blue) is a 2D building material for carbon materials of all other dimensionalities. It can be wrapped up into 0D fullerenes (green), rolled into 1D nanotubes (purple) or stacked into 3D graphite (dark blue). Figure borrowed from reference [5].

All of the aforementioned properties make CNSs deeply interesting components for the construction of devices for the next generation of catalysts for solar cells and water splitting,[11]–[13] electronics,[14] health,[15]–[17] environmental applications[18]–[21] and others.[22], [23] Nevertheless, if we want CNSs to be part of macroscopic organised structures with high-end determined properties, they need to be assembled into more sophisticated and hierarchical architectures in order to design exploitable integrated systems. One of the most interesting strategies for the future



expansion of this technology is to functionalize them with inorganic nanocrystals (NCs).

### **0.1. NANOCRYSTALS: SYNTHESIS, CHALLENGES AND CHARACTERISTICS**

Nanocrystals typically possess a diameter of under <100 nm and contain from hundreds to tens of thousands of atoms, they are constituted of an inorganic core, with tuneable composition, size, and shape, and covered with surfactants or ligands. Because of their size, nanocrystals are unique in that the number of surface atoms is a large fraction of the total. Their intrinsic properties are also transformed by size effects and/or the spatial confinement of excitations.[24] Size control allows the study, understanding and application of fundamental properties of NCs, such as fluorescence of semiconductor NCs plasmonic behaviour of noble metal NCs (i.e. Au or Ag) and the superparamagnetic moment in magnetic NCs (i.e. Fe<sub>3</sub>O<sub>4</sub> or Co).[25] The diversity of examples illustrates the control of the material, size, shape, and composition of NCs that is now to be potentially achievable. Bottom-up wet-chemistry synthesis strategies can be used to prepare, understand, and design new and improved systems.

Bottom-up wet-chemistry synthesis routes deal with chemical reactions in the solution phase using precursors at proper experimental conditions. [26] Working in the liquid phase allows to easily tune the final product structurally, compositionally, and morphologically with small changes in the overall reaction such as the solvent properties or the addition of ligands. The process of transformation of precursors to colloidal NCs involve (a) the chemical reduction of metal salts, (b) the nucleation and growth of inorganic nanocrystals in suspension, (c) the seeded growth approach in which small (<5 nm) nanoparticles act as seed for the epitaxial attachment of metal ions, (d) precipitation methods, involving a stoichiometric precipitation of ionic species, and

others not explored in the following work such as (e) biogenic approaches to inorganic nanostructures, micro emulsion methods, sonolysis and radiolysis. [27] These methods usually involve the use of inorganic or organometallic precursors, and organic ligands or surfactants. The key concept is the controlled temporal separation of particle nucleation and growth by supersaturation of monomers in solution, as plotted in **Figure 3**. This can be achieved either by hot-injection methods, which involves rapid addition of precursor species that induce a short burst of nucleation, followed by the growth of the initially formed nuclei [28]-[30] or heat-up methods the reaction mixture is prepared at a lower temperature and heated to the reaction temperature at which the formation of nanocrystals takes place.[31], [32] The selection of one of the other strategy depends on the choice of precursor.

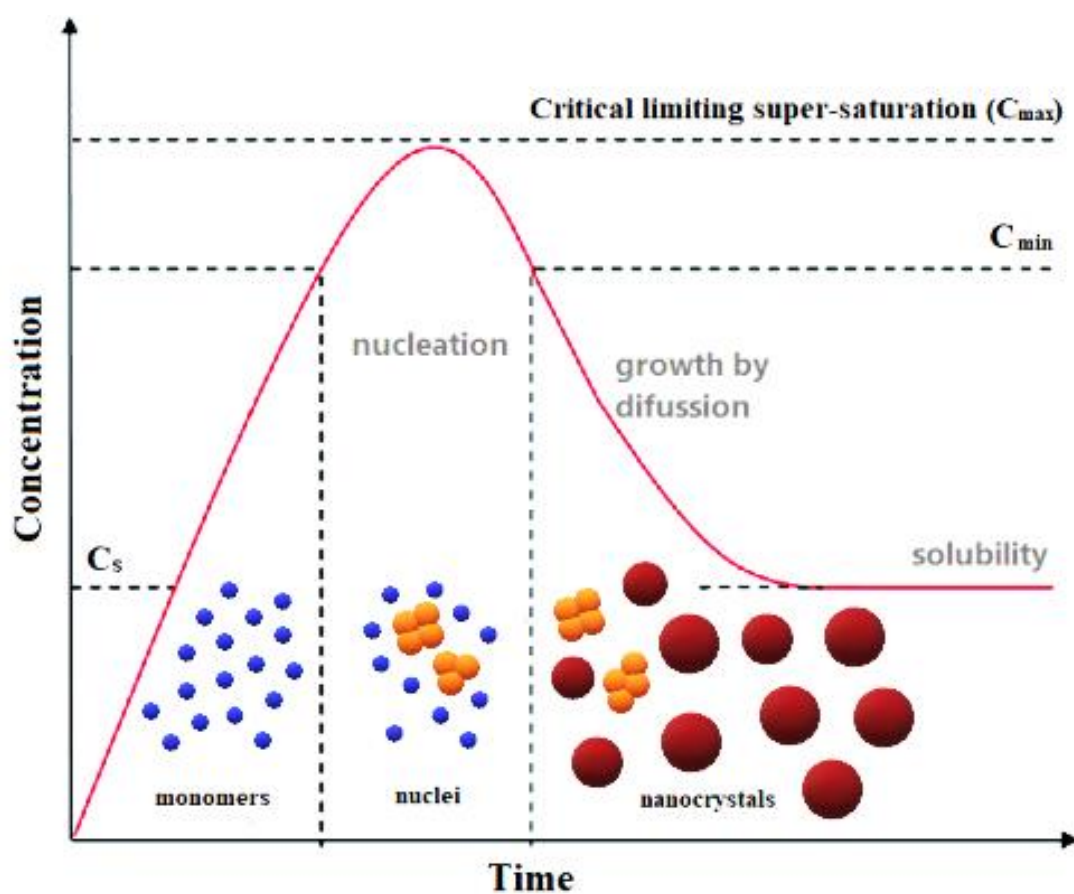


**Figure 3.** Traditional LaMer model applied to the generation of atoms, nucleation, and growth of colloidal synthesis. [26]

The combination of specific surfactants and high temperatures facilitate the formation of NCs with narrower size distributions and with fewer internal defects, hence having well-defined physical properties. [33], [34] During the synthesis, the surfactants play the key role in tuning the reactivity of the monomers, and in regulating the temporal evolution of the NC size and shape over time. [35]

Summarizing, the classical concepts of size distribution control, i.e., burst nucleation, separation of nucleation and growth, and diffusion-controlled growth, are applied consistently to both the hot-injection and heat-up models. [36], [37] Although a two-step model where the crystalline nucleus appears after the generation of pre-existing metastable clusters followed by its reorganization into NCs, has been proved as a modification of the classical one. [38]

Same concepts used for size-control can be extended to shape by tuning the reactivity of the different NCs facets.[35], [39], [40] The preferential binding of ligands to certain crystal planes allows their introduction to the system as shape-control agents because of the hindering of growth of those facets by lowering their reactivity.[41], [42] In addition to surfactants, halogen ions ( $F^-$ ,  $Cl^-$ ,  $Br^-$ , and  $I^-$ ) can strongly adsorb on certain crystal planes and thus stabilize specific facets being therefore used as shape-control agents via selective attachment, especially for pure metals and alloys.[43]–[45] Tuning the pH of the media can also control the growth of metal oxides, due to the differential hydroxylation of surfaces, such that  $OH^-$  or  $H^+$  ions are used as selective capping agents on specific facets. Also, the pH in the solution modulates the surface potential and reactivity of NPs leading to different stabilities of metal oxide and metal hydroxide surfaces, and thus affecting the growth of specific facets. [42]

These strategies can be used as a toolbox for widening the NCs family as represented in **Figure 4** and its possibilities as each one of them plays a role on the properties of the final product (i.e.: plasmonic response of Ag NCs is varies as a function of its size [46], shape [45], morphology).

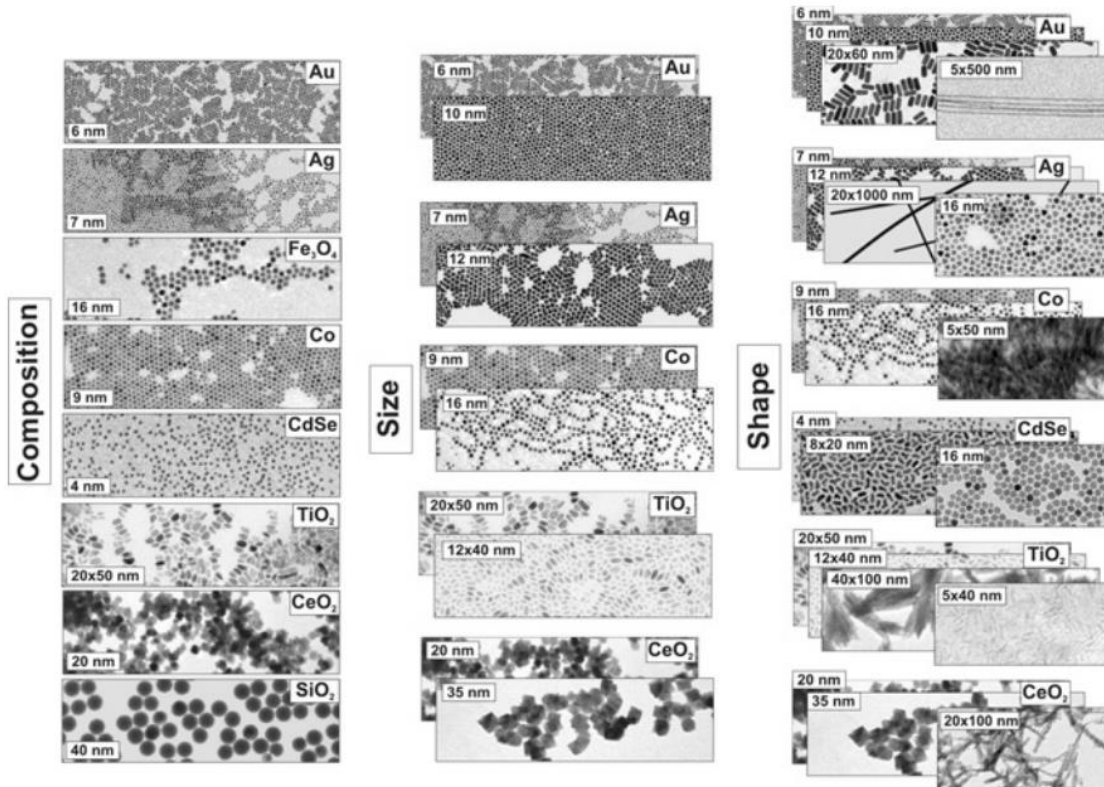


**Figure 4.** Control of the Composition, Size, and Shape of Colloidal Inorganic Nanocrystals. Representative Transmission Electron Microscopy (TEM) images of colloidal solutions of NCs of different compositions, sizes and shapes. Extracted from reference [20].

## 0.2. STRATEGIES FOR THE SYNTHESIS OF CARBON NANOSTRUCTURE – NANOPARTICLE HYBRIDS

Carbon nanostructure-nanocrystal hybrids are innovative and of deep interest because they can take advantage of the aforementioned tenability of the NCs characteristics – and therefore properties – and create an interface of tailorable and predictable properties. To develop a hybrid involving both CNSs and NCs is to achieve a heterojunction with an area of less than 10 nm<sup>2</sup>, which is more than significantly

unique from the material development point of view. From this modular point of view, the possibilities of generating new materials are immense, thus increasing the chances of being able to address the technological challenges of the future.

At the present moment, the performance of NP-CNS hybrid structures has been reported as outstanding in different fields, from energy to health and environment.<sup>1</sup> [20], [48], [50] For instance, the decoration of graphene (G) by metal or metal oxide NPs has been shown to affect the charge transfer behaviour in G through the modification of the local electronic structure. [51], [52] As a result, this type of composite material can show improved performance as catalysts. On the other hand, in sensing applications, the combination of NPs, which have excellent conductivity and catalytic properties, with CNSs allows for the enhancement of achievable sensitivity and selectivity over either CNSs or NP-based sensors alone. Similarly, by combining CNSs with NPs, it is possible to develop new multifunctional platforms for imaging. [53], [54]

*In situ* and *ex situ* methods for the decoration of CNSs with inorganic nanoparticles via covalent or non-covalent interactions (**Figure 5**). [47]–[49] The paradigm of the *in-situ* case is to grow the NPs directly onto the surface of the CNSs via of inorganic precursors absorbed by functional groups present at the surface of the CNSs. [55]–[57] Hybrid structures can also be achieved by the *ex-situ* assembly of NPs onto the CNSs surface, where the NPs are synthesized attached to the surface of the graphene via linking agents that can utilize van der Waals interactions, hydrogen bonding,  $\pi$ – $\pi$  stacking, or electrostatic interactions.[51], [58]–[62]

---

<sup>1</sup> Although in this thesis we will focus on the coupling of NCs and CNSs, in this introduction we will describe general nanoparticle (NP)-CNS structures, because the examples from the literature may be valid for non-crystalline species.

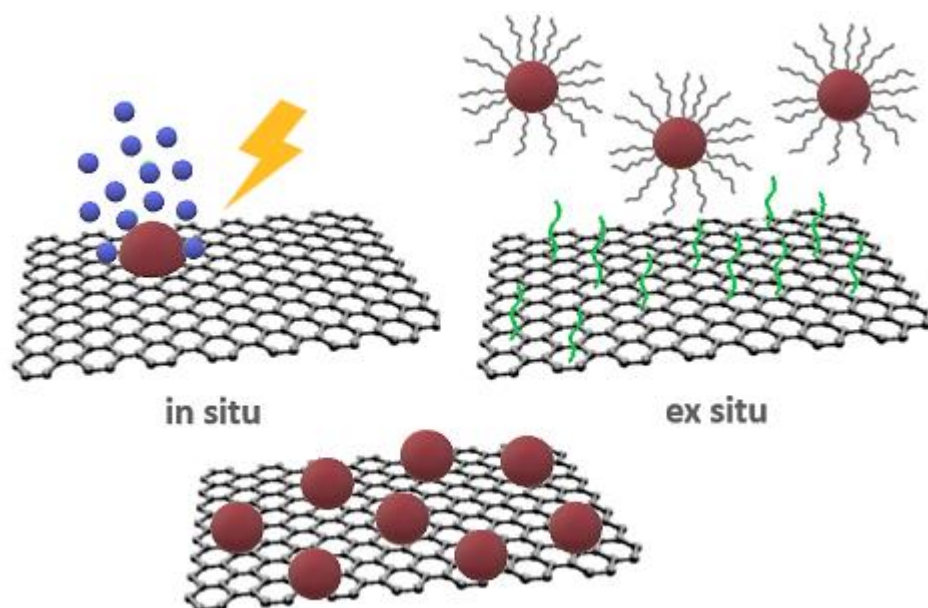


**Figure 5.** General graphical representation of *in-situ* and *ex-situ* approaches for nanoparticle decoration of CNSs.

### 0.3. MOTIVATION

Summarizing, to develop the applicability of CNS–NP hybrid materials it is of vital importance to i) produce high quality components that allow for a robust, reproducible, and versatile coupling methodology and ii) for the method to be technologically relevant, including safety and sustainability considerations in its design that allow for scale-up, which open up the conversation on the translation of nanoscience to nanotechnology. [63]–[66]

Both challenges are addressed in **CHAPTER 1** of the present work. **CHAPTER 2** and **CHAPTER 3** of this thesis address the synergies of NCs and CNSs in the catalysis and the remediation field respectively. Both subjects have been chosen because of the unavoidable relationship between them and the societal urge of being attended since energy and pollution are at the core of the current environmental crisis.

#### 0.4. REFERENCES

- [1] O. D. Velev and S. Gupta, "Materials fabricated by micro- and nanoparticle assembly - The challenging path from science to engineering," *Adv. Mater.*, vol. 21, no. 19, pp. 1897–1905, May 2009.
- [2] S. C. Glotzer, M. J. Solomon, and N. A. Kotov, "Self-assembly: From nanoscale to microscale colloids," *AIChE J.*, vol. 50, no. 12, pp. 2978–2985, Dec. 2004.
- [3] M. Tirrell, "Modular materials by self-assembly," *AIChE J.*, vol. 51, no. 9, pp. 2386–2390, Sep. 2005.
- [4] H. W. Kroto, J. R. Heath, S. C. O'Brien, R. F. Curl, and R. E. Smalley, "C60: Buckminsterfullerene," *Nat. 1985 3186042*, vol. 318, no. 6042, pp. 162–163, 1985.
- [5] S. Iijima, "Helical microtubules of graphitic carbon," *Nat. 1991 3546348*, vol. 354, no. 6348, pp. 56–58, 1991.
- [6] R. S. Ruoff and D. C. Lorents, "Mechanical and thermal properties of carbon nanotubes," *Carbon N. Y.*, vol. 33, no. 7, pp. 925–930, Jan. 1995.
- [7] Z. Zhen and H. Zhu, "Structure and Properties of Graphene," *Graphene Fabr. Charact. Prop. Appl.*, pp. 1–12, Jan. 2018.
- [8] A. K. Geim and K. S. Novoselov, "The rise of graphene," *Nanosci. Technol. A Collect. Rev. from Nat. Journals*, pp. 11–19, Jan. 2009.
- [9] M. S. Dresselhaus and M. Terrones, "Carbon-based nanomaterials from a historical perspective," *Proc. IEEE*, vol. 101, no. 7, pp. 1522–1535, 2013.
- [10] C. Alvial-Palavicino and K. Konrad, "The rise of graphene expectations: Anticipatory practices in emergent nanotechnologies," *Futures*, vol. 109, pp. 192–202, May 2019.
- [11] K. S. Subrahmanyam, A. K. Manna, S. K. Pati, and C. N. R. Rao, "A study of graphene decorated with metal nanoparticles," *Chem. Phys. Lett.*, vol. 497, no. 1–3, pp. 70–75, Sep. 2010.
- [12] I. V. Lightcap, T. H. Kosel, and P. V. Kamat, "Anchoring semiconductor and metal nanoparticles on a two-dimensional catalyst mat. storing and shuttling electrons with reduced graphene oxide," *Nano Lett.*, vol. 10, no. 2, pp. 577–583, Feb. 2010.
- [13] P. V. Kamat, "Graphene-based nanoarchitectures. Anchoring semiconductor and metal nanoparticles on a two-dimensional carbon support," *J. Phys. Chem. Lett.*, vol. 1, no. 2, pp. 520–527, Jan. 2010.

- 
- [14] A. Cao *et al.*, “A facile one-step method to produce craphene-CdS quantum dot nanocomposites as promising optoelectronic materials,” *Adv. Mater.*, vol. 22, no. 1, pp. 103–106, Jan. 2010.
- [15] H. Vedala, D. C. Sorescu, G. P. Kotchey, and A. Star, “Chemical sensitivity of graphene edges decorated with metal nanoparticles,” *Nano Lett.*, vol. 11, no. 6, pp. 2342–2347, Jun. 2011.
- [16] A. C. Joshi, G. B. Markad, and S. K. Haram, “Rudimentary simple method for the decoration of graphene oxide with silver nanoparticles: Their application for the amperometric detection of glucose in the human blood samples,” *Electrochim. Acta*, vol. 161, pp. 108–114, Apr. 2015.
- [17] W. Shao, X. Liu, H. Min, G. Dong, Q. Feng, and S. Zuo, “Preparation, characterization, and antibacterial activity of silver nanoparticle-decorated graphene oxide nanocomposite,” *ACS Appl. Mater. Interfaces*, vol. 7, no. 12, pp. 6966–6973, Apr. 2015.
- [18] A. O. Adeola and P. B. C. Forbes, “Advances in water treatment technologies for removal of polycyclic aromatic hydrocarbons: Existing concepts, emerging trends, and future prospects,” *Water Environment Research*. John Wiley and Sons Inc., 2020.
- [19] L. A. Al-Khateeb, S. Almotiry, and M. A. Salam, “Adsorption of pharmaceutical pollutants onto graphene nanoplatelets,” *Chem. Eng. J.*, vol. 248, pp. 191–199, Jul. 2014.
- [20] S. Mura *et al.*, “Graphene Oxide/Iron Oxide Nanocomposites for Water Remediation,” *ACS Appl. Nano Mater.*, vol. 1, no. 12, pp. 6724–6732, Dec. 2018.
- [21] S. M. Maliyekkal *et al.*, “Graphene: A reusable substrate for unprecedented adsorption of pesticides,” *Small*, vol. 9, no. 2, pp. 273–283, Jan. 2013.
- [22] M. Valcárcel, S. Cárdenas, B. M. Simonet, Y. Moliner-Martínez, and R. Lucena, “Carbon nanostructures as sorbent materials in analytical processes,” *TrAC Trends Anal. Chem.*, vol. 27, no. 1, pp. 34–43, Jan. 2008.
- [23] Y. H. Wu, T. Yu, and Z. X. Shen, “Two-dimensional carbon nanostructures: Fundamental properties, synthesis, characterization, and potential applications,” *J. Appl. Phys.*, vol. 108, no. 7, p. 071301, Oct. 2010.
- [24] E. Roduner, “Size matters: Why nanomaterials are different,” *Chem. Soc. Rev.*, vol. 35, no. 7, pp. 583–592, 2006.
- [25] N. G. Bastús *et al.*, “Exploring new synthetic strategies for the production of advanced complex inorganic nanocrystals,” *Zeitschrift fur Phys. Chemie*, vol. 229, no. 1–2, pp.



- 65–83, 2015.
- [26] W. J. Parak, “Complex Colloidal Assembly,” *Science* (80-. ), vol. 334, no. 6061, pp. 1359–1360, Dec. 2011.
- [27] S. Diodati, P. Dolcet, M. Casarin, and S. Gross, “Pursuing the Crystallization of Mono- and Polymetallic Nanosized Crystalline Inorganic Compounds by Low-Temperature Wet-Chemistry and Colloidal Routes,” *Chem. Rev.*, vol. 115, no. 20, pp. 11449–11502, Oct. 2015.
- [28] V. K. Lamer and R. H. Dinegar, “Theory, Production and Mechanism of Formation of Monodispersed Hydrosols,” *J. Am. Chem. Soc.*, vol. 72, no. 11, pp. 4847–4854, Nov. 2002.
- [29] C. B. Murray, D. J. Norris, and M. G. Bawendi, “Synthesis and characterization of nearly monodisperse CdE (E = sulfur, selenium, tellurium) semiconductor nanocrystallites,” *J. Am. Chem. Soc.*, vol. 115, no. 19, pp. 8706–8715, Sep. 2002.
- [30] C. De Mello Donegá, P. Liljeroth, and D. Vanmaekelbergh, “Physicochemical Evaluation of the Hot-Injection Method, a Synthesis Route for Monodisperse Nanocrystals,” *Small*, vol. 1, no. 12, pp. 1152–1162, Dec. 2005.
- [31] G. K. Soon and T. Hyeon, “Colloidal Chemical Synthesis and Formation Kinetics of Uniformly Sized Nanocrystals of Metals, Oxides, and Chalcogenides,” *Acc. Chem. Res.*, vol. 41, no. 12, pp. 1696–1709, Dec. 2008.
- [32] J. Van Embden, A. S. R. Chesman, and J. J. Jasieniak, “The Heat-Up Synthesis of Colloidal Nanocrystals,” *Chem. Mater.*, vol. 27, no. 7, pp. 2246–2285, Apr. 2015.
- [33] T. Hyeon, Su Seong Lee, J. Park, Y. Chung, and Hyon Bin Na, “Synthesis of highly crystalline and monodisperse maghemite nanocrystallites without a size-selection process,” *J. Am. Chem. Soc.*, vol. 123, no. 51, pp. 12798–12801, Dec. 2001.
- [34] J. Park *et al.*, “Ultra-large-scale syntheses of monodisperse nanocrystals,” *Nat. Mater.*, vol. 3, no. 12, pp. 891–895, Dec. 2004.
- [35] C. M. Phan and H. M. Nguyen, “Role of Capping Agent in Wet Synthesis of Nanoparticles,” *J. Phys. Chem. A*, vol. 121, no. 17, pp. 3213–3219, May 2017.
- [36] S. G. Kwon and T. Hyeon, “Formation Mechanisms of Uniform Nanocrystals via Hot-Injection and Heat-Up Methods,” *Small*, vol. 7, no. 19, pp. 2685–2702, Oct. 2011.
- [37] C. B. Whitehead, S. Özkar, and R. G. Finke, “LaMer’s 1950 Model for Particle Formation of Instantaneous Nucleation and Diffusion-Controlled Growth: A Historical

- Look at the Model's Origins, Assumptions, Equations, and Underlying Sulfur Sol Formation Kinetics Data," *Chem. Mater.*, vol. 31, no. 18, pp. 7116–7132, Sep. 2019.
- [38] D. Erdemir, A. Y. Lee, and A. S. Myerson, "Nucleation of Crystals from Solution: Classical and Two-Step Models," *Acc. Chem. Res.*, vol. 42, no. 5, pp. 621–629, May 2009.
- [39] L. Manna, E. C. Scher, and A. P. Alivisatos, "Synthesis of Soluble and Processable Rod-, Arrow-, Teardrop-, and Tetrapod-Shaped CdSe Nanocrystals," *J. Am. Chem. Soc.*, vol. 122, no. 51, pp. 12700–12706, Dec. 2000.
- [40] D. Milliron *et al.*, "Colloidal nanocrystal heterostructures with linear and branched topology," *Nat. 2004 4306996*, vol. 430, no. 6996, pp. 190–195, Jul. 2004.
- [41] C. R. Bealing, W. J. Baumgardner, J. J. Choi, T. Hanrath, and R. G. Hennig, "Predicting nanocrystal shape through consideration of surface-ligand interactions," *ACS Nano*, vol. 6, no. 3, pp. 2118–2127, Mar. 2012.
- [42] Z. Wu, S. Yang, and W. Wu, "Shape control of inorganic nanoparticles from solution," *Nanoscale*, vol. 8, no. 3, pp. 1237–1259, Jan. 2016.
- [43] M. Meyns *et al.*, "Shape evolution of CdSe nanoparticles controlled by halogen compounds," *Chem. Mater.*, vol. 26, no. 5, pp. 1813–1821, Mar. 2014.
- [44] M. Grzelczak, J. Pérez-Juste, P. Mulvaney, and L. M. Liz-Marzán, "Shape control in gold nanoparticle synthesis," *Chem. Soc. Rev.*, vol. 37, no. 9, pp. 1783–1791, Aug. 2008.
- [45] J. Patarroyo, A. Genç, J. Arbiol, N. G. Bastús, and V. Puntès, "One-pot polyol synthesis of highly monodisperse short green silver nanorods," *Chem. Commun.*, vol. 52, no. 73, pp. 10960–10963, Sep. 2016.
- [46] N. G. Bastús, F. Merkoçi, J. Piella, and V. Puntès, "Synthesis of highly monodisperse citrate-stabilized silver nanoparticles of up to 200 nm: Kinetic control and catalytic properties," *Chem. Mater.*, vol. 26, no. 9, pp. 2836–2846, May 2014.
- [47] X. Peng, J. Chen, J. A. Misewich, and S. S. Wong, "Carbon nanotube-nanocrystal heterostructures," *Chemical Society Reviews*, vol. 38, no. 4, pp. 1076–1098, 2009.
- [48] G. G. Wildgoose, C. E. Banks, and R. G. Compton, "Metal nanoparticles and related materials supported on Carbon nanotubes: Methods and applications," *Small*, vol. 2, no. 2, pp. 182–193, 2006.
- [49] Q. Li, N. Mahmood, J. Zhu, Y. Hou, and S. Sun, "Graphene and its composites with nanoparticles for electrochemical energy applications," *Nano Today*, vol. 9, no. 5, pp.

668–683, Oct. 2014.

- [50] X. Huang *et al.*, “Graphene-Based Materials: Synthesis, Characterization, Properties, and Applications,” *Small*, vol. 7, no. 14, pp. 1876–1902, Jul. 2011.
- [51] G. M. A. Rahman, D. M. Guldi, E. Zambon, L. Pasquato, N. Tagmatarchis, and M. Prato, “Dispensable carbon nanotube/gold nanohybrids: Evidence for strong electronic interactions,” *Small*, vol. 1, pp. 527–530, 2005.
- [52] C. N. R. Rao and R. Voggu, “Charge-transfer with graphene and nanotubes,” *Mater. Today*, vol. 13, no. 9, pp. 34–40, Sep. 2010.
- [53] P. K. Jain, X. Huang, I. H. El-Sayed, and M. A. El-Sayed, “Noble Metals on the Nanoscale: Optical and Photothermal Properties and Some Applications in Imaging, Sensing, Biology, and Medicine,” *Acc. Chem. Res.*, vol. 41, no. 12, pp. 1578–1586, Dec. 2008.
- [54] J. J. Davis, K. S. Coleman, B. R. Azamian, C. B. Bagshaw, and M. L. H. Green, “Chemical and biochemical sensing with modified single walled carbon nanotubes,” *Chem. - A Eur. J.*, vol. 9, pp. 3732–3739, 2003.
- [55] H. C. Choi, M. Shim, S. Bangsaruntip, and H. Dai, “Spontaneous reduction of metal ions on the sidewalls of carbon nanotubes,” *J. Am. Chem. Soc.*, vol. 124, pp. 9058–9059, 2002.
- [56] Z. Zhang *et al.*, “Sodium citrate: A universal reducing agent for reduction / decoration of graphene oxide with au nanoparticles,” *Nano Res.*, vol. 4, no. 6, pp. 599–611, 2011.
- [57] X. Z. Tang *et al.*, “Synthesis of graphene decorated with silver nanoparticles by simultaneous reduction of graphene oxide and silver ions with glucose,” *Carbon N. Y.*, vol. 59, pp. 93–99, Aug. 2013.
- [58] M. J. Moghaddam, S. Taylor, M. Gao, S. Huang, L. Dai, and M. J. McCall, “Highly Efficient Binding of DNA on the Sidewalls and Tips of Carbon Nanotubes Using Photochemistry,” *Nano Lett.*, vol. 4, pp. 89–93, 2004.
- [59] K. Jiang *et al.*, “Selective attachment of gold nanoparticles to nitrogen-doped carbon nanotubes,” *Nano Lett.*, vol. 3, pp. 275–277, 2003.
- [60] X. Li, Y. Liu, L. Fu, L. Cao, D. Wei, and Y. Wang, “Efficient synthesis of carbon nanotube-nanoparticle hybrids,” *Adv. Funct. Mater.*, vol. 16, pp. 2431–2437, 2006.
- [61] S. Guo and S. Sun, “FePt nanoparticles assembled on graphene as enhanced catalyst for oxygen reduction reaction,” *J. Am. Chem. Soc.*, vol. 134, no. 5, pp. 2492–2495, Feb.

- 2012.
- [62] S. Guo, S. Zhang, L. Wu, and S. Sun, “Co/CoO Nanoparticles Assembled on Graphene for Electrochemical Reduction of Oxygen,” *Angew. Chemie Int. Ed.*, vol. 51, no. 47, pp. 11770–11773, Nov. 2012.
- [63] W. K. Boyes *et al.*, “A comprehensive framework for evaluating the environmental health and safety implications of engineered nanomaterials,” *Crit. Rev. Toxicol.*, vol. 47, no. 9, pp. 771–814, Oct. 2017.
- [64] A. Sánchez, S. Recillas, X. Font, E. Casals, E. González, and V. Puentes, “Ecotoxicity of, and remediation with, engineered inorganic nanoparticles in the environment,” *TrAC - Trends in Analytical Chemistry*, vol. 30, no. 3. Elsevier B.V., pp. 507–516, 01-Mar-2011.
- [65] H. T. Phan and A. J. Haes, “What Does Nanoparticle Stability Mean?,” *J. Phys. Chem. C*, vol. 123, no. 27, pp. 16495–16507, Jul. 2019.
- [66] Y. Geng, J. Sarkis, and R. Bleischwitz, “How to globalize the circular economy,” *Nature*, vol. 565, no. 7738. Nature Research, pp. 153–155, 10-Jan-2019.



# 1. TOWARDS A GENERAL STRATEGY FOR THE FUNCTIONALIZATION OF CARBON NANOSTRUCTURES BY INORGANIC NANOCRYSTALS

Carbon-based nanostructures (CNS), including graphene (G), graphene oxide (GO), reduced graphene oxide (rGO), and carbon nanotubes (CNTs), play a central role in materials science thanks to their unique structural and morphological features, as well as excellent electrical, mechanical, and thermal properties. [1], [2] While promising and exciting, this applicability can be increased by combining CNSs with inorganic nanoparticles (NPs). These hybrid structures are especially alluring not only because they display the individual properties of each component but also because they exhibit additional advantageous and often synergistic behaviour. [3], [4] The combination of those materials might be used for catalysis, in solar cells, for water splitting, [4]–[6] for health, [7]–[9] electronics, [10] and environmental applications. [11]–[13] Additionally, studies on the fundamental aspect of charge transfer between the components can be studied in such systems. [14]

Recent efforts in this area have been focused on the development of *in-situ* and *ex-situ* methods to functionalize CNSs with inorganic NPs via covalent or non-covalent interactions. A very simple approach is to grow the NPs directly onto the CNS surface following a chemical treatment –reduction, heating, or electrodeposition– of inorganic

precursors electrostatically absorbed by functional groups present at the surface of the CNS. [15]–[17] This process is especially useful when using the oxidised form of the CNS as a substrate [18], [19], as it has multiple defects and oxygen functionalities where seeding can take place and it is widely used in the case of GO. [20]–[22] Alternatively, graphene-NP composites can also be produced by the *ex-situ* assembly of NPs onto the surface in a process where the NPs are synthesized in advance and attached to the surface of the graphene via linking agents that can utilize van der Waals interactions, hydrogen bonding,  $\pi$ – $\pi$  stacking, or electrostatic interactions. [16], [17], [22] Both approaches present interesting benefits but important limitations. While the direct deposition is simpler and large amounts of NPs can be immobilized onto the CNS, the features of the NP –size, shape, composition, and the percentage of NPs deposited– are very difficult to control in the presence of the CNS. On the contrary, the attachment of pre-formed NPs on CNSs is a more complicated procedure that involves a multi-reaction sequential process (synthesis of the NPs, chemical modifications of both components, and their affinity). However, this approach allows selecting the NPs and, to some extent, adjust the loading of the CNS.

Remarkably, none of them allow to easily produce graphene–NP hybrid structures composed of different types of NPs. By fabricating such a structure, synergism and other emergent properties may be achieved between the different NP species that are present in it, between the NPs and the CNSs and also the anchored NPs and the media. Another important limitation of the methods reported is that none of them are universal. This point is especially important when considering the chemical nature of the different CNSs; while CNSs are hydrophobic in nature, the presence of oxygen atoms bound with carbon makes their oxidized form hydrophilic. [23], [24]

The most crucial point for the future expansion of Carbon-based-NP hybrid structures is to develop synthetic methodologies to produce the materials with reproducible properties and performances that preserve not only the properties of the carbonaceous structure but also that allows tuning the physicochemical features of the NPs that are deposited on it.

In the following chapter, we aim to offer the community a general, facile, and non-intrusive method for nanocrystal (NCs) decoration of CNSs. The presented protocol (**Figure 1**) allows the control of shape, size, composition, and population density onto the carbonaceous substrate by controlling the process at two different levels: i) NCs synthesis and ii) graphene decoration. The quality of the produced hybrid depends inherently on the NC's quality. In this work, highly monodisperse metal and metal oxide NCs have been prepared both in aqueous and non-aqueous media and attached non-covalently to the CNS surface without the need of further chemical treatment by a ligand exchange process resulting from the progressive depletion of stabilizer in the media. The robustness of the hybrid has been proved and detailed characterization performed.

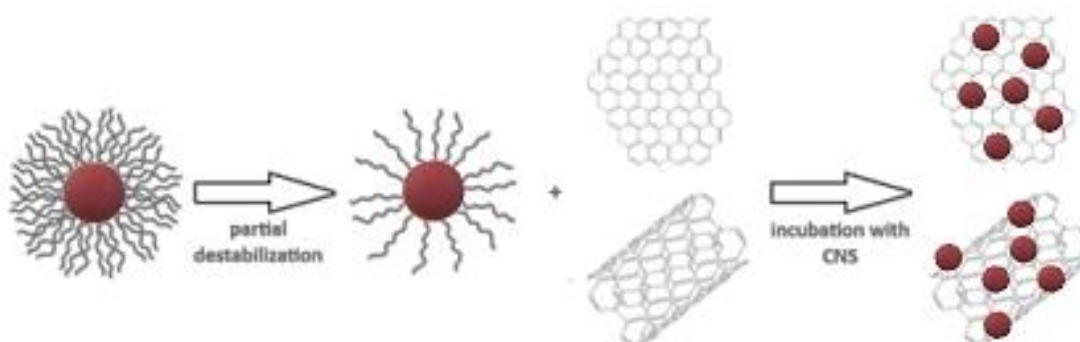


**Figure 1.** Schematic representation of the approached used for successful NCs decoration of CNSs.



## **1.1. MATERIALS AND METHODS**

Materials are listed by their order of appearance in this chapter.

Oleylamine (OIAm, technical grade 70%), 1-octadecanol (1-ODOL, 95%), octadecene (1-ODE, technical grade 90%), oleic acid (OIAc, technical grade 90%), titanium fluoride (TiF<sub>4</sub>), titanium chloride (TiCl<sub>4</sub> 99.9% trace metals basis), 2-propanol (70% in H<sub>2</sub>O), methanol (anhydrous, 99.8%), silver nitrate (AgNO<sub>3</sub>, ≥99.0%), selenium (Se, pellets, <5 mm, ≥99.99% trace metals basis), cadmium oxide (CdO, 99.998%), 3 g of trioctylphosphine oxide (TOPO, 98%), 0.280 g of octadecylphosphonic acid (ODPA, 98%), trisodium citrate (SC, ≥98%), tannic acid (TA, ACS reagent), gallic acid (GA, ≥98.0%), hydrogen tetrachloroaurate(III) trihydrate (HAuCl<sub>4</sub>·3H<sub>2</sub>O, ≥99.9% trace metals basis), cerium(III) nitrate hexahydrate (Ce(NO<sub>3</sub>)<sub>3</sub>, 99% trace metals basis), iron (III) chloride (FeCl<sub>3</sub>, reagent grade, 97%), iron(II) chloride tetrahydrate (FeCl<sub>2</sub>·4H<sub>2</sub>O, puriss. p.a., ≥99.0%), tetramethylammonium hydroxide (TMAOH, 25 wt. % in H<sub>2</sub>O), 11-mercaptoundecanoic acid (MUA, 95%) and hexadecyltrimethylammonium bromide (CTAB, ≥98%) were purchased from Sigma-Aldrich. All chemicals were used as received without further purification. Distilled water passed through a Millipore system (ρ = 18.2 MΩ) was used in all experiments. All glassware was first rinsed with acetone and then with Millipore water before use.

### **1.1.1. Synthesis of semiconductor and metal nanocrystals**

**Synthesis of titanium oxide nanocrystals (TiO<sub>2</sub> NCs):** Titanium oxide nanocrystals were synthesized using the method proposed by Murray et al. [25] Shape-controlled synthesis of TiO<sub>2</sub>-NCs was achieved by non-aqueous surfactant-assisted synthesis using standard Schlenk line techniques under an inert atmosphere. Briefly, in a 125 mL flask, 30 mmol of cosurfactant (OIAm or 1-ODOL) 10.2 mL of 1-ODE, and

1.5 mmol of Oleic Acid (OIAc) are combined and degassed at 120 °C for 1 h. After degassing the flask, 1.5 mL of the titanium precursor is added at 60 °C under Argon atmosphere. Titanium precursor could be TiF<sub>4</sub>, TiCl<sub>4</sub> stock solutions (0.2M halogenated titanium compound and 1M OIAc using 1-ODE as solvent, each which have been prepared inside the glovebox prior to use) or a 1:1 mixture of both, depending on the desired final shape. Then, the solution is quickly heated to 290 °C, and the temperature is held for 10 min to allow the formation of seed crystals. An 8 mL portion of the stock solution is then pumped into the flask kept at 290 °C at 0.3 mL min<sup>-1</sup> using a syringe pump. In this synthesis, the choice of co-surfactant and precursor will be key for the final shape, size and thus properties of the resulting TiO<sub>2</sub> NCs [25]. **Table 1** summarizes the different reaction iterations of the process.

**Table 1.** Summary of detailed experimental conditions for achieving diverse TiO<sub>2</sub> shapes and sizes described in the reported method.

Shape	Size	Purge, 120°C, Argon, 1hour					60°C, Argon			290°C, Argon, 1 hour		
		Purge REAGENTS					NUCLEATION			GROWTH		
		Flask Volume	Solvent (1-ODE)	Surfactant (OIAc)	Cosurfactant		Stock Solution			Stock Solution		
OIAm	1-ODOL				TiCl <sub>4</sub> (0.2 M)	TiF <sub>4</sub> (0.2M)	(1:1) Mixture	TiCl <sub>4</sub> (0.2 M)	TiF <sub>4</sub> (0.2M)	(1:1) Mixture		
Bypyramids	~ 20 nm side	100 mL	10 mL	0.48 mL (1.5 mmol)	9.87 mL (30 mmol)		1.5 mL (14mgTi)			8 mL (77mgTi)		
Bypyramids	~ 10 nm side	100 mL	10 mL	0.48 mL (1.5 mmol)	9.87 mL (30 mmol)			1.5 mL (14mgTi)				8 mL (77mgTi)
Rods	~ 40 nm side, ~ 5 nm width	100 mL	10 mL	0.48 mL (1.5 mmol)	9.87 mL (30 mmol)	1.5 mL (14mgTi)				8 mL (77mgTi)		
Nanoplates	~ 200 nm side	100 mL	10 mL	0.48 mL (1.5 mmol)			1.5 mL (14mgTi)				8 mL (77mgTi)	
Nanoplates	~ 40 nm side, ~ 10 nm width	100 mL	10 mL	0.48 mL (1.5 mmol)				1.5 mL (14mgTi)				8 mL (77mgTi)

Afterward, the heating mantle is removed, and the flask is left to cool naturally to ambient temperature. After the synthesis, the reaction contents are first diluted with a small volume of toluene and centrifuged at 6000 rpm to purify the NCs. The NCs are then re-dispersed through the addition of toluene, 100 µL of OIAm, and sonication. Insoluble surfactant and agglomerated particles are removed through centrifugation. A mixture of 2-propanol and methanol is added to precipitate the NCs, and centrifugation

at 6000 rpm is used to recover the NCs. This washing process is repeated twice and adjusted to a final volume of 20 mL of toluene.

**Synthesis of silver selenide nanocrystals ( $\text{Ag}_2\text{Se}$  NCs):** Silver selenide nanocrystals of ~50 nm in diameter were synthesized by a modified approach to a previously reported method found in the literature. [26] Briefly, 10 mL of OIAm and 0.5 g of  $\text{AgNO}_3$  were mixed in a flask, heated up to 180 °C and vigorously magnetically stirred for 10 minutes. Afterwards, 0.12 g of molted Se were added to the mixture. Post-preparation steps were the same as previously described for  $\text{TiO}_2$  NCs, leading in this case to a dense, brown solution.

**Synthesis of cadmium selenide and cadmium selenide@cadmium sulfide core@shell nanocrystals ( $\text{CdSe}$  and  $\text{CdSe@CdS}$ ):** Cadmium selenide and cadmium selenide@cadmium sulfide quantum dots (QDs) of around 10 nm in diameter were synthesized following a previously proposed ‘flash’ seeded-growth method by Cirillo et al. [27] Briefly, in order to synthesize  $\text{CdSe}$  QDs, 0.06 g of  $\text{CdO}$ , 3 g of TOPO and 0.280 g of ODPA were mixed in a 25 mL three-neck Pyrex flask, the mixture was heated to 150 °C and left under vacuum for 1h. Afterwards, the solution was heated to 345 °C under inert atmosphere. By then, the solution was colorless, which indicated the proper dissolution of  $\text{CdO}$ , and 1.8 mL of TOP was injected. When the temperature recovered, a solution containing 0.058 g of selenium in 0.360 g of TOP and prepared under inert condition was injected. After, the reaction was quenched by a sudden drop of the temperature using a water bath and allowed to cool down to room temperature. For the synthesis of  $\text{CdSe@CdS}$ ,  $\text{CdO}$  solution was prepared as previously described. After the temperature had recovered, 1.8 mL of a solution containing 87 nmol of  $\text{CdSe}$  core QDs and sulfur in TOP was injected. After 3 min, the reaction was quenched by a sudden

drop of the temperature using a water bath, followed by the injection of 10 mL of toluene. The resulting QDs were washed as previously described for TiO<sub>2</sub> NCs.

**Synthesis of aqueous silver nanocrystals (Ag NCs):** Silver nanocrystals of different size growing from ~15 nm to 35 nm in diameter were prepared by a slightly modified approach to the seeded-growth method previously reported by Bastús et al. [28] In a typical experiment, silver seeds were obtained by filling a three-neck round bottomed flask with a 100 mL aqueous solution containing 5 mM trisodium citrate (SC) and 0.1 mM of tannic acid (TA) and heated up with a heating mantle up to 100°C. After boiling had commenced, 1 mL of 25 mM AgNO<sub>3</sub> was injected into this solution under vigorous stir. The as-obtained silver seeds were grown by cooling down the solution to 90°C and sequentially injecting 100 µL of 25 mM SC, 250 µL of 2.5 mM gallic acid (GA) and, 250 µL of 25 mM AgNO<sub>3</sub>. This process was repeated up to four times, at that point, Ag NCs were ~15nm in diameter. In the same vessel, the seed solution was diluted by extracting 20 mL of sample and adding 17 mL of Milli-Q water, then 500 µL of 25 mM SC, 1.5 mL of 2.5 mM GA and, 1 mL of 25 mM AgNO<sub>3</sub> were sequentially injected, again. This process was repeated up to 7 times, progressively growing the size of the AgNCs until reaching the desired size (~35 nm). The obtained AgNCs were not further purified.

**Synthesis of aqueous gold nanocrystals (Au NCs):** Gold nanocrystals of different size growing from ~15 nm to 35 nm in diameter were prepared by a slightly modified approach to the seeded-growth method previously reported by Bastús et al. [29] In a typical experiment, gold seeds were obtained by filling a three-neck round bottomed flask with a 150 mL aqueous solution containing 2.2 mM sodium citrate (SC) heated up with a heating mantle up to 100°C. After 10 minutes of boiling, 1 mL of 25 mM HAuCl<sub>4</sub> was injected into this solution under vigorous stir. The as-obtained gold

seeds were grown by cooling down the solution to 90 °C and sequentially injecting 1 mL of 25 mM HAuCl<sub>4</sub> twice within a 20 min separation each, at that point, Au NCs were ~15 nm in diameter. In the same vessel, the seed solution was diluted by extracting 55 mL of sample and adding 53 mL of Milli-Q water, then 2.5 mL of 60 mM SC were injected, again. This growing process was repeated up to 5 times, progressively growing the size of the Au NCs until reaching the desired size (~35 nm). The obtained Au NCs were not further purified.

**Synthesis of aqueous core@shell Au@CeO<sub>2</sub> nanocrystals:** Colloidal solutions of highly monodisperse Au@CeO<sub>2</sub> NCs were obtained by a method previously reported. [30] Briefly, in a 250 mL three-neck round bottomed flask, 1 mL of 25 HAuCl<sub>4</sub> and 5 mL of 25 mM Ce(NO<sub>3</sub>)<sub>3</sub> solutions were added sequentially to a 100 mL refluxing aqueous solution of 10 mM SC and left to react for four hours. The obtained Au@CeO<sub>2</sub> NCs were not further purified.

**Synthesis of aqueous Fe<sub>3</sub>O<sub>4</sub> NCs:** Synthesis of Fe<sub>3</sub>O<sub>4</sub> magnetic NCs was achieved by following a method previously reported by our group. [31] In a 250 mL round bottom flask, 1.824 g of FeCl<sub>3</sub> anhydrous and 0.996 g of FeCl<sub>2</sub>·4H<sub>2</sub>O are sequentially added to 50 mL of milli-Q water deoxygenated under N<sub>2</sub> bubbling for 30 minutes and stirred until complete dissolution. Afterwards, 50 mL of 1M TMAOH previously deoxygenated under N<sub>2</sub> bubbling for 30 minutes are poured continuously onto the solution containing the Fe(II) and Fe(III) precursors stirred at 600 rpm under N<sub>2</sub> atmosphere. The mixture is left stirring for 30 min. Once the reaction is completed the sample is washed twice by magnetically aided sedimentation and finally resuspended in 10 mM TMAOH. Sample is stored under nitrogen atmosphere to avoid its degradation.

**Synthesis of aqueous CeO<sub>2</sub> NCs:** Synthesis of CeO<sub>2</sub> NCs was achieved by following a method previously reported by our group. [32] In a typical procedure, a 50 mL solution of TMAOH 50 mM was added to a 50 mL of a solution containing 20 mM of Ce(NO<sub>3</sub>)<sub>3</sub> and 40 mM of sodium citrate in a 250 mL glass bottle. The reaction mixture was left under stirring at room temperature overnight. Later, the reaction mixture was added to a three necked round bottom flask and left under refluxing at 100 °C for 4h. During this time, the colour of the solution changed from yellow to pale yellow. The resultant CeO<sub>2</sub> NCs were not further purified.

### **1.1.2. Post-synthesis procedure: preparation of the hybrid**

In this section the preparation of hybrids involving the described synthesized NCs and CNS such as Single-Walled Carbon Nanotubes and Graphene is explained. Since these syntheses provided of final products which were stored in either organic solvents or aqueous media, two different approaches had to be developed:

**The case of CNS-NCs coupling in organic solvents:** the approach is based on the incubation of NCs with CNSs which have been destabilized by change of the solvent polarization, resulting in a controlled deposition of the previously synthesized semiconductor NCs. Briefly, all of as-synthesized nanocrystals have been purified by centrifugation up to four times and resuspended in toluene in order to partially destabilize them. Afterwards, 1 mL of the purified nanocrystals ( $\sim 3,66 \cdot 10^{15}$  NCs/mL) have been diluted in 2 mL of toluene and 0.25 mL of CNS solution (0.005 mg/mL) and left under stirring for incubation for 12 h. This method has proved to be highly reproducible for small nanocrystals (10-20 nm) synthesized in organic conditions, up to seven different species have been tested, and scalable up to a total volume of 50 mL solution.

**The case of CNS-NCs coupling in aqueous conditions:** For the attachment of NCs to the graphene structure,  $2 \times 10^{13}$  NCs were mixed with 625  $\mu\text{L}$  of 0.005 mg/mL suspension of Graphene in  $\text{H}_2\text{O}$  ( $6.4 \times 10^{13}$  NCs/mg graphene) were dialyzed versus  $\text{H}_2\text{O}$  in 100 kDa, 5 mL dialysis bags for 3 days, constantly stirred and renewing the dialysis water once per day. After the procedure was completed, the dialyzed samples were precipitated under 2000 g centrifugation for 10 minutes and the supernatant containing non-attached crystals was removed and replaced with 5 mL Milli-Q Water, this process was performed twice. The NCs/Graphene hybrids were treated under sonication for 1 h being non-affected by it. Same treatment in the presence of CTAB and MUA leads to the same results, no obvious detachment of the crystals can be noticed.

Study of the deposition mechanism and the hybrid formation control was performed by synthesis of the hybrid at different and defined Graphene to Nanocrystal ratios. Three syntheses of each composition were performed. In a first one, the amount of incubated NCs was of  $3.2 \times 10^{15}$  NCs/mg graphene. The other two were of one order of magnitude above and below of the first one. Concentrations of NCs were calculated by taking in account the size, composition and concentration of precursors in the original synthesis, as well as its yield.

### **1.1.3. Dynamic characterization experiments**

These experiments were conducted in order to assess the stability and robustness of the synthesized hybrid, the possible detachment of the NCs from the graphene and the inherent limits of the technique. In these experiments samples were exposed to ultrasonication both with and without presence of an excess of molecules with known affinity respect either the Ag, Au and  $\text{Au@CeO}_2$  NCs or the graphene substrate for extended times.

*Experimental control:* The absorbance in the UV-Vis spectra of these supernatants were compared with control  $4 \times 10^{12}$  NCs/ mL solutions of the used Au, Ag and Au@CeO<sub>2</sub> NCs species. These amounts are equivalent to the ones used at the start of the procedure (**Figure 4**, black line).

*Analysis of the supernatant:* For a first quantification of the yield of the decoration process, the supernatant resulting from the precipitation (centrifuging the samples at 800 G for 5 minutes) of the hybrid was analyzed by UV-Vis spectroscopy. The pellets were resuspended in 5 mL of Milli-Q Water (**Figure 4**, dashed line).

*Endurance test (ultrasonication in presence of affine molecules):* 4 aliquots of 1 mL each were taken from the different samples, precipitated and resuspended in 1 mL of 1 mM or 10 mM MUA and 1 mL of 1 mM or 10 mM CTAB solutions, respectively. Aliquots were ultrasonicated for 30 min. The supernatant resulting from the precipitation (samples centrifuged at 800 G for 5 minutes) of the hybrid was analyzed by UV-Vis spectroscopy. The pellets were resuspended in 1 mL of Milli-Q Water.

## **1.2. CHARACTERIZATION TECHNIQUES**

The characterisation techniques and equipment used in this Chapter are UV–Vis Spectroscopy, Transmission Electron Microscopy (TEM) and X-ray Photoelectron Spectroscopy (XPS) and Image analysis and the ultrasonication bath. Details on the equipment, settings and use are explained in **APPENDIX I**.

## **1.3. RESULTS AND DISCUSSION**

### **1.3.1. Method validation and characterization**

Metal, metal oxide and semiconductor NCs-CNS hybrids were prepared by surfactant depletion of previously synthesized NCs to the substrate. In this way we have been able to synthesize composites with different composition, size, shape and particle



density on the surface of different CNSs. The synthesis of the NCs has been performed following previously reported methods which can be divided in non-aqueous [25]–[27], [33] and aqueous [28]–[30] surfactant-assisted approaches. These products have been attached to the CNSs by progressive and slow depletion of the surfactant, accomplished either by several centrifugation processes in the first case and dialysis in the later. These investigations can be understood as a ligand exchange process in which the removal of the stabilizers (surfactant depletion) results in the NCs attaching to the CNS in a similar fashion to the ones described before in the scientific literature for other NCs-CNS such as Pt-CNTs. [34] Hybrids are stable and can overcome long periods of ultra-sonication (US) with little to zero morphological changes.

For decoration of CNS by semiconductors synthesized in non-aqueous media we use an approach based on the incubation of NCs with Single-Walled Carbon Nanotubes (SWCNTs). Semiconductor NCs have been partially destabilized repeating a purification process based in the change of the solvent polarization combined with centrifugation. This operation results in a controlled deposition of the previously synthesized semiconductor NCs on the SWCNTs surface. In this survey, several semiconductors such as TiO<sub>2</sub> (brookite and anatase), Ag<sub>2</sub>Se, CdSe and CdSe@CdS were synthesized and coupled to SWCNTs with positive results (**Figure** ). The NCs densely covered the SWCNTs in a homogeneous manner, especially for smaller particles.

The synthesis of NCs was carried out following reported methods, [25]–[27] which are based on the decomposition of an organometallic precursor in a hot, liquid mixture of surfactants. Molecular precursor species were introduced into the growing medium via fast injection. During the synthesis, the surfactants played a key role in

tuning the reactivity of the monomers and regulating the temporal evolution of the NC size over time. The combination of specific surfactants and high temperatures facilitated the formation of NCs with narrow size distributions and few internal defects, hence having well defined physical properties. This process could also be extended to the use of graphene as a CNS, which has been proved for the case of Pt NCs (not shown in **Figure 2**).

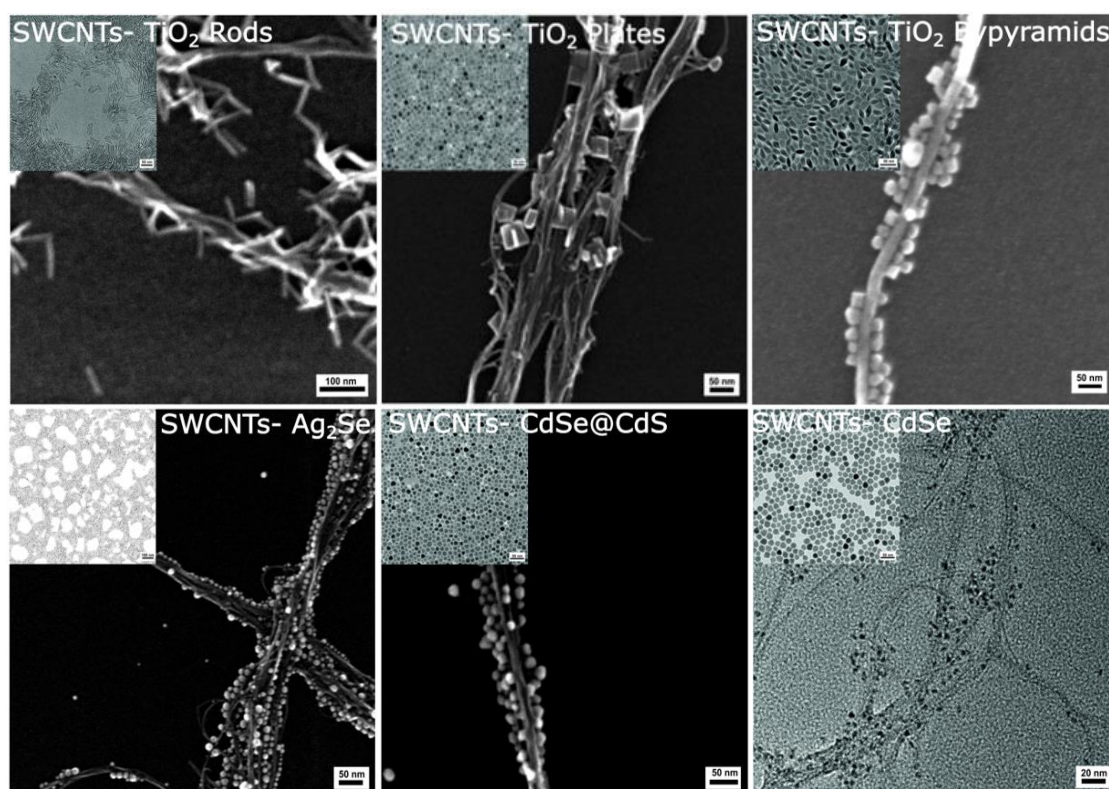


**Figure 2.** SEM microscopy of the synthesized semiconductor-SWCNTs hybrid in non-aqueous media. Inset shows STEM Bright Field microscopy of the semiconductor NCs as synthesised.

Deposition of noble metal NCs onto graphene flakes was studied by adhesion of Au, Ag and Au@CeO<sub>2</sub> NCs onto its surface. The decoration of metal NCs to graphene nanoflakes was achieved by mixing a determined amount of  $6.4 \times 10^{13}$  NCs/mg graphene were dialyzed against H<sub>2</sub>O in 100 kDa 5 mL dialysis bags for 3 days, constantly stirred and renewing the dialysis water once per day. The resulting suspension was centrifuged at low speed twice and the supernatant kept for future characterization. The acquired

pellet was studied with electronic microscopy (**Figure 33**). Timid decoration of the graphene can be observed in the case of Ag NCs (~15 nm), where small amounts of NCs can be observed onto the substrate mostly in form of aggregates. For the samples containing Au (~15 nm) and Au@CeO<sub>2</sub> NCs the deposition is densely and homogeneously observed (see section 1.3.2.). This difference might be either to remnant traces of TA used for the synthesis of the Ag NCs seeds, remarkably, if the deposition of the Ag NCs is performed by using TA instead of GA during the growth process, very low decoration is observed under the microscope suggesting the big size of the TA and its hard anchoring to the surface of Ag NCs may hinder the surfactant depletion. [28]

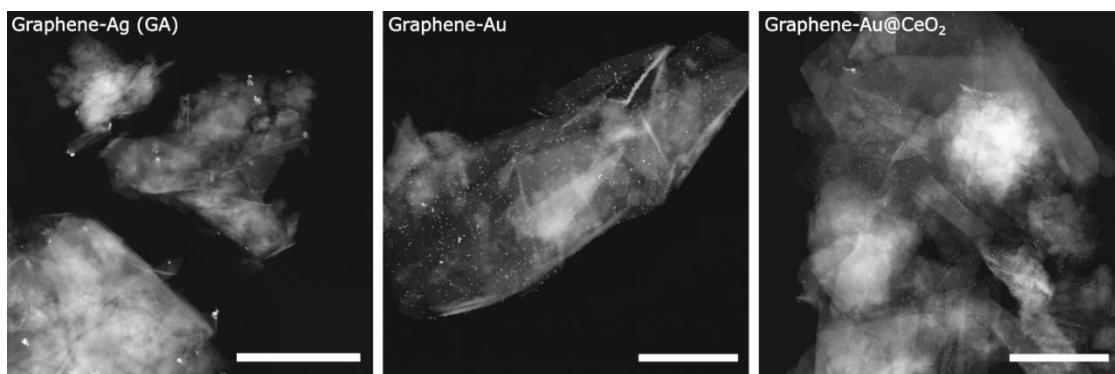


**Figure 3.** STEM (HAADF) microscopy of the synthesized hybrid. From left to right: Graphene-Ag, Graphene-Au, Graphene Au@CeO<sub>2</sub>. Scale bar corresponds to 1 $\mu$ m.

### **1.3.2. Assessment of the reproducibility, robustness and scalability of the decoration method**

In order to evaluate the yield of the decoration process samples were purified twice by mild centrifugation and the supernatant analysed by UV-Vis spectroscopy. Ag NCs remained in the supernatant with some aggregation (**Figure 4**). Yield of the incubation of GA synthesized Ag NCs was around 58%, showing 2 nm red-shift of both samples versus the control demonstrating that surfactant is depleted from the NCs surface during the incubation process. For the Au NCs and Au@CeO<sub>2</sub> was considered of 100% since no signal was observed in the supernatant. For better understanding of

the robustness of the system, samples were exposed to ultrasound (US) treatment for 1h in presence of affine molecules in order to evaluate the reversibility of the method. In this case, hybrids were exposed to 1 mM and 10 mM solutions of Cetrimonium Bromide (CTAB) and Mercaptoundecanoic Acid (MUA) under US. The supernatant was evaluated by UV-Vis spectroscopy and contrasted versus a control solution containing  $4 \cdot 10^{12}$  NCs/mL in order to semi quantify the loss of sample related to this test (**Figure 4**).

No significant losses were observed after the US treatment for the Ag NCs-Graphene hybrid but results were not as conclusive for the Au NCs-Graphene and Au@CeO<sub>2</sub> NCs-Graphene cases due to noise signal from the remnant graphene flakes in solution. In those cases, the sample was spiked and normalized to have clear data. By these results it can be affirmed that the loss of material should be <10% of the original NCs. Microscopy of the product was performed after the sonication process (**Figure 4**) were a detachment of the sample cannot be appreciated, although loss of clarity is observed in samples containing CTAB due to the crystallization of the compound.

Deposition of non-noble metal oxide NCs was studied by adhesion of CeO<sub>2</sub> and Fe<sub>3</sub>O<sub>4</sub> NCs. In the case of CeO<sub>2</sub> NCs, STEM microscopy (**Figure 5**) could only give a qualitative observation of the sample, either due to the small size of the NCs, synthesis concentration or intrinsic characteristics as an oxide. Interestingly, the sample containing Fe<sub>3</sub>O<sub>4</sub> showed a conservation of the magnetic properties of the NCs onto the graphene which will be analyzed and studied in **CHAPTER 3**.

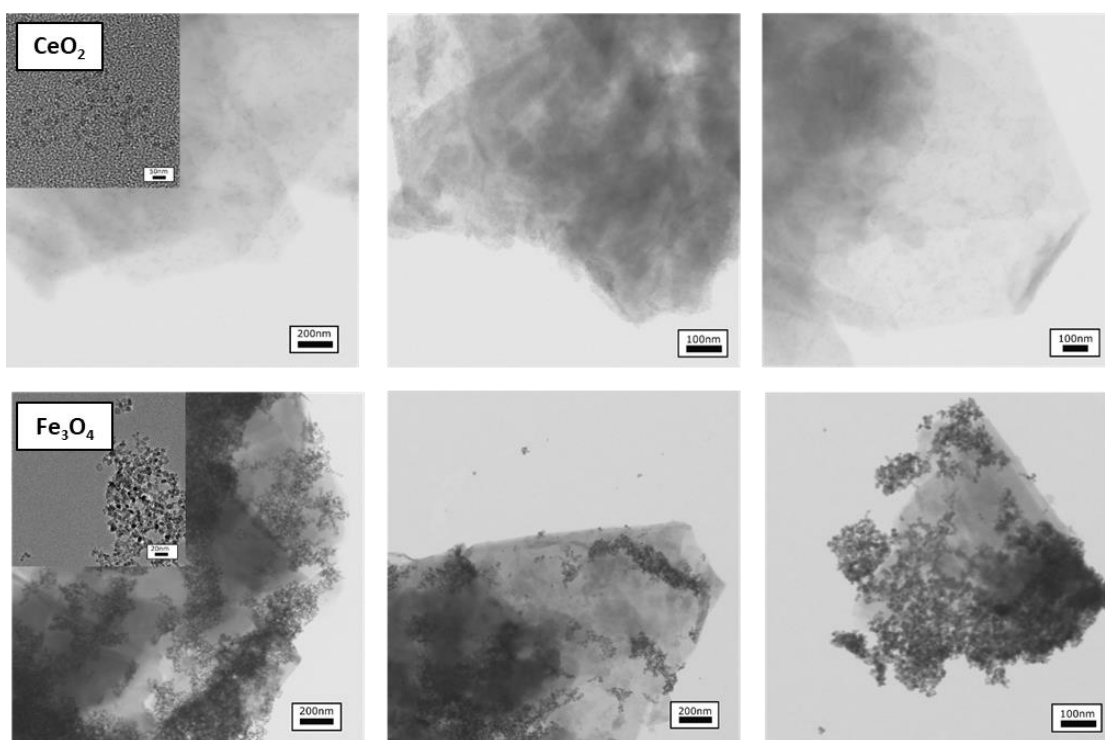


**Figure 5.** STEM BF microscopy images of the metal oxides NCs – Graphene hybrid. Scale bar 100 nm.

Distribution of NCs over the sample was evaluated by analyzing the distance in between the nanocrystals deposited on the graphene CNSs TEM images up to the 12<sup>th</sup> neighbor (**Figure 6**). These distances are found by the assessment of the eccentricity and grayscale on the images. Image analysis does not suggest any clear order or assembly in the NCs distribution.

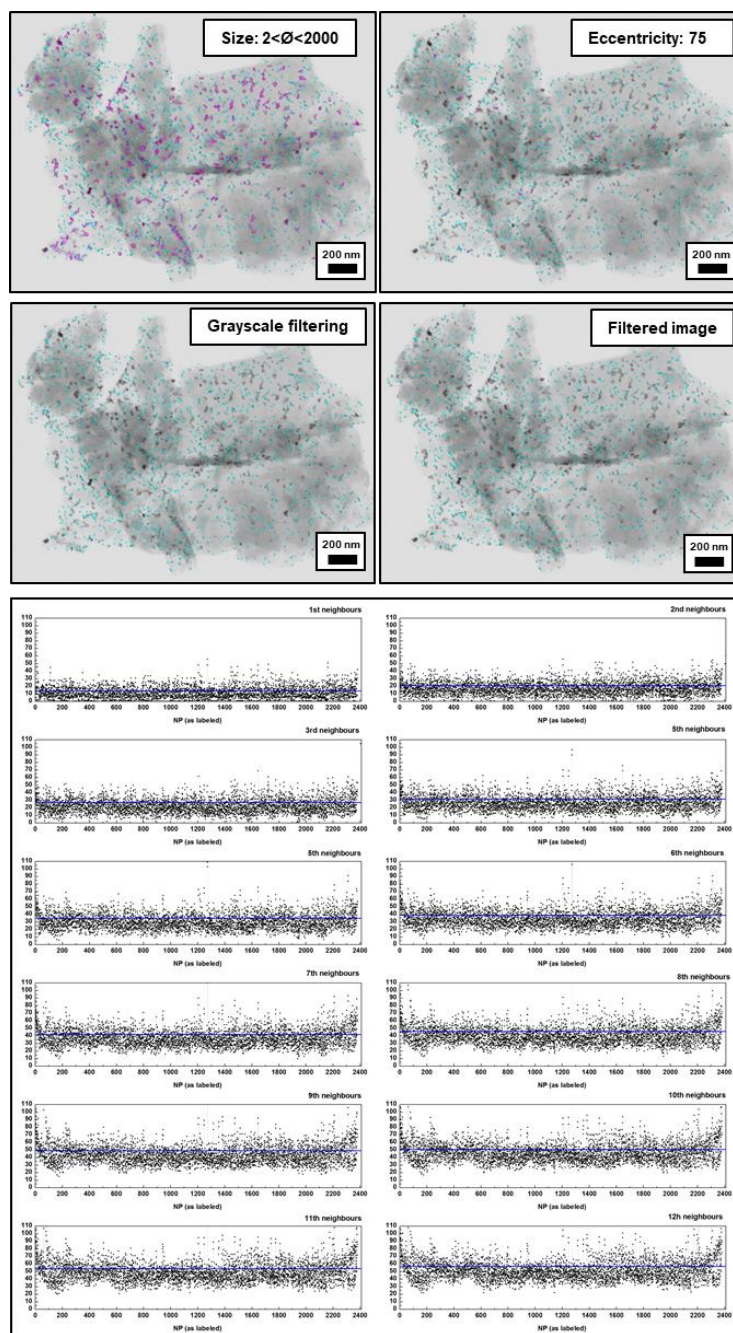


**Figure 6.** Left: Image treatment for analysis. Right: Graphs resolving the distance between neighbour up to the 12<sup>th</sup>.

Once the decoration approach had been proved to serve for different metal and oxide NPs coming from organic and aqueous media, better understanding and control of the product was desired. In a first experiment, several ratios of Au, Au@CeO<sub>2</sub> or CeO<sub>2</sub> NCs–Graphene were incubated in order to better understand the behavior of the system. For doing so, the NCs concentration was explored one order of magnitude above or below from the original synthesis. STEM microscopy (**Figure7**) showed an obvious visual correlation of the amount of NCs onto the graphene surface and the

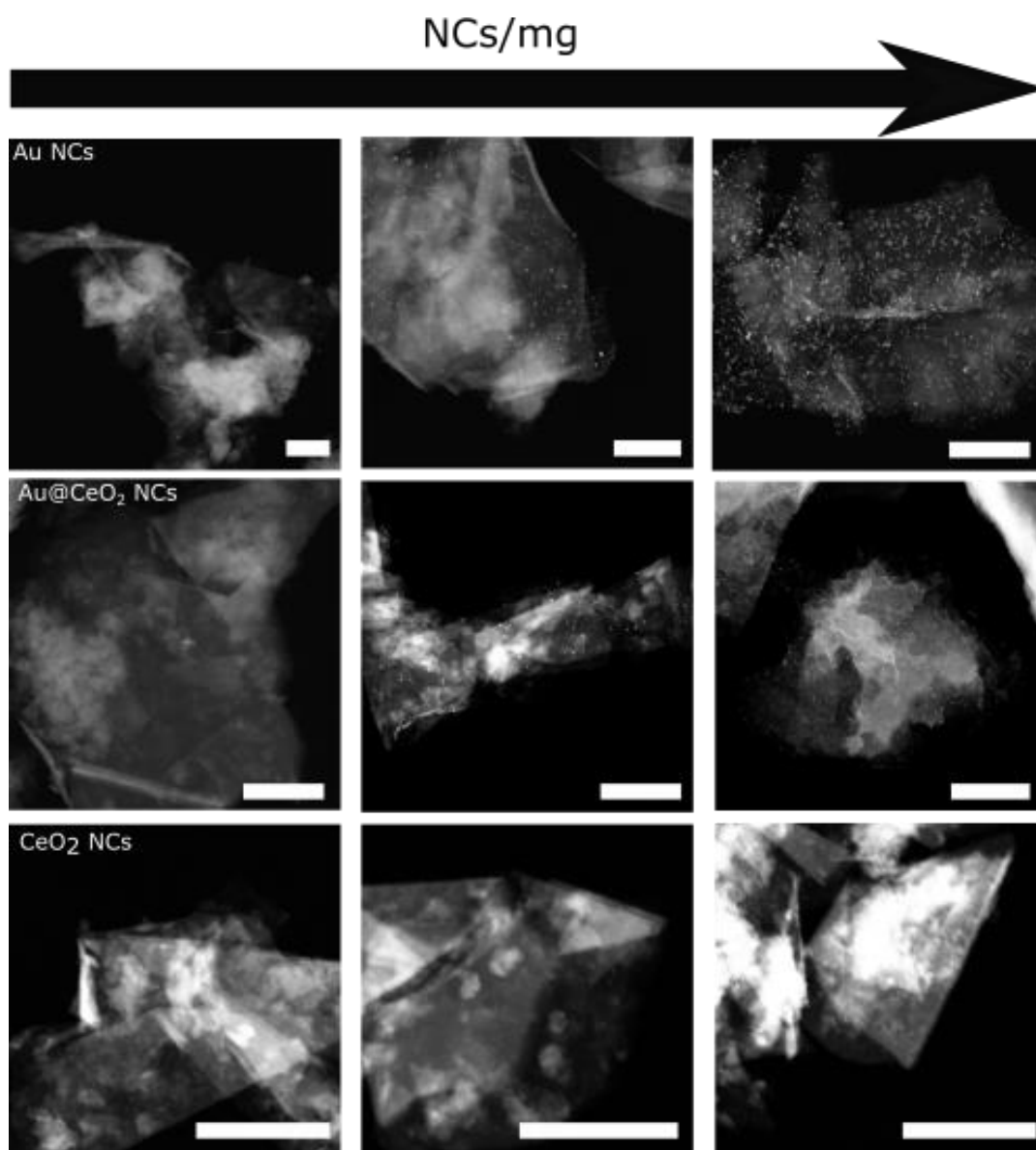


**Figure 7.** STEM-HAADF microscopy evaluating different particle concentration deposition onto graphene flakes for the Au, Au@CeO<sub>2</sub> and CeO<sub>2</sub> NCs. Scale bar: 500 nm.

incubated one as well an apparent homogeneous distribution of them. This allows for the system to be tunable in future applications, since proves the surface coverage as tunable too.

### **1.3.3. Advanced characterization of the hybrids**

Deeper characterization of the Au NCs-Graphene interactions was performed by High Resolution TEM (analyzed and reported by GaEN group at ICN2) and XPS. In **Figure 8** the HRTEM images of the Au NCs deposited on graphene are shown. Here it is possible to distinguish the support from the particle itself as it presents a layered structure evidenced in the frequency filtered structural map reported in the top right of the image. On the bottom left of **Figure 8** a blow-up of the Au nanoparticle is reported, evidencing that it has a cubic structure and the particle in the figure is oriented along the [1 1 0] zone axis.

On the bottom right a 3D model reconstruction of the particle together with the TEM image simulation are reported proving there is no evidence of remaining surfactant in the interface. Furthermore, (-111) Au direction is almost 4° rotated with respect to the (0002) graphene plane. All of this information drives to the conclusion of intimate contact between the graphene surface and the Au NCs. Similar results have been observed for the case of Au@CeO<sub>2</sub> NCs.



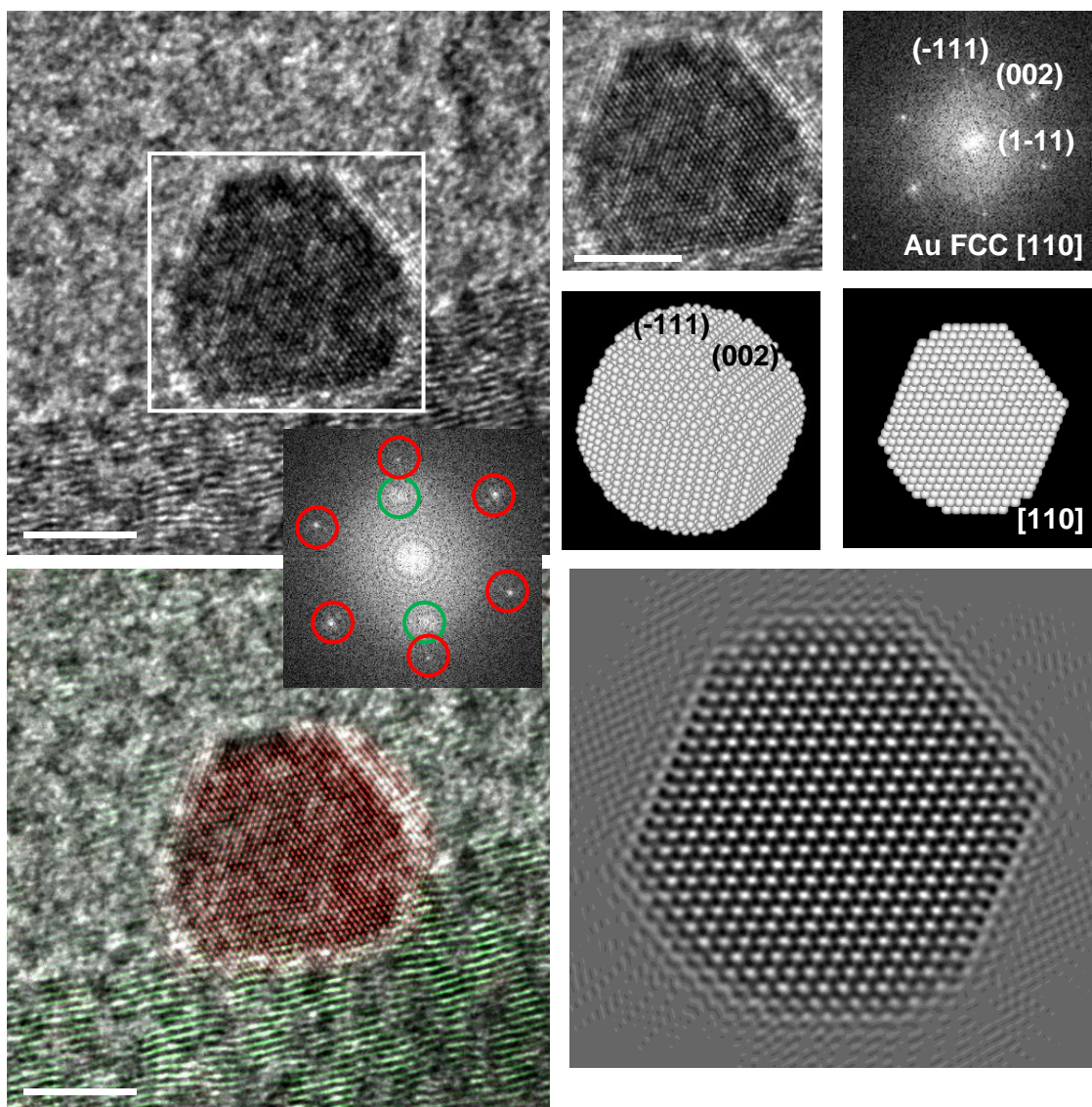


**Figure 8.** HRTEM image of the sample. On the top right, the coloured frequency filtered structural map where the different marked orientations are reported in different colour (red for the Au nanocrystals and green for the graphene multilayer), scale bar 5nm. On the bottom left: blow-up of the crystals in the white box and the corresponding indexed power spectrum. On the bottom right: a 3D atomic model reconstruction of the particle together with the TEM image simulation are reported.

For the XPS experiments, Au-Graphene hybrid was compared to a graphene control and a naked Au NCs sample (centrifuged and resuspended twice in distilled water). As shown in **Figure 9**, there were no changes of position in any of the cases. On one hand, the C1s spectrum from the graphene control and the Au-graphene sample

show a peak at 284 eV satellite features can be observed several eV in higher energies from the main peak. These two features correspond to samples with high concentration of  $sp^2$  carbon.[35]–[37] On the other hand, the Au control and Au-Graphene show both a pair of peaks at BE 87.5 eV and 84 eV, corresponding to the positions of the first and most important pair of peaks which characterize the Au  $4f_{7/2}$  and Au  $4f_{5/2}$  spin-orbit coupling (BEs of 84 and 87.3 eV) and are related to elemental gold ( $Au^0$ ). [38] As stated before, though, there are no significant differences between both spectrums, therefore it can be assumed, the graphene substrate has not undergone through any chemical changes and either have Au NCs.

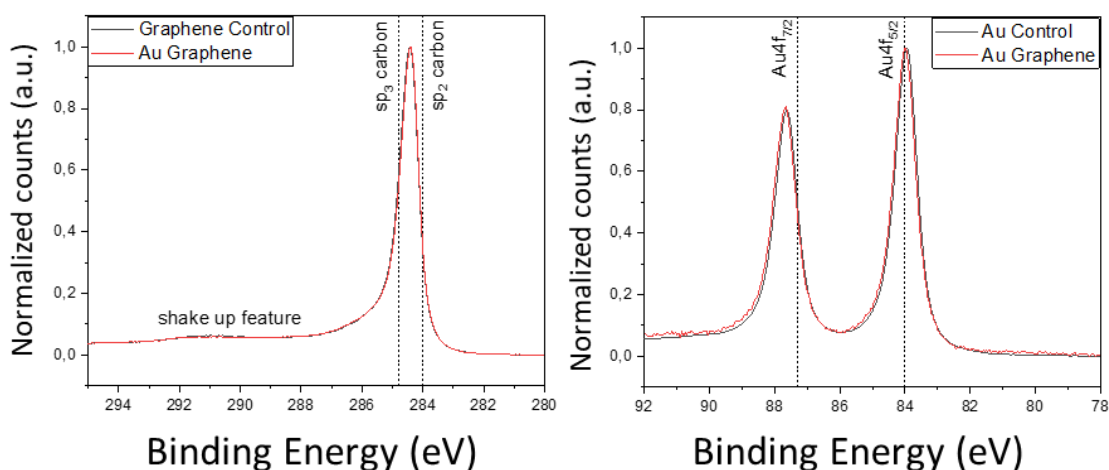


**Figure 9.** XPS spectra of the Au-Graphene sample, plotting the Carbon region of interest at the left and the Gold one at the right.

For better understanding of the deposition preferences of the system, mixes of different composition NCs were prepared. Briefly, a total amount of  $2 \cdot 10^{13}$  NCs distributed equally between Au, Au@CeO<sub>2</sub>, Ag, CeO<sub>2</sub> and Fe<sub>3</sub>O<sub>4</sub> NCs was deposited onto the typical amount of graphene of other synthesis, resulting in a total of  $3.2 \cdot 10^{15}$  NCs/mg Graphene. The resultant material was observed via STEM - Electron Energy Loss Spectroscopy (EELS) (**Figure 10**). In this case attention was focused detecting all the elements, so two images were acquired with different camera length, relative atomic

composition calculation was, therefore, not possible but imaging of other less populated zones verified the composition of the NCs was the one expected, where Ag NCs had. There was no obvious sign of assembly between the crystals, nor by size or composition.

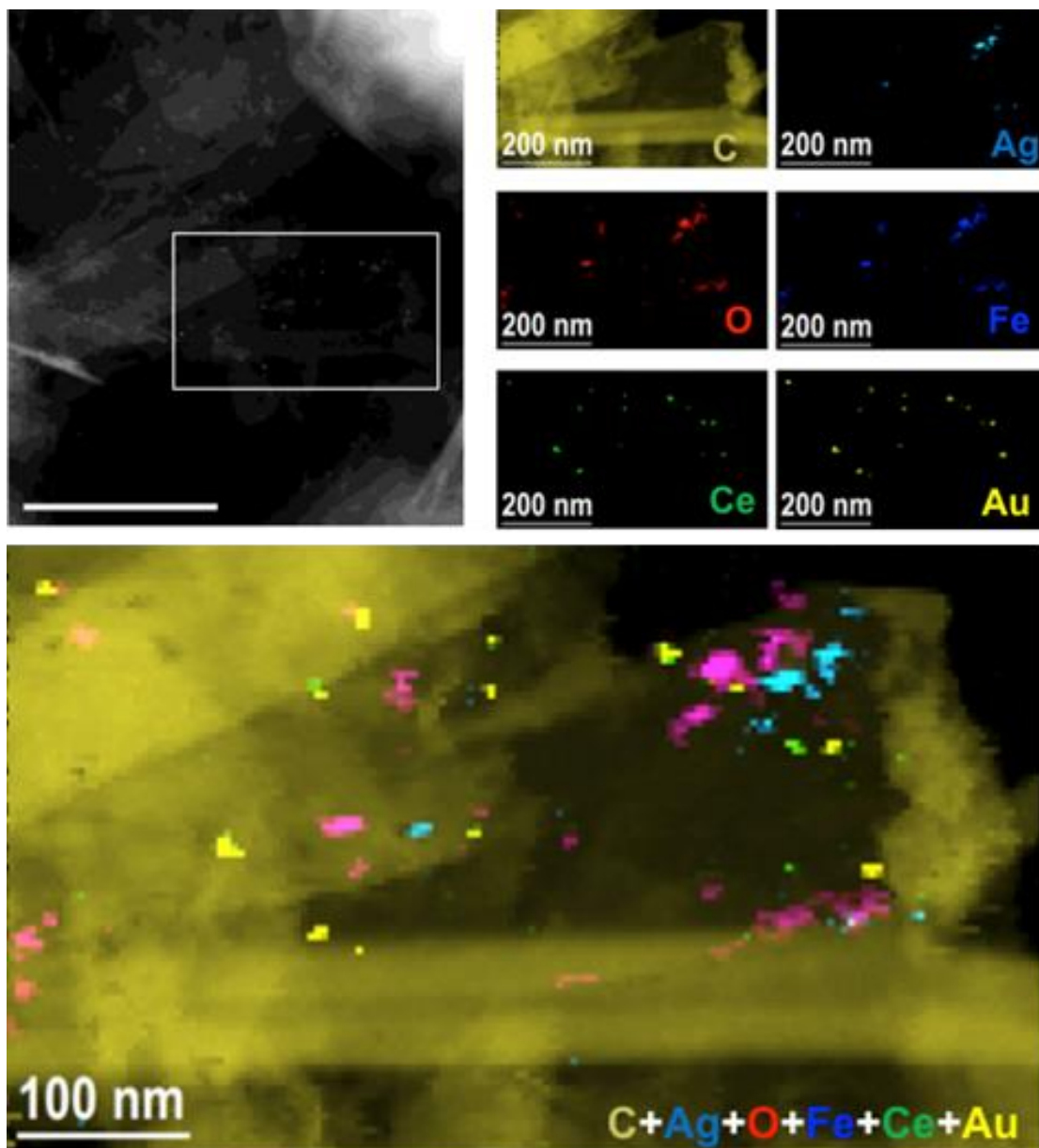


**Figure 10.** HAADF STEM and STEM-EELS elemental maps obtained on the selected areas (white box). Images obtained by using: Au M-edge at 2206 eV (bright yellow), Fe L-edge at 708 eV (blue), Ce M-edge at 883 eV (green), O K-edge at 532 eV (red), C K-edge at 284 eV (dark yellow) and Ag M-edge at 367 eV (light blue) as well as composites of C-Ag-Au-Ce-Fe-O.

## **1.4. CONCLUSIONS**

In this first chapter, a general approach for the decoration of CNSs has been explored. This method is based on the nature of both surfaces involved in the process. Carbon nanostructures exhibit a hydrophobic behavior whilst NCs are traditionally stabilized using surfactants that avoid their aggregation or dissolution. We have studied how a slow depletion of the surfactant will allow for the NC to meet with the CNS before NC-NC aggregation. This will happen because of the difference of size affects the mobility: since NCs have a much higher mobility, the density of surfactant needed at their surface for avoiding NC-NC interaction is smaller than the needed to avoid NC-CNS interaction. It has been possible to generalize this strategy, allowing for a powerful tool that is thought for the community to use in order to achieve a carbon-nanoparticle structure with better control of the properties. This control extends from the inherent quality of the compounds –since both CNSs and nanoparticles can be prepared in scientific facilities for better understanding, tuning, and characterization of their individual properties– to all of the possible compounds resulting from the iterations related to those. This is conceived to allow enhanced studies of the properties and possibilities these hybrids promise with predictable components and synergies.

## **1.5. REFERENCES**

- [1] A. K. Geim and K. S. Novoselov, “The rise of graphene,” *Nanosci. Technol. A Collect. Rev. from Nat. Journals*, pp. 11–19, Jan. 2009.
- [2] Y. Zhu *et al.*, “Graphene and graphene oxide: Synthesis, properties, and applications,” *Adv. Mater.*, vol. 22, no. 35, pp. 3906–3924, Sep. 2010.
- [3] X. Li, Y. Liu, L. Fu, L. Cao, D. Wei, and Y. Wang, “Efficient synthesis of carbon nanotube-nanoparticle hybrids,” *Adv. Funct. Mater.*, vol. 16, pp. 2431–2437, 2006.
- [4] P. V. Kamat, “Graphene-based nanoarchitectures. Anchoring semiconductor and metal nanoparticles on a two-dimensional carbon support,” *J. Phys. Chem. Lett.*, vol. 1, no. 2,

- pp. 520–527, Jan. 2010.
- [5] K. S. Subrahmanyam, A. K. Manna, S. K. Pati, and C. N. R. Rao, “A study of graphene decorated with metal nanoparticles,” *Chem. Phys. Lett.*, vol. 497, no. 1–3, pp. 70–75, Sep. 2010.
- [6] I. V. Lightcap, T. H. Kosel, and P. V. Kamat, “Anchoring semiconductor and metal nanoparticles on a two-dimensional catalyst mat. storing and shuttling electrons with reduced graphene oxide,” *Nano Lett.*, vol. 10, no. 2, pp. 577–583, Feb. 2010.
- [7] H. Vedala, D. C. Sorescu, G. P. Kotchey, and A. Star, “Chemical sensitivity of graphene edges decorated with metal nanoparticles,” *Nano Lett.*, vol. 11, no. 6, pp. 2342–2347, Jun. 2011.
- [8] A. C. Joshi, G. B. Markad, and S. K. Haram, “Rudimentary simple method for the decoration of graphene oxide with silver nanoparticles: Their application for the amperometric detection of glucose in the human blood samples,” *Electrochim. Acta*, vol. 161, pp. 108–114, Apr. 2015.
- [9] W. Shao, X. Liu, H. Min, G. Dong, Q. Feng, and S. Zuo, “Preparation, characterization, and antibacterial activity of silver nanoparticle-decorated graphene oxide nanocomposite,” *ACS Appl. Mater. Interfaces*, vol. 7, no. 12, pp. 6966–6973, Apr. 2015.
- [10] A. Cao *et al.*, “A facile one-step method to produce craphene-CdS quantum dot nanocomposites as promising optoelectronic materials,” *Adv. Mater.*, vol. 22, no. 1, pp. 103–106, Jan. 2010.
- [11] A. O. Adeola and P. B. C. Forbes, “Advances in water treatment technologies for removal of polycyclic aromatic hydrocarbons: Existing concepts, emerging trends, and future prospects,” *Water Environment Research*. John Wiley and Sons Inc., 2020.
- [12] L. A. Al-Khateeb, S. Almotiry, and M. A. Salam, “Adsorption of pharmaceutical pollutants onto graphene nanoplatelets,” *Chem. Eng. J.*, vol. 248, pp. 191–199, Jul. 2014.
- [13] S. Mura *et al.*, “Graphene Oxide/Iron Oxide Nanocomposites for Water Remediation,” *ACS Appl. Nano Mater.*, vol. 1, no. 12, pp. 6724–6732, Dec. 2018.
- [14] C. N. R. Rao and R. Voggu, “Charge-transfer with graphene and nanotubes,” *Mater. Today*, vol. 13, no. 9, pp. 34–40, Sep. 2010.
- [15] X. Peng, J. Chen, J. A. Misewich, and S. S. Wong, “Carbon nanotube-nanocrystal heterostructures,” *Chemical Society Reviews*, vol. 38, no. 4, pp. 1076–1098, 2009.

- [16] B. H. Juárez, C. Klinke, A. Kornowski, and H. Weller, "Quantum dot attachment and morphology control by carbon nanotubes," *Nano Lett.*, vol. 7, no. 12, pp. 3564–3568, Dec. 2007.
- [17] A. B. Hungria, B. H. Juárez, C. Klinke, H. Weller, and P. A. Midgley, "3-D characterization of CdSe nanoparticles attached to carbon nanotubes," *Nano Res.*, vol. 1, no. 1, pp. 89–97, Jul. 2008.
- [18] H. C. Choi, M. Shim, S. Bangsaruntip, and H. Dai, "Spontaneous reduction of metal ions on the sidewalls of carbon nanotubes," *J. Am. Chem. Soc.*, vol. 124, pp. 9058–9059, 2002.
- [19] X. Huang *et al.*, "Graphene-Based Materials: Synthesis, Characterization, Properties, and Applications," *Small*, vol. 7, no. 14, pp. 1876–1902, Jul. 2011.
- [20] X. Z. Tang *et al.*, "Synthesis of graphene decorated with silver nanoparticles by simultaneous reduction of graphene oxide and silver ions with glucose," *Carbon N. Y.*, vol. 59, pp. 93–99, Aug. 2013.
- [21] Z. Zhang *et al.*, "Sodium citrate: A universal reducing agent for reduction / decoration of graphene oxide with Au nanoparticles," *Nano Res.*, vol. 4, no. 6, pp. 599–611, 2011.
- [22] Y. Li, J. Chu, J. Qi, and X. Li, "An easy and novel approach for the decoration of graphene oxide by Fe<sub>3</sub>O<sub>4</sub> nanoparticles," *Appl. Surf. Sci.*, vol. 257, no. 14, pp. 6059–6062, May 2011.
- [23] K. Krishnamoorthy, M. Veerapandian, K. Yun, and S. J. Kim, "The chemical and structural analysis of graphene oxide with different degrees of oxidation," *Carbon N. Y.*, vol. 53, pp. 38–49, Mar. 2013.
- [24] M. Veerapandian, M. H. Lee, K. Krishnamoorthy, and K. Yun, "Synthesis, characterization and electrochemical properties of functionalized graphene oxide," *Carbon N. Y.*, vol. 50, no. 11, pp. 4228–4238, Sep. 2012.
- [25] T. R. Gordon *et al.*, "Nonaqueous synthesis of TiO<sub>2</sub> nanocrystals using TiF<sub>4</sub> to engineer morphology, oxygen vacancy concentration, and photocatalytic activity," *J. Am. Chem. Soc.*, vol. 134, pp. 6751–6761, 2012.
- [26] D. Wang, T. Xie, Q. Peng, and Y. Li, "Ag, Ag<sub>2</sub>S, and Ag<sub>2</sub>Se nanocrystals: Synthesis, assembly, and construction of mesoporous structures," *J. Am. Chem. Soc.*, vol. 130, pp. 4016–4022, 2008.

- [27] M. Cirillo *et al.*, “Flash synthesis of CdSe/CdS core-shell quantum Dots,” *Chem. Mater.*, vol. 26, pp. 1154–1160, 2014.
- [28] N. G. Bastús, F. Merkoçi, J. Piella, and V. Puntès, “Synthesis of highly monodisperse citrate-stabilized silver nanoparticles of up to 200 nm: Kinetic control and catalytic properties,” *Chem. Mater.*, vol. 26, no. 9, pp. 2836–2846, May 2014.
- [29] N. G. Bastús, J. Comenge, and V. Puntès, “Kinetically controlled seeded growth synthesis of citrate-stabilized gold nanoparticles of up to 200 nm: Size focusing versus ostwald ripening,” *Langmuir*, vol. 27, no. 17, pp. 11098–11105, Sep. 2011.
- [30] N. G. Bastús *et al.*, “Robust one-pot synthesis of citrate-stabilized Au@CeO<sub>2</sub> hybrid nanocrystals with different thickness and dimensionality,” *Appl. Mater. Today*, vol. 15, pp. 445–452, Jun. 2019.
- [31] E. Casals *et al.*, “Programmed Iron Oxide Nanoparticles Disintegration in Anaerobic Digesters Boosts Biogas Production,” *Small*, vol. 10, no. 14, pp. 2801–2808, Jul. 2014.
- [32] R. Barrena, E. Casals, J. Colón, X. Font, A. Sánchez, and V. Puntès, “Evaluation of the ecotoxicity of model nanoparticles,” *Chemosphere*, vol. 75, no. 7, pp. 850–857, May 2009.
- [33] S. I. Lim, I. Ojea-Jiménez, M. Varon, E. Casals, J. Arbiol, and V. Puntès, “Synthesis of platinum cubes, polypods, cuboctahedrons, and raspberries assisted by cobalt nanocrystals,” *Nano Lett.*, vol. 10, no. 3, pp. 964–973, Mar. 2010.
- [34] B. Ritz *et al.*, “Reversible attachment of platinum alloy nanoparticles to nonfunctionalized carbon nanotubes,” *ACS Nano*, vol. 4, no. 4, pp. 2438–2444, 2010.
- [35] A. Siokou, F. Ravani, S. Karakalos, O. Frank, M. Kalbac, and C. Galiotis, “Surface refinement and electronic properties of graphene layers grown on copper substrate: An XPS, UPS and EELS study,” *Appl. Surf. Sci.*, vol. 257, no. 23, pp. 9785–9790, 2011.
- [36] S. Rey and F. Le Normand, “Surface transformations of carbon (graphene, graphite, diamond, carbide), deposited on polycrystalline nickel by hot filaments chemical vapour deposition,” *Thin Solid Films*, vol. 519, no. 14, pp. 4426–4428, 2011.
- [37] J. Liu, S. Fu, B. Yuan, Y. Li, and Z. Deng, “Toward a universal ‘adhesive nanosheet’ for the assembly of multiple nanoparticles based on a protein-induced reduction/decoration of graphene oxide,” *J. Am. Chem. Soc.*, vol. 132, no. 21, pp. 7279–7281, 2010.

- [38] M. P. Casaletto, A. Longo, A. Martorana, A. Prestianni, and A. M. Venezia, “XPS study of supported gold catalysts: the role of Au<sup>0</sup> and Au<sup>+δ</sup> species as active sites,” *Surf. Interface Anal.*, vol. 38, no. 4, pp. 215–218, 2006.





## 2. HYBRID MOLECULAR-NANOPARTICLE MATERIALS FOR LIGHT INDUCED WATER SPLITTING\*

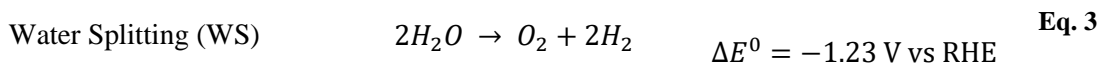
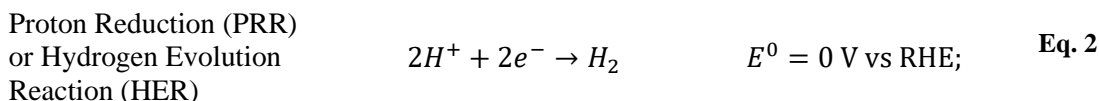
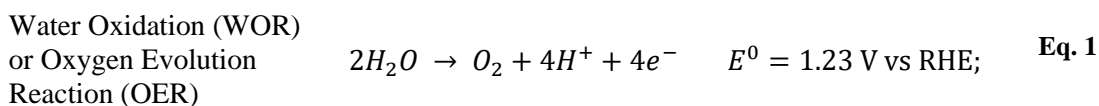
Depletion of the earth's fossil fuels and their prejudicial environmental impact has urged the scientific community to find solutions to sustain current energy needs using more sustainable methods. [1] Inspired by nature, artificial photosynthesis has been recently explored for alternative to produce zero carbon emission combustible fuels. The result of the photosynthesis process is the transformation of CO<sub>2</sub> and H<sub>2</sub>O into oxygen and carbohydrates; while in biological systems catalytic processes are accomplished by specific proteins, in artificial photosynthesis this job is performed by inorganic catalysts.[2] Light-induced water splitting is a paradigmatic case of artificial photosynthesis where the electrons and protons generated in the water oxidation half-reaction (**Eq. 1**) are used to produce hydrogen (**Eq. 2**). The overall reaction is an endergonic process that requires 475 kJ/mol (**Eq. 3**), this energy is the minimum required to perform the reaction and, ideally, should be provided exclusively by the sun.[3], [4] Several side reactions can hinder the reaction, therefore, use of a catalyst is required to lower the energy of activation. One of the most important challenges of this

---

\* The following chapter is an adaptation with special focus on the hybrid point of view from the work reported by the author and co-workers in: Ventosa, M., Oliveras J. et. al. Nanocrystal–Molecular Hybrids for the Photocatalytic Oxidation of Water. ACS Appl. Energy Mater. (2020), hence the figures showed are extracted from the article. The electrochemical measurements were performed and reported by the Artificial Photosynthesis Group at ICIQ.

technology is the functional and structural limitations of current existing molecular catalysts, including their efficiency, cost, and lack of technology for their production.

[5]



Such challenges can be addressed by colloidal nanocrystals (NCs) with uniform size and well-defined morphology. [6] The performance of a catalyst is directly correlated to the length and time scale of charge carriers and the atomic distribution of the material, terms that are better controlled when working at the nanoscale. As a consequence, NCs with uniform size and well-defined morphology and structure provide a unique platform to improve energy generation, storage, transport, and conversion processes. [7], [8] An effective photocatalyst consists of a photoabsorber that absorbs solar energy and uses it to generate excited electrons and holes to be used in subsequent redox reactions. For each desired reaction, the photoabsorber must have a suitable bandgap and proper conduction and valence band edge potentials. For effective water splitting, the conduction band needs to be at a potential less than 0 V vs. NHE ( $H^+/H_2$ ) while the valence band needs to be at a potential more than 1.23 V, which corresponds to light of 1008 nm. Reports regarding colloidal NCs being used as light absorbers to drive water splitting have increased notably in the last years, with studies on hydrogen evolution reaction (HER) greatly outnumbering those on oxygen evolution reaction (OER). The band structure of different types of semiconductors with respect to the redox potentials of water splitting is summarized in (**Figure 1**). Amongst

photoabsorbers [9], TiO<sub>2</sub> is the most popular and investigated due to its outstanding activity under UV irradiation (3.2 eV), high stability against photocorrosion, and low cost. [10], [11]

However, there are still several functional and structural aspects to be addressed including both their efficiency and the technology for their production. Two major drawbacks are i) the low photocatalytic efficiency due to low generation of charge carriers and rapid recombination, and ii) the lack of satisfactory broad-band visible and near-infrared (NIR) light-responsive photocatalytic materials, large bandgap photo catalysts only absorb the light in the near-ultraviolet (UV) region (wavelength <400 nm), which accounts for only ~7% of the solar spectrum, while most of the low bandgap photo catalysts absorbing in the visible (48% of the incoming solar energy) do not maintain photo activity over a sufficiently long time.[12], [13] Moreover, after their generation, electron-hole pairs may diffuse inducing undesired potential degradation. Consequently, significant challenges remain in developing a photoabsorber that is both efficient and robust enough to harvest and convert visible solar irradiation for H<sub>2</sub> harvesting and solar fuel production. [14]–[16]

A possible contribution to the solution of this issue is the combination of molecular catalysts with semiconductor NCs acting as photoabsorbers. Straightforward methods have been explored by the scientific community such as simple deposition, based on van der Waal interactions or linkage of the catalyst to the semiconductor NCs surface via organic linkers. [17] Catalyst leaching and inefficient electronic interaction are the main drawbacks of the first case, and the stability of the bond during the water-splitting process for the second. [18]

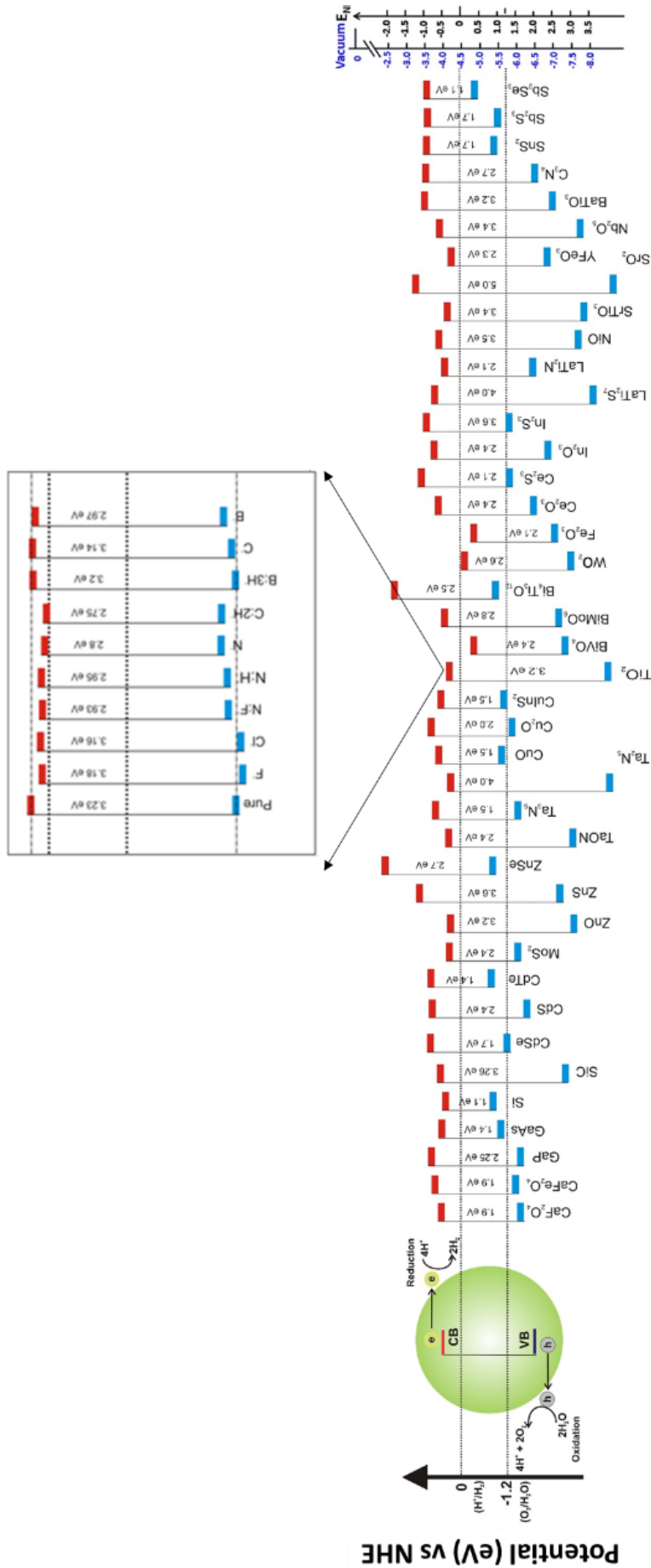
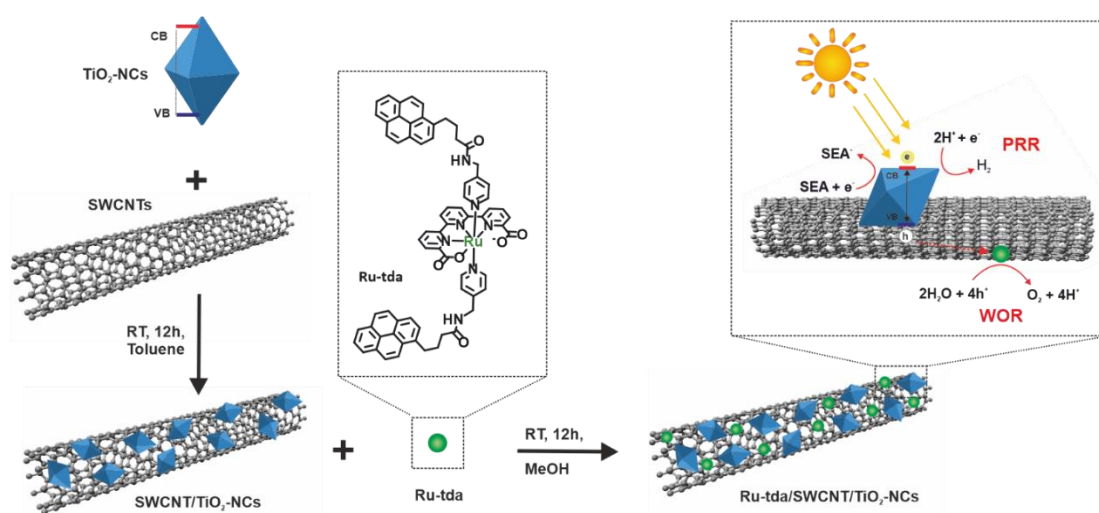


Figure 1. Bandgap structure of different types of semiconductors with respect to the redox potentials of water splitting.

The experiments and discussions included in this chapter have been performed in the context of the IGNITE (BIST) project SOLHYCAT, stemming out a collaboration between the Inorganic Nanoparticles group at ICN2 and the Artificial Photosynthesis group at ICIQ, the results of which have already been published [19]. SOLHYCAT aimed to generate a hybrid photocatalyst made of i) inorganic NCs as light absorbers, ii) molecular water oxidation/reduction catalysts (WOC and OEC respectively) for water splitting and iii) graphitic materials as linkers and electron transfer platforms (**Figure 2**).

For doing so, an array of semiconductor NCs which fulfill the bandgap requirements explained before has been synthesized, characterized, and coupled to SWCNTs, as described in CHAPTER 1 of this thesis.



**Figure 2.** Schematic representation of the synthetic steps to obtain the colloidal photocatalyst Ru-tda/SWCNT/ $\text{TiO}_2$ -NCs, starting with the attachment of  $\text{TiO}_2$ -NCs to SWCNTs followed by the final loading of the molecular WOC.

## 2.1. MATERIALS AND METHODS

Materials are listed by their order of appearance in this chapter.

Titanium fluoride (TiF<sub>4</sub>), Titanium(IV) chloride (TiCl<sub>4</sub>), Oleic Acid (OlAc, Technical Grade, 90%), Octadecanol (1-ODE), 2-Propanol, and Single-Walled Carbon Nanotubes (SWCNTs) were purchased from Sigma-Aldrich and used as received. Toluene and Methanol, technical grade were purchased from Fluka.

### 2.1.1. Synthesis of Ru-tda/SWCNT/TiO<sub>2</sub>-NCs

Highly monodisperse ( $9.27 \pm 1.5$  nm in side and  $15.4 \pm 1.8$  nm in diagonal, **Figure 3**) TiO<sub>2</sub> NCs were synthesized using the method proposed by Murray *et al.* [20] Shape-controlled synthesis of TiO<sub>2</sub>-NCs was achieved by non-aqueous surfactant-assisted synthesis using standard Schlenk line techniques under an inert atmosphere as previously described in CHAPTER 1. Titanium precursor is in this specific case a 1:1 mixture of TiF<sub>4</sub> and TiCl<sub>4</sub> stock solutions (0.2M halogenated titanium compound, 1 M OlAc in 1-ODE each) which have been mixed at equal volume inside the glovebox prior to use. For controlled NCs deposition onto SWCNTs, as-synthesized NCs were purified by centrifugation up to four times as described in CHAPTER 1 and finally resuspended in the original volume of 20 mL of toluene. Afterward, 1 mL of the purified NCs are diluted in 2 mL of toluene. To this solution, 0.25 mL of a 5 g/L single-walled carbon nanotubes solution was added and then left under stirring for 12 h. This method has proved to be scalable up to a total volume of 50 mL solution.

The synthesis of Ru-tda water oxidation catalyst precursor is reported in the literature. [21]

The Ru-tda catalyst precursor was anchored by soaking and stirring the SWCNT/TiO<sub>2</sub>-NCs material in a 1mM methanolic solution of Ru-tda for 8 h. Then, the

sample was centrifuged, and the pellets were washed three times with methanol for purification from non-anchored catalyst.

### **2.1.2. Photocatalytic experiments**

O<sub>2</sub> detection was performed in a liquid phase by a Clark-type electrode (custom-made DW2/2 electrode chamber equipped with quartz glass, Hansatech Instruments®). Prior to the experiments calibration of the electrode was performed with saturated and non-saturated O<sub>2</sub> aqueous solutions at 25 °C before the photocatalytic experiment.

In a glass vial, 4 mg of Ru-tda/SWCNT/TiO<sub>2</sub>-NCs or SWCNT/TiO<sub>2</sub>-NCs were added to a 2 mL pH 7 phosphate buffer solution (25 mM). The mixture was sonicated until a dispersed colloidal suspension was formed. The suspension was transferred to a water-jacketed 2 mL chamber (Hansatech® Instruments) in the dark and Na<sub>2</sub>S<sub>2</sub>O<sub>8</sub> was added to give a final concentration of 10 mM and reaching a final ionic strength of the solution of 0.1 M. The cell was sealed with a Teflon cap with a double septum and the solution was bubbled with N<sub>2</sub>. Afterward, the data was recorded both in the dark and under irradiation keeping the mixture at 25°C. The light source used was a 150 W Xe Arc Lamp previously calibrated to “3 suns” with a Si photodiode.

## **2.2. CHARACTERIZATION TECHNIQUES**

Electronic microscopy, UV-Vis spectra and X-Ray diffraction were used for sample characterization. Details on the equipment, settings and use are explained in

### **APPENDIX I.**

**Electrochemical methods:** Buffer solutions at pH 7 were prepared with Na<sub>2</sub>HPO<sub>4</sub> and NaH<sub>2</sub>PO<sub>4</sub> and adjusted to 0.1 M ionic strength. Cyclic voltammetry experiments were performed with a CHI660D potentiostat in a one-compartment cell, three-electrode system using platinum disk as the counter electrode (Ø = 3 mm) and mercury-mercurous sulfate, Hg/Hg<sub>2</sub>SO<sub>4</sub>, as a reference electrode. The working



electrode consisted of Ru-tda/SWCNT/TiO<sub>2</sub>-NCs on top of a glassy carbon (GC) disk ( $\varnothing = 3$  mm). The preparation of the working electrode was done following a dropcasting methodology. The as-prepared photocatalyst was dissolved in THF (50mg/mL) and the colloidal solution was stirred until homogeneity. Subsequently, 25  $\mu$ L of the solution were drop-cast 3 times onto previously polished glassy-carbon electrodes and left to air dry.

## 2.3. RESULTS AND DISCUSSION

### 2.3.1. Synthesis of Ru-tda/SWCNT/TiO<sub>2</sub>-NCs and characterization

Highly monodisperse TiO<sub>2</sub> tetragonally distorted square bipyramidal NCs with a high-intense UV light absorption (**Figure 3A**) were synthesized following a non-aqueous surfactant-assisted method which has been previously reported by Murray and co-workers[20] and in CHAPTER 1 of this thesis. In this specific case, TiO<sub>2</sub> NCs were obtained by injecting a 1:1 mixture of TiF<sub>4</sub>:TiCl<sub>4</sub> solutions in a liquid media composed of surfactants and co-reagents under a controlled atmosphere. The size of the TiO<sub>2</sub> NCs was assessed by measuring their edge and diagonal dimensions using the aforementioned TEM microscopy, giving the size values of  $9.27 \pm 1.5$  nm in side and  $15.4 \pm 1.8$  nm in diagonal (**Figure 3B**). Optical characterization by UV-Vis spectroscopy (**Figure 3C**) shows a sharp absorption edge at 300 nm (3.2 eV) corresponding to the typical high energy UV light absorption of TiO<sub>2</sub> NCs, which in this case broadens beyond this wavelength into the visible region, giving the solution a sky-blue colour.[22], [23] Structural characterization by X-ray diffraction (**Figure 3D**) shows well-defined peaks accordingly with the high crystallinity of the sample. Crystal texture is observed in the enhanced relative intensity of 37.5° and 48° peaks, corresponding to the elongation of the “a” axis in the bipyramids as described in the same article followed for the synthesis, broadening of the XRD peaks in comparison to the model is attributed

to limited crystal size and defects in the crystal structure as a result of oxygen vacancies [20], [24].

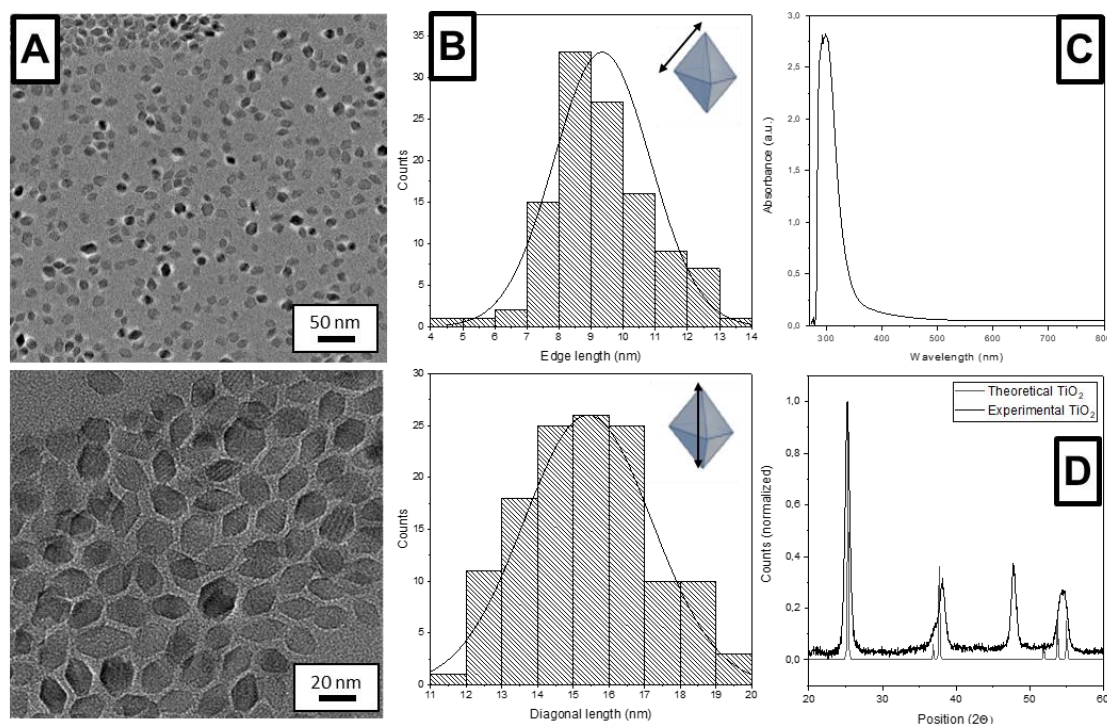


**Figure 3.** Complete characterization of TiO<sub>2</sub> NCs: A) TEM microscopy, B) size distribution histograms, C) UV-Vis spectra and D) XRD analysis.

Summarizing, all of these unique characteristics of the sample are explained from the synthetic point of view and are an almost paradigmatic example of how the choice of surfactants and precursors tunes the final properties of a given synthesis. The use of TiF<sub>4</sub> as a precursor leads to reduced (substoichiometric) TiO<sub>2</sub> (TiO<sub>2-x</sub>, 0 < x < 0.2) NCs with a high percentage of highly active {101} facets and a large number of oxygen vacancies. [25] Oxygen vacancies give the solution a sky-blue color which allow the NCs to be more photoactive than stoichiometric TiO<sub>2</sub>, which is white in color. [25], [26]

In order to build the SWCNT/TiO<sub>2</sub>-NCs hybrid, TiO<sub>2</sub> NCs were mixed at room temperature with a suspension of SWCNTs after being washed several times. Slow depletion of surfactant at the NCs surface allowed the system to be progressively destabilized to a point in which it would aggregate to the SWCNTs before NP-NP

aggregation, after a relatively long time (> 6 h). The addition of SWCNTs to such system allows the NCs to attach to them in a randomly distributed manner before aggregation, as previously discussed in CHAPTER 1. The decoration process leads to SWCNTs homogeneously coated with high densities of TiO<sub>2</sub> NCs (3·10<sup>15</sup> NCs/mg SWCNT), in the c.a. 80% of the SWCNT exposed surface (**Figure 4A**). Calculations on the amount of deposited NCs can be simply performed by analyzing its geometry and the synthesis reaction as explained next:

- 1) From the geometrical data it is possible to calculate the volume of a single ideal NC, which can be translated to mass via TiO<sub>2</sub> density.

Geometrical data (nm)			Volume (nm <sup>3</sup> )	Density (mg/nm <sup>3</sup> )	Mass 1NC (mg)
d <sub>1</sub>	d <sub>2</sub>	h	[d <sub>1</sub> ·d <sub>2</sub> ·h/3]		
10	10	15	500	4,23·10 <sup>-18</sup>	2,115·10 <sup>-15</sup>

- 2) Total mass of TiO<sub>2</sub> in solution can be calculated from the content of precursor and following the stoichiometric synthesis reaction. Yield of reaction has been considered 100%.

$$\begin{aligned} \frac{\text{TiO}_2\text{NCs}}{\text{mL}} &= \frac{m_{\text{TiO}_2}}{20\text{mL}} = \frac{91\text{mg Ti in precursor} \cdot \frac{79.866 \frac{\text{mgTiO}_2}{\text{mmol}}}{47.867 \frac{\text{mg Ti}}{\text{mmol}}}}{2.115 \cdot 10^{-15}\text{mg}} \\ &= 3.66 \cdot 10^{15}\text{TiO}_2\text{NCs/mL} \end{aligned}$$

- 3) Finally, from the volume of colloidal TiO<sub>2</sub> NCs solution and SWCNTs mixture used the ratio of both can be easily extracted as follows.

$$\frac{\text{TiO}_2\text{NCs}}{\text{mL hybrid}} = \frac{3.66 \cdot 10^{15}\text{TiO}_2\text{NCs}}{\text{mL colloid}} \cdot \frac{1\text{mL colloid}}{3.25\text{mL hybrid}} \sim 1 \cdot 10^{15}\text{TiO}_2\text{NCs/mL hybrid}$$

### **2.3.2. Electrochemical characterization of the sample**

The Ru complex [Ru(tda)(pypyr)<sub>2</sub>], where tda<sup>2-</sup> = [2,2':6',2''-terpyridine]-6,6''-dicarboxylato and pypyr = 4-(pyren-1-yl)-N-(pyridin-4-ylmethyl) butanamide) reported earlier [21], and abbreviated as “Ru-tda” from here on, has been used as WOC in this work. The axial position is occupied by two pyridyl ligands that are functionalized with pyrene units, which are responsible for the anchoring on the SWCNTs via  $\pi,\pi$ -stacking interactions (**Figure 4**).[21] Cyclovoltametry (CV) experiments were very useful to electrochemically corroborate the presence of the molecular Ru compound on top of the conductive SWCNTs. By drop-casting the Ru-tda/SWCNT/TiO<sub>2</sub>-NCs molecular hybrids onto a glassy carbon working electrode and carrying out a CV at pH 7, two redox waves at  $E_{1/2} = 0.61$  V and  $E_{1/2} = 1.06$  V (vs NHE) appeared, corresponding to the characteristic Ru<sup>III/II</sup> and Ru<sup>IV/III</sup> couples, respectively (**Figure 4B**).[27] We calculated coverage of  $\Gamma = 2.18 \cdot 10^{-8}$  mol<sub>Ru</sub> · g<sub>molecular/hybrid</sub> (**Equation 4**), which accounts for a ratio of 10<sup>4</sup>:1 TiO<sub>2</sub>-NCs:Ru-tda as follows:

**Equation 4.** Q is the charge under the oxidative peak of the reversible, one-electron wave obtained by integration of the CV, which is  $9.1 \times 10^{-6}$  C. n is the number of electrons involved in that oxidation process, which is 1 (Ru<sup>II</sup> to Ru<sup>III</sup>). m is the hybrid catalyst mass on the electrode and F is the Faradaic constant (96,485 C/mol).

$$\Gamma \text{ (mol/g)} = \frac{Q}{n \cdot m \cdot F}$$

By using the surface coverage value, TiO<sub>2</sub>-NCs: Ru-tda was calculated as:

$$\frac{\text{TiO}_2\text{NCs}}{\text{atom Ru}} = \frac{1 \cdot 10^{15} \text{TiO}_2\text{NCs}}{1 \text{mL hybrid}} \cdot \frac{1 \text{mL hybrid}}{4.5 \text{mg hybrid}} \cdot \frac{1 \text{g hybrid}}{2.18 \cdot 10^{-8} \text{mol RuOEC}} \cdot \frac{1 \text{mol RuOEC}}{6.02 \cdot 10^{23} \text{molec RuOEC}} \cdot \frac{1 \text{molec RuOEC}}{1 \text{atom Ru}} = \frac{10 \text{ TiO}_2\text{NCs}}{\text{atom Ru}}$$

The capacity of the new molecular hybrid material, Ru-tda/SWCNT/TiO<sub>2</sub>-NCs, to catalytically oxidize water was assessed in a thermostated reactor at 25 °C, under 3 suns irradiation, using peroxydisulfate (S<sub>2</sub>O<sub>8</sub><sup>2-</sup>) as a sacrificial electron acceptor (SEA) in a pH 7 phosphate buffer solution. Once the sample is illuminated, electrons and holes should be generated at the photoactive TiO<sub>2</sub> NCs, transferred through the SWCNTs and used to induce the chemical reactions that are responsible for final oxygen evolution (**Figure 4C**). A control experiment was performed in the absence of the Ru-catalyst. The SWCNT/TiO<sub>2</sub>-NCs hybrid generates an increasing amount of oxygen during the first 50 minutes of illumination, via hydroxyl radical formation and its evolution as it has been previously described in the literature. [28] Then the oxygen production continuously decreases until it fades away, which indicates degradation or blocking of the surface of the TiO<sub>2</sub> NCs.

In the presence of the Ru-tda catalyst precursor, the molecular hybrid material Ru-tda/SWCNT/TiO<sub>2</sub>-NCs generates no net molecular oxygen during the first 30 minutes when compared to the blank. During this period of time the catalyst active species are generated from the catalyst precursor which is progressively oxidized from Ru(II) to Ru(IV), which will coordinate to a solvent OH<sup>-</sup> generating Ru seven-coordinated species, [Ru<sup>IV</sup>(O)(tda)(pypyr)<sub>2</sub>] (abbreviated as Ru<sup>IV</sup>(O)-tda), responsible for water oxidation catalysis. This is a process that has been described previously in homogeneous phase and is known to be slow at pH 7. [27], [29] After this period, there is a sustained generation of O<sub>2</sub> as long as there is illumination. The fact that under the presence of Ru complex the photoactivity of the TiO<sub>2</sub> component is maintained throughout of 2.7 h indicates that the Ru complex acts as a protecting agent for the surface of TiO<sub>2</sub> avoiding the formation of HO• and reacting in a fast manner with the holes generated upon excitation, thus avoiding TiO<sub>2</sub> surface degradation.[30]

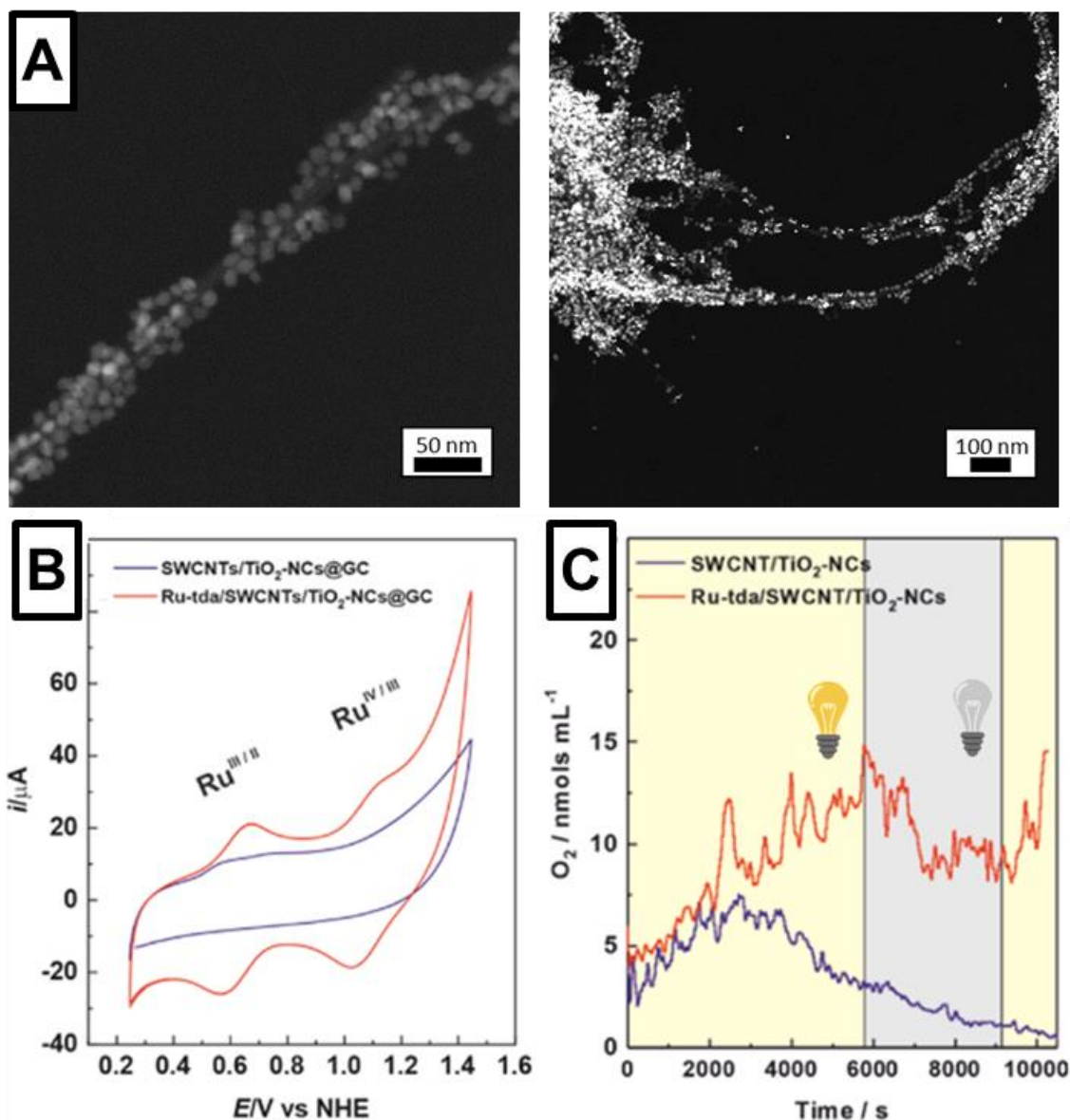


**Figure 4.** Characterization of the Ru-tda/SWCNT/TiO<sub>2</sub>-NCs hybrid A) HAADF STEM microscopy images of the hybrid, B) Cyclic Voltammetry: In blue, a blank of SWCNT/TiO<sub>2</sub>-NCs dropcast on glassy carbon, GC, as the working electrode and in red the freshly prepared Ru-tda/SWCNT/ TiO<sub>2</sub>-NCs on GC as a working electrode, C) oxygen evolution profile obtained during illumination of a mixture containing 2 mg/mL Ru-tda/SWCNT/TiO<sub>2</sub>-NCs (red) or 2 mg/mL SWCNT/TiO<sub>2</sub>-NCs (blue).

Remarkably, the hybrid material Ru<sup>IV</sup>(O)-tda/SWCNT/TiO<sub>2</sub>-NCs achieves a Turnover Number (TON) of 229 (**Equation 5**) based on the Ru catalyst amount which is the highest reported for these type of systems.[31], [32] The apparent quantum yield (AQY) of the water oxidation reaction at pH 7 and 25 °C was measured to be

approximately 0.9% at the peak of absorbance of TiO<sub>2</sub>-NCs at  $\lambda = 310$  nm (**Equation 6**). On one hand, this low value can be attributed to the large excess of light absorber versus catalyst and, on the other hand, to the high complexity of these systems. Similar quantum yields, albeit a bit lower 0.10-0.27%, have been recently reported for related hybrid molecular photocatalytic material using a Ru complex as WOC and CdSe as light absorber, [30] although in this case TONs were below 1.

**Equation 5.** The turnover number, TON, is defined as the number of moles of substrate transformed by 1 mol of both forms of the Ru-tda present on the surface of the colloidal photocatalyst.

$$TON = \frac{\text{moles O}_2}{\text{moles OEC}} = \frac{20 \text{ nmols O}_2}{8.72 \cdot 10^{-11} \text{ moles OEC}} = 229.36$$

**Equation 6.** The absorbed photons in the formula [33] were estimated by integrating the solar spectrum (AM 1.5) in the 300-350 nm range, where the TiO<sub>2</sub>-NCs absorber shows the maximum absorption and assuming full absorption in this range.

$$\begin{aligned} AQY(\%) &= \frac{\text{Rate of reacted electrons}}{\text{Rate of absorbed photons}} \times 100 \\ &= \frac{(4 \times \text{molecules O}_2)_t}{(\text{absorbed photons})_t \cdot \text{area irradiated}} \times 100 = \\ &= \frac{4 \times 2 \cdot 10^{-8} \text{ moles O}_2 \times 6.022 \cdot 10^{23} \text{ moles}^{-1}}{3 \times (2.31 \cdot 10^{19}) \text{ photons} \cdot \text{s}^{-1} \cdot \text{m}^{-2}} \times 100 = 0.07\% \end{aligned}$$

A high ratio of semiconductor NCs versus catalyst is desirable to perform light-induced water oxidation efficiently, as previously observed in photocatalytic molecular systems for the water oxidation reaction although this will obviously decrease quantum yields.[29], [34], [35] This can be explained by the fact that all the TiO<sub>2</sub> moieties that are not accessible by the highly mobile anchored Ru will lose their photoactivity, as we have observed in the blank experiment, and thus they will not be involved in the light-harvesting process.[28], [36] The low quantum yield also reflects the complexity of the

system studied here where a large number of competing reactions are operating at the same time. An additional challenge of single colloidal devices, as compared to typical two-compartment photoelectrochemical cells (PECs), is that oxidation and reduction reactions are not spatially separated. Therefore, it can lead to non-productive reactions that again will be responsible for a decrease of quantum efficiency unless that molecular catalyst are able to compartment both reactions in the colloidal phase

Interestingly, after the catalytic test was performed the sample was observed again via TEM microscopy which demonstrated the robustness of the sample since the TiO<sub>2</sub> NCs were still attached to the SWCNTs surface. Ru traces were observable via EDX which opens a door for possible long term use of the hybrid (**Figure 5**).

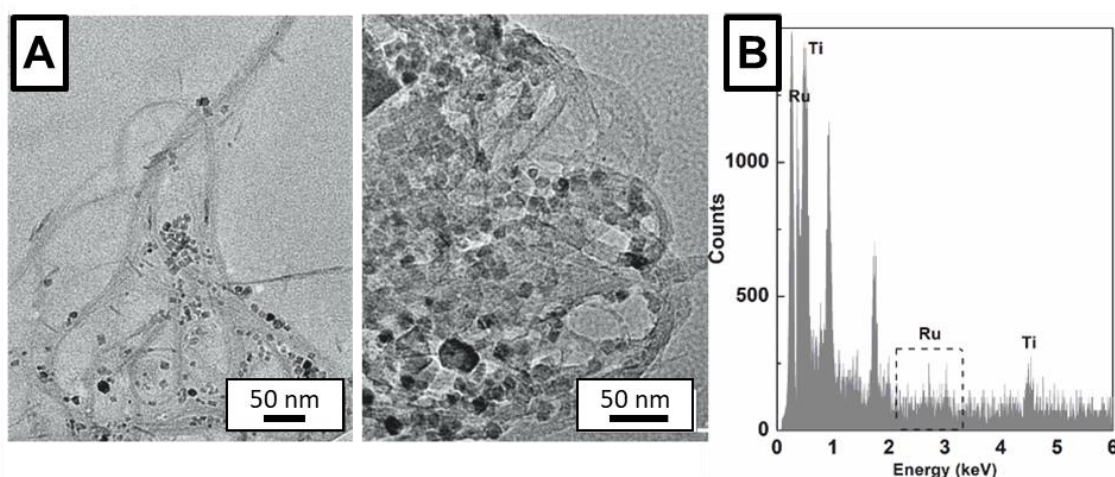


**Figure 5.** Characterization of Ru-tda/SWCNT/TiO<sub>2</sub>-NCs hybrid structure after catalytic testing A) TEM microscopy B) EDX spectra from the sample in B revealing the presence of atomic Ru in the hybrid structures.

## 2.4. CONCLUSIONS AND PERSPECTIVES

The system presented here is remarkable because it is capable of overcoming all the challenges just described at neutral pH. Although the AQY is low, it is still within the best values reported in the literature up to now. Under these conditions, the molecular hybrid material Ru<sup>IV</sup>(O)-tda/SWCNT/TiO<sub>2</sub>-NCs achieves a remarkable TON of 229 upon illumination, which is the highest reported for this type of devices, thanks



to favorable overall kinetics. Furthermore, the modular approach reported here establishes a very versatile platform. Each of the constituting entities, such as the light absorber, linker, and the catalyst, can be easily and independently replaced. For this reason, it is an optimal and efficient methodology for device discovery to foster the production of clean and renewable fuels.

The reported results are the seed of a broad and interesting line of research that could lead to a new family of hybrid catalysts for the production of clean and renewable product, hydrogen, with a high impact to our society. Some of the parameters that would need further development are:

- Investigation of the Ru-tda: TiO<sub>2</sub> NCs ratio: The amount of highly active Ru catalyst used in this work is extremely low (2.2 μg<sub>Ru</sub>/g<sub>molecular hybrid</sub>), in line with the scarcity of that element. [37], [38] As discussed, though, this leads to a high amount of photoabsorber that triggers the WOC reaction by being degraded and fostering secondary reactions. This issue should be tackled by systematically testing several ratios.
- Addition of a co-catalyst such as Pt NCs in the surface of the carbon structure to perform complete hv-WS experiments. Tentative investigations of this initiative have been performed by adding 1%(wt.) K<sub>2</sub>PtCl<sub>6</sub> to the reaction media with positive results. This leads to a simplified charge carrier dynamics scheme since the sacrificial agent reactions are suppressed and oxygen reduction reaction is heavily hindered by Pt. Although replicates and quantitative measurements still need to be performed, to the best of our knowledge, it is the first time that O<sub>2</sub> and H<sub>2</sub> have been detected in a TiO<sub>2</sub> based homogeneous-heterogeneous hybrid without the need for sacrificial agents boosting conversion efficiency. The preparation of the hybrid is

already proven as feasible since, following the reported method, several types of NCs can be easily deposited onto a carbon nanostructure as proven in CHAPTER 1.

## 2.5. REFERENCES

- [1] N. S. Lewis and D. G. Nocera, "Powering the planet: Chemical challenges in solar energy utilization," *Proc. Natl. Acad. Sci.*, vol. 103, no. 43, pp. 15729–15735, 2006.
- [2] M. E. El-Khouly, E. El-Mohsnawy, and S. Fukuzumi, "Solar energy conversion: From natural to artificial photosynthesis," *J. Photochem. Photobiol. C Photochem. Rev.*, vol. 31, pp. 36–83, 2017.
- [3] Y. Tachibana, L. Vayssieres, and J. R. Durrant, "Artificial photosynthesis for solar water-splitting," *Nat. Photonics*, vol. 6, p. 511, Jul. 2012.
- [4] J. Barber, "Photosynthetic energy conversion: Natural and artificial," *Chem. Soc. Rev.*, vol. 38, no. 1, pp. 185–196, Dec. 2009.
- [5] N. None, "Report of the Basic Energy Sciences Roundtable on Liquid Solar Fuels," Apr. 2019.
- [6] H. Imahori, Y. Mori, and Y. Matano, "Nanostructured artificial photosynthesis," *J. Photochem. Photobiol. C Photochem. Rev.*, vol. 4, no. 1, pp. 51–83, 2003.
- [7] N. G. Bastús *et al.*, "Exploring new synthetic strategies for the production of advanced complex inorganic nanocrystals," *Zeitschrift fur Phys. Chemie*, vol. 229, no. 1–2, pp. 65–83, 2015.
- [8] A. P. Alivisatos, "Perspectives on the physical chemistry of semiconductor nanocrystals," *J. Phys. Chem.*, vol. 100, no. 31, pp. 13226–13239, 1996.
- [9] X. Chen, S. Shen, L. Guo, and S. S. Mao, "Semiconductor-based photocatalytic hydrogen generation," *Chem. Rev.*, vol. 110, no. 11, pp. 6503–6570, Nov. 2010.
- [10] A. Fujishima, T. N. Rao, and D. A. Tryk, "Titanium dioxide photocatalysis," *J. Photochem. Photobiol. C Photochem. Rev.*, vol. 1, pp. 1–21, 2000.
- [11] A. Fujishima, X. Zhang, and D. A. Tryk, "TiO<sub>2</sub> photocatalysis and related surface phenomena," *Surf. Sci. Rep.*, vol. 63, no. 12, pp. 515–582, Dec. 2008.
- [12] X. Huang, S. Han, W. Huang, and X. Liu, "Chemical Society Reviews Enhancing solar cell efficiency: the search for luminescent materials as spectral converters," *Chem. Soc.*

*Rev.*, vol. 42, no. 1, p. 173, 2013.

- [13] Y. Qu and X. Duan, "Progress, challenge and perspective of heterogeneous photocatalysts," *Chemical Society Reviews*, vol. 42, no. 7. The Royal Society of Chemistry, pp. 2568–2580, 11-Mar-2013.
- [14] T. Hisatomi, J. Kubota, and K. Domen, "Recent advances in semiconductors for photocatalytic and photoelectrochemical water splitting," *Chemical Society Reviews*, vol. 43, no. 22. Royal Society of Chemistry, pp. 7520–7535, 21-Nov-2014.
- [15] F. E. Osterloh, "Inorganic nanostructures for photoelectrochemical and photocatalytic water splitting," *Chemical Society Reviews*, vol. 42, no. 6. The Royal Society of Chemistry, pp. 2294–2320, 21-Mar-2013.
- [16] F. F. Wang, Q. Li, and D. S. Xu, "Recent progress in semiconductor-based nanocomposite photocatalysts for solar-to-chemical energy conversion," *Adv. Energy Mater.*, vol. 7, no. 23, pp. 1–19, 2017.
- [17] J. Willkomm, K. L. Orchard, A. Reynal, E. Pastor, J. R. Durrant, and E. Reisner, "Dye-sensitised semiconductors modified with molecular catalysts for light-driven H<sub>2</sub> production," *Chem. Soc. Rev.*, vol. 45, no. 1, pp. 9–23, 2016.
- [18] K. L. Materna, R. H. Crabtree, and G. W. Brudvig, "Anchoring groups for photocatalytic water oxidation on metal oxide surfaces," *Chemical Society Reviews*, vol. 46, no. 20. Royal Society of Chemistry, pp. 6099–6110, 21-Oct-2017.
- [19] M. Ventosa, J. Oliveras, N. G. Bastús, C. Gimbert-Suriñach, V. Puntès, and A. Llobet, "Nanocrystal–Molecular Hybrids for the Photocatalytic Oxidation of Water," *ACS Appl. Energy Mater.*, Sep. 2020.
- [20] T. R. Gordon *et al.*, "Nonaqueous synthesis of TiO<sub>2</sub> nanocrystals using TiF<sub>4</sub> to engineer morphology, oxygen vacancy concentration, and photocatalytic activity," *J. Am. Chem. Soc.*, vol. 134, pp. 6751–6761, 2012.
- [21] J. Creus *et al.*, "A Million Turnover Molecular Anode for Catalytic Water Oxidation," *Angew. Chemie Int. Ed.*, vol. 55, no. 49, pp. 15382–15386, Dec. 2016.
- [22] B. Choudhury and A. Choudhury, "Oxygen defect dependent variation of band gap, Urbach energy and luminescence property of anatase, anatase-rutile mixed phase and of rutile phases of TiO<sub>2</sub> nanoparticles," *Phys. E Low-Dimensional Syst. Nanostructures*, vol. 56, pp. 364–371, Feb. 2014.
- [23] G. Liu *et al.*, "Enhanced Photoactivity of Oxygen-Deficient Anatase TiO<sub>2</sub> Sheets with

Dominant {001} Facets.”

- [24] N. Zhang, M. Q. Yang, S. Liu, Y. Sun, and Y. J. Xu, “Waltzing with the Versatile Platform of Graphene to Synthesize Composite Photocatalysts,” *Chem. Rev.*, vol. 115, no. 18, pp. 10307–10377, 2015.
- [25] U. Diebold, “The surface science of titanium dioxide,” *Surface Science Reports*, vol. 48, no. 5–8. North-Holland, pp. 53–229, 01-Jan-2003.
- [26] M. Gharagozlou and R. Bayati, “Photocatalytic activity and formation of oxygen vacancies in cation doped anatase TiO<sub>2</sub> nanoparticles,” *Ceram. Int.*, vol. 40, no. 7 PART B, pp. 10247–10253, Aug. 2014.
- [27] R. Matheu *et al.*, “Intramolecular Proton Transfer Boosts Water Oxidation Catalyzed by a Ru Complex,” *J. Am. Chem. Soc.*, vol. 137, no. 33, pp. 10786–10795, Jul. 2015.
- [28] A. L. Linsebigler, G. Lu, and J. T. Yates, “Photocatalysis on TiO<sub>2</sub> Surfaces: Principles, Mechanisms, and Selected Results,” *Chem. Rev.*, vol. 95, no. 3, pp. 735–758, 1995.
- [29] L. Francàs *et al.*, “Kinetic Analysis of an Efficient Molecular Light-Driven Water Oxidation System,” *ACS Catal.*, vol. 7, no. 8, pp. 5142–5150, Aug. 2017.
- [30] C. M. Wolff *et al.*, “All-in-one visible-light-driven water splitting by combining nanoparticulate and molecular co-catalysts on CdS nanorods,” *Nat. Energy*, vol. 3, no. 10, pp. 862–869, 2018.
- [31] R. Abe, K. Sayama, and H. Sugihara, “Development of new photocatalytic water splitting into H<sub>2</sub> and O<sub>2</sub> using two different semiconductor photocatalysts and a shuttle redox mediator IO<sub>3</sub><sup>-</sup>/I<sup>-</sup>,” *J. Phys. Chem. B*, vol. 109, no. 33, pp. 16052–16061, Aug. 2005.
- [32] C. Costentin, S. Drouet, M. Robert, and J. M. Savéant, “Turnover numbers, turnover frequencies, and overpotential in molecular catalysis of electrochemical reactions. Cyclic voltammetry and preparative-scale electrolysis,” *J. Am. Chem. Soc.*, vol. 134, no. 27, pp. 11235–11242, Jul. 2012.
- [33] N. Serpone and A. Salinaro, “Terminology, relative photonic efficiencies and quantum yields in heterogeneous photocatalysis. Part I: Suggested protocol (Technical Report),” *Pure Appl. Chem.*, vol. 71, no. 2, pp. 303–320, 1999.
- [34] S. Berardi *et al.*, “Efficient Light-Driven Water Oxidation Catalysis by Dinuclear Ruthenium Complexes,” *ChemSusChem*, vol. 8, no. 21, pp. 3688–3696, Nov. 2015.
- [35] Y. Xu *et al.*, “Chemical and Light-Driven Oxidation of Water Catalyzed by an Efficient

- Dinuclear Ruthenium Complex,” *Angew. Chemie Int. Ed.*, vol. 49, no. 47, pp. 8934–8937, Nov. 2010.
- [36] M. Setvin *et al.*, “Following the Reduction of Oxygen on TiO<sub>2</sub> Anatase (101) Step by Step,” *J. Am. Chem. Soc.*, vol. 138, no. 30, pp. 9565–9571, Aug. 2016.
- [37] E. Roduner, “Size matters: Why nanomaterials are different,” *Chem. Soc. Rev.*, vol. 35, no. 7, pp. 583–592, 2006.
- [38] P. C. K. Vesborg and T. F. Jaramillo, “Addressing the terawatt challenge: Scalability in the supply of chemical elements for renewable energy,” *RSC Advances*, vol. 2, no. 21. The Royal Society of Chemistry, pp. 7933–7947, 21-Aug-2012.

### **3. SYNTHESIS AND APPLICATION STUDY OF $\text{Fe}_3\text{O}_4$ /GRAPHENE HYBRID FOR WATER REMEDIATION**

In a world where 1.2 billion people have no access to clean water, emerging pollutants (personal care products, pesticides, drugs, and their metabolites) found in drinking water have recently been of great concern [1]–[4]. The consequences of water contamination are also relevant to the ecosystem health: it is well established, from models and empirical observations, the ecological thresholds of contaminants to which biological systems are susceptible. [5], [6] When these thresholds are surpassed, the environment is damaged. If the stressor is recognized before passed this tipping point it can be acted upon, thus, avoiding drastic and unexpected ecosystem responses such as biodiversity narrowing or foundation species loss. [7], [8] Nevertheless, these thresholds are often met at very low concentrations of pollutants, and so, noticeable in catastrophic responses on small organisms such as algae or sea flies, which will lead to a cascade effect on bigger species. It is only when bigger animal species collapse that the issue meets the public eye, for instance, on the almost extinguishment of vultures in India from DCF intoxication [9], [10] –vultures feed on animal carcasses, which helps avoiding the spreading of sicknesses– or the reproduction problems caused by IBP to

some fish species. [11], [12] These observed effects, are usually past the tipping point of the ecosystem.

Up to now, over 200 pharmaceutical compounds have been detected in freshwaters [13], the most commonly found are antibiotics –100 to 200 kilotons consumed per year on average [14]– followed by painkillers, analgesics and antidepressants, which affect plants and animal's life including human beings. [15] Pharmaceuticals are inherently designed to be robust, so they can be stored, distributed and have long expiration dates, and also they are designed to interact with biological mechanisms, and because of that they persist in nature and accumulate damaging biological systems. [16] These compounds are usually excreted non-metabolised by humans and livestock [17], directly to wastewater and after water processing in sludge that is later used as fertiliser.[18] While it is true that regulated pollutants have a longer environmental half-lives, the main concern when talking about pharmaceutical drugs is its continuous disposal to the water, which makes them persistent. [19] The existence of pharmaceuticals in drinking water is a potential threat for life of unknown risk.

The reported environmental concentrations of nonsteroidal anti-inflammatory drugs (NSAIDs) have been mainly found to be at the µg/L-mg/L range in seawaters and surface waters [20], and in the lower ng/L level in groundwaters and drinking waters [21], but they tend to steadily increase due to their wide usage and irresponsible disposal. Even at very low concentrations, such pollutants can impact aquatic ecosystems causing irreversible harm. [22]–[25] Evidences show mixtures of these pollutants allow them to be more harmful at lower concentrations. [26] Among them, Ibuprofen (IBP) and Diclofenac (DCF), estimated to be consumed in several kilotons per year globally, are considered Class I pharmaceuticals which must be dealt with in urgency [27].

These pollutants cannot be monitored with common detection methods, moreover, traditional water treatment methods fail to remove them.[2], [15], [28]–[30] Of all the technologies that have been proposed – including photocatalytic degradation, biodegradation, ozonation, electrochemical techniques, reverse osmosis and other advanced oxidation processes [13], [31] - adsorption is globally recognized as the most promising one for wastewater treatment because of its versatility, wide applicability and economic feasibility. [32] Adsorption does not intercede with the targeted contaminants and allows the waste to be treated and processed whilst techniques involving the degradation of the pharmaceuticals often produce compounds which end up being more problematic than the initial ones. [33]–[35] Adsorption techniques are known for being easily optimized depending of tunable parameters such as pH, temperature and physiochemical features of the pollutant-adsorbent pair, [36] with the added adversity of being adsorbed when in traces concentration. [37]

Activated carbon, carbon nanotubes, clays and others have been traditionally used for absorption of pharmaceutical pollutants. [32] Today, graphene and graphene oxide have shown better results and behavior since they efficiently remove persistent pollutants [38] and organic compounds [39] due to its high surface area ( $\sim 2630 \text{ m}^2 \text{ g}^{-1}$ ), delocalized pi ( $\pi$ ) electrons, and tunable chemical properties, which make them potential outstanding adsorbents for environmental decontamination applications.[40], [41] Graphene both in a pristine and modified or oxidized state has been tested to take full advantage of its high adsorption capacity. [42] In this context, the addition of magnetic nanoparticles to graphitic structures has recently been studied to help remove the adsorbent materials from the treated water easily once the pollutant has been adsorbed. [38], [39], [43]–[45] In the following pages, we explore the adsorption of



NSAIDs such as Ibuprofen and Diclofenac at low concentrations, giving a practical and realistic approach to this issue.

In this work a graphene-based magnetic hybrid material decorated with Fe<sub>3</sub>O<sub>4</sub> nanocrystals (NCs) is prepared for effective removal of emerging pollutants when they are present at low concentrations. A green preparation of this hybrid, a study of its application and performance and a simple, direct method of detection and quantification by UV-Vis are presented in the following pages. Several variations of the Fe<sub>3</sub>O<sub>4</sub>/Graphene hybrid were fabricated such as Fe<sub>3</sub>O<sub>4</sub>/Graphene oxide and a multimodal Fe<sub>3</sub>O<sub>4</sub>-TiO<sub>2</sub>/Graphene hybrid which explored the photocatalytic degradation of the captured drugs.

### **3.1. MATERIALS AND METHODS**

Materials are listed by their order of appearance in this chapter.

Iron III Chloride (FeCl<sub>3</sub> anhydrous, powder, ≥99.99% trace metals basis), Iron(II) chloride tetrahydrate (FeCl<sub>2</sub>·4H<sub>2</sub>O puriss. p.a., ≥99.0% (RT)), stored in a glovebox under inert conditions, diclofenac (DCF) and Tetramethylammonium hydroxide solution (TMAOH), Sodium Hydroxide (NaOH), Hydrochloric Acid (HCl) and Hydrogen Peroxide (30 v/v) were purchased from Sigma-Aldrich and. Float-A-Lyzer devices of 0.5-1kDa were purchased from Spectrum Labs and used after activation with 10% Ethanol solution as described by the company. 4-Isobutyl-alpha-methylphenylacetic acid, 99% (Ibuprofen-IBP) was purchased from Alfa Aesar. Titanium Isopropoxide was purchased from Fluka. Graphene flakes were kindly donated by Arben Merkoçi group at ICN2.

All chemicals were used as received without further purification. Distilled water passed through a Millipore system ( $\rho = 18.2 \text{ M}\Omega$ ) was used in all experiments.

### **3.1.1. Synthesis of Fe<sub>3</sub>O<sub>4</sub>/Graphene and Fe<sub>3</sub>O<sub>4</sub>-TiO<sub>2</sub>/Graphene hybrids**

**Synthesis of Fe<sub>3</sub>O<sub>4</sub> NCs:** Synthesis of Fe<sub>3</sub>O<sub>4</sub> magnetite NCs of ~7 nm has been performed following a previously reported method. [46], [47] Briefly, in a 250mL round bottom flask, 1.824g of FeCl<sub>3</sub> anhydrous and 0.996g of FeCl<sub>2</sub>·4H<sub>2</sub>O are sequentially added to 50 mL of mQ water deoxygenated under N<sub>2</sub> bubbling for 30 minutes and stirred until complete dissolution. Afterwards, 50mL of 1M TMAOH previously deoxygenated under N<sub>2</sub> bubbling for 30 minutes are poured continuously onto the solution containing the Fe(II) and Fe(III) precursors stirred at 600rpm under Nitrogen atmosphere. The mixture is left stirring for 30 min. Once the reaction is completed the sample is washed twice by magnetically aided sedimentation and finally resuspended in 10mM TMAOH. Sample is stored under nitrogen atmosphere to avoid its degradation.

**Synthesis of TiO<sub>2</sub> NCs:** Synthesis of TiO<sub>2</sub> anatase NCs of ~4 nm has been performed following a previously reported method. [48] Briefly, NaOH 3M and HCl 3M solutions were prepared. Afterwards, 2.07 mL of Titanium Isopropoxide were added to the 10 mL of the acid solution. Once the solution was homogeneous, 30 mL of mQ water and 5 mL of the base solution were carefully added to the solution containing the Titanium precursor, pH was then adjusted to pH 5. The solution was left covered in an oven at 70 °C without stirring for 24 h. The resulting nanoparticles were centrifuged twice, the first time at 500 G and the second one at 1000 G and resuspended in water. Afterwards, they were thoroughly sonicated in a sonics bath for several hours, centrifuged at 1000 G and resuspended in 10mM TMAOH.

**Synthesis of graphene oxide:** Synthesis of graphene oxide was performed by adaptation of a simplified Hummer's method previously reported in the literature. [49] Briefly, 0.5 g of graphene flakes were mixed with 66.5 mL of H<sub>2</sub>SO<sub>4</sub> in a 250 mL cooled by an ice bath. Afterward, 3 g of KMnO<sub>4</sub> were slowly added under vigorous stirring, at

this point the solution was purplish green. Solution was left stirring for 3 and 6 days capped, and it gradually turned to a deep green color. After this time had passed, the solution was poured in a 500 mL flask containing 66.5 mL of cold Mili-Q Water, this reaction was exothermic and effervescent, and the solution turned to a reddish brown color. Finally, 4.5 mL of H<sub>2</sub>O<sub>2</sub> were added and the solution was left stirring for 10 minutes, turning to a light-yellow color. The final graphene oxide solution was washed 3 times centrifuging at 10000 G for 15 minutes and replacing the supernatant with 3 M HCl in order to remove the metal impurities that may had remained, finally the centrifugation process was repeated, replacing the supernatant with Mili-Q Water until the pH of the solution was 4-5.

**Post-synthesis procedure, preparation of the hybrid:** For the attachment of NCs to the graphene structure a calculated amount of  $2 \cdot 10^{12}$  NCs were mixed with 625  $\mu$ L of 5 mg/mL suspension of Graphene in H<sub>2</sub>O ( $6.4 \cdot 10^{12}$  NCs/mg graphene) and dialyzed versus H<sub>2</sub>O in 0.5-1kDa, 5 mL dialysis bags for 3 days, constantly stirred and renewing the dialysis water once per day. After the procedure was completed, the dialyzed samples were precipitated under 2000 G centrifugation for 10 minutes and the supernatant containing non-attached crystals was removed and replaced with 5mL Milli-Q-Water, this process was performed twice. In the case of Fe<sub>3</sub>O<sub>4</sub>-TiO<sub>2</sub>/Graphene hybrids, TiO<sub>2</sub> NCs were added to the dialysis bag after the afformented process was completed and decoration was accomplished by following the same steps. TiO<sub>2</sub> NCs were washed prior to dialysis via centrifugation and the pellet was resuspended in water. Study of the deposition mechanism and the hybrid formation control was performed by synthesis of the hybrid at different and defined Graphene-to-Nanocrystal ratios. Concentrations of NCs were calculated by taking in account the size, composition and concentration of precursors in the original synthesis, as well as its yield. This process

was easily scalable and for the following experiments, 3.75 mL of Graphene suspension were used per each synthesis.

### 3.2. CHARACTERIZATION TECHNIQUES

Electronic microscopy and UV-Vis spectra were used for sample characterization. Details on the equipment, settings and use are explained in **APPENDIX I**.

**Superconducting Quantum Interference Device (SQUID) magnetometry measurements:** Magnetic susceptibility measurements were carried out at the Unitat de Mesures Magnètiques of the Centres Científics i Tecnològics of the Universitat de Barcelona on a Quantum Design SQUID MPMS- XL susceptometer.

**Termogravimetric analysis (TGA):** Thermogravimetric analysis measurements were performed under air flow of 24 mL/min heating from 25 °C to 900 °C at a heating rate of 10 °C/min using a Pyris 8000 Thermo Gravimetric Analyzer.

### 3.3. RESULTS AND DISCUSSION

#### 3.3.1. Synthesis and characterization of Fe<sub>3</sub>O<sub>4</sub>/Graphene and Fe<sub>3</sub>O<sub>4</sub>-TiO<sub>2</sub>/Graphene hybrids

Monodisperse 7 nm TMAOH stabilized magnetite Fe<sub>3</sub>O<sub>4</sub> NCs used in the present work were synthesized in the aqueous phase, following a modified previously reported method by Casals et. al. [46] consisting of nanoparticle precipitation at room temperature under basic conditions of a mixture of ferric salts working with stoichiometric amounts of precursors [47] in an inert atmosphere. Synthesis resulted in a black, dense, magnetic, highly concentrated (1g NCs/L) colloidal suspension of Fe<sub>3</sub>O<sub>4</sub> magnetite NCs. Transmission Electron Microscopy (TEM) image (**Figure 1A**) of as obtained Fe<sub>3</sub>O<sub>4</sub> NCs show uniform particles. Stable Fe<sub>3</sub>O<sub>4</sub> NCs were mixed with a graphene suspension and dialyzed against H<sub>2</sub>O for 3 days, allowing this way a slow and progressive depletion of the surfactant at the NCs surface, which leads to a

destabilization of the system that would typically result in aggregation. Addition of a graphitic structure to the system allows the NCs to attach to them in a randomly distributed manner instead (**Figure 1B**). The resulting Fe<sub>3</sub>O<sub>4</sub>/Graphene hybrid robustness has been tested by undergoing ultra-sonication in a bath for up to 6 h without any observable change in morphology or NCs detachment.

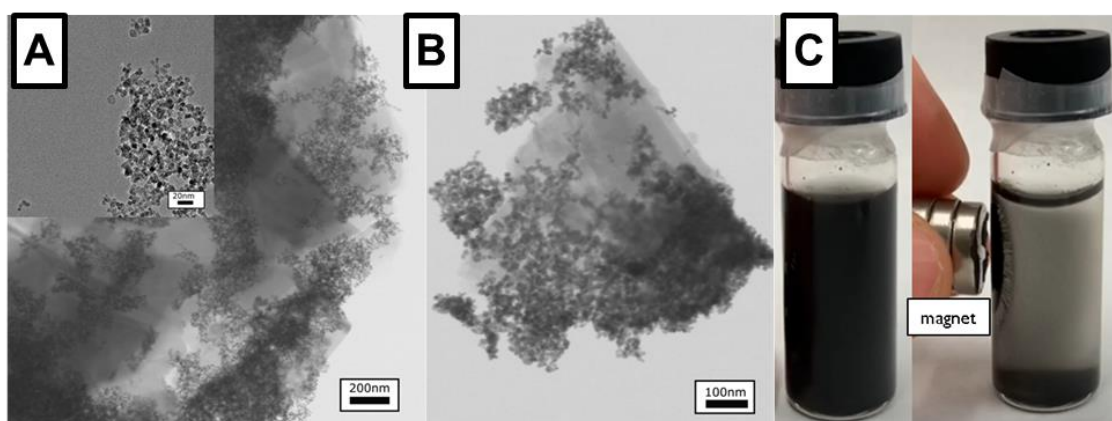


**Figure 1.** A) Fe<sub>3</sub>O<sub>4</sub> NCs TEM Bright Field Microscopy, B) Fe<sub>3</sub>O<sub>4</sub>/Graphene hybrids TEM Bright Field Microscopy images, C) Pictures of the sample before and after magnetic field exposition.

Magnetic behavior of the hybrid was assessed at 10 and 300K with a first immanation of 1T and 2T. The resulting hysteresis loops show small area (**Figure 2**), which is interpreted as a behavior with little to no energy losses (superparamagnetism). A small paramagnetic contribution was observed at high field and 300 K. Weight percentage of Fe<sub>3</sub>O<sub>4</sub> was calculated to be around 4% from using as a reference the  $M_{\text{Fe}_3\text{O}_4}$  value reported in the literature [50] (3.91-4.46%) of the sample, which is in accordance with the measurements extracted from the TGA (**Figure 2**).

The hereby presented method is effective, straightforward, versatile, highly reproducible, and scalable, thereby representing an exciting approach for the modular development of inorganic carbon-supported hybrid structures, as concluded in CHAPTER 1 of this thesis.

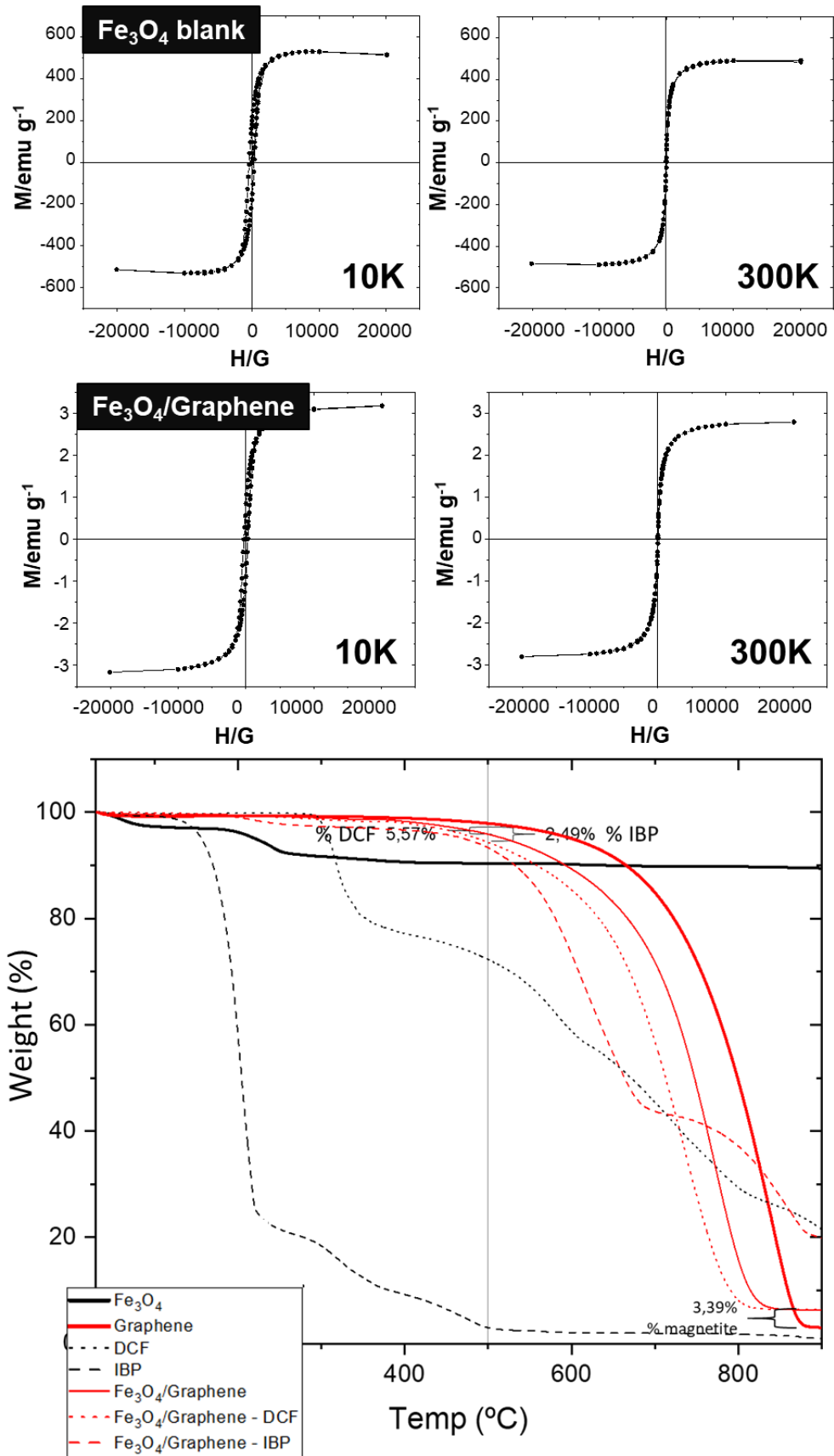


**Figure 2.** Top: SQUID hysteresis loops from  $Fe_3O_4$  NCs and  $Fe_3O_4$ /Graphene and bottom: Termogravimetric curves of the Graphene- $Fe_3O_4$  samples exposed to DCF and IBP.

### **3.3.2. Fe<sub>3</sub>O<sub>4</sub>/Graphene hybrids as an adsorbent for pharmaceutical wastewater**

In order to test the capability of graphene as adsorbent, adsorption isotherm experiments have been performed. Several drug loading experiments systematically testing drug and hybrid concentration have been executed, exposing both plain graphene as control and Fe<sub>3</sub>O<sub>4</sub>/Graphene hybrids for further comparison. All of the Fe<sub>3</sub>O<sub>4</sub>/Graphene NCs samples were still magnetic after the exposition process regardless of the particle population density, drug composition or its concentration (**Figure 1C**).

In a first experiment adsorption isotherms of both IBP and DCF, mixed with Graphene flakes were performed (**Figure 3A,B**). Briefly, 1 g/L suspensions of graphene flakes in drug solutions ranging 10-50 mg/L were prepared and vigorously shaken for the adsorption to carry on homogeneously. In the case of IBP solutions, those were prepared at pH ~6.3 Phosphate Buffer Solution (PBS) for optimal dissolution of the compound [51], while DCF could be directly dissolved in Milli-Q Water. In a second experiment the complementary study was developed (**Figure 3B, D**), drug concentration was fixed to be 68 mg/L and 100 mg/L for DCF and IBP respectively, value at which can be considered in the range of acute toxicity based on calculated short-term half maximal effective concentration (EC<sub>50</sub>) for sentinel aquatic species (*Daphnia Magna*). [26] After 24h all of the samples were centrifuged at 10.000 G for 10 minutes. The supernatant of these operations was observed by UV-Vis and loss of signal quantified versus drug control calibrations (**Figure 4**), DCF signal was monitored at 275 nm[52] whilst IBP signal was observed at the characteristic band at 222 nm and the one of its temporary products at 262 nm.[53] Three replicates of each experiment were performed and adsorption was calculated.

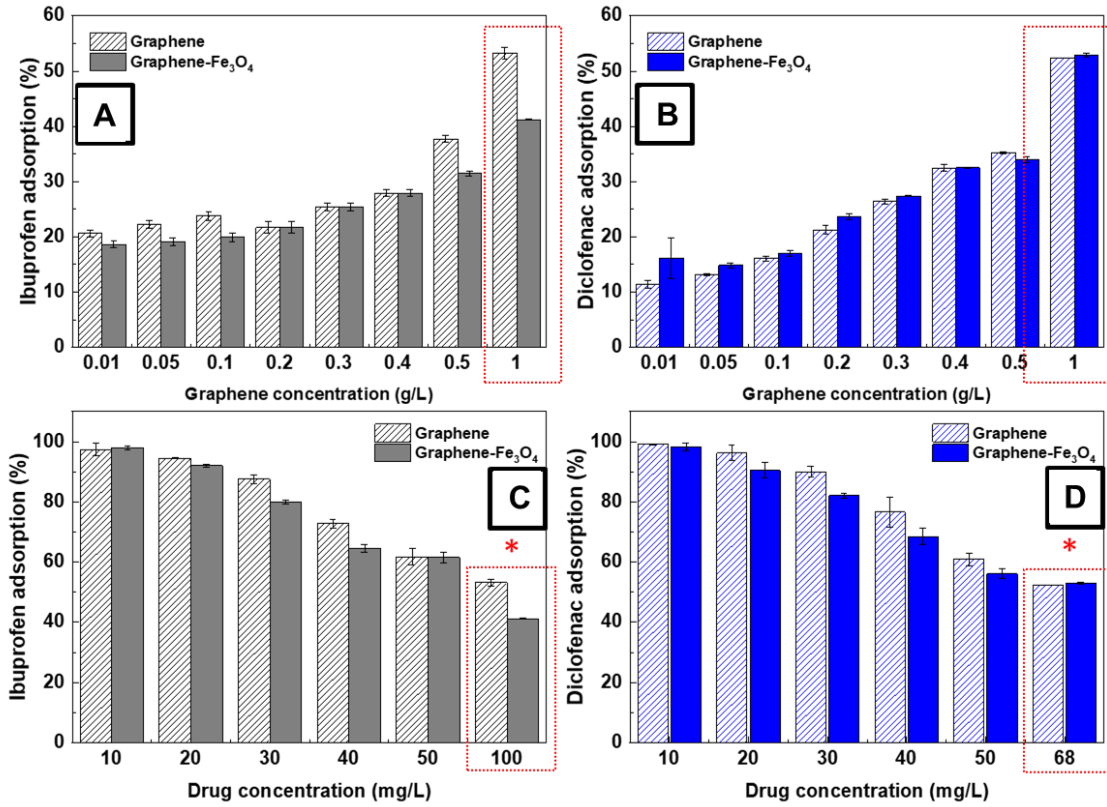


**Figure 3.** Adsorption isotherms of non-decorated graphene and Fe<sub>3</sub>O<sub>4</sub>/Graphene. A, B) final concentration of drug in solution exposed to EC<sub>50</sub> concentrations of IBP and DCF respectively being exposed to a range of solutions of differently concentrated graphene suspensions, C, D) final concentration of drug in solutions of different concentrations of IBP and DCF respectively exposed to 1 g/L graphene suspensions. Red squares show equivalent ratios of drug vs G and the concentrations used for remediation working conditions.

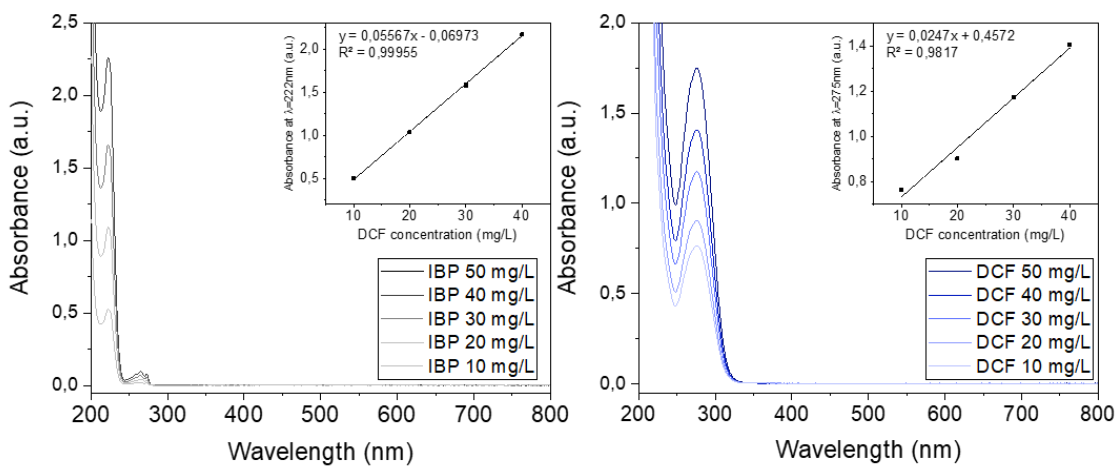


**Figure 4.** Calibration curve of DCF and IBP controls.



In both adsorption isotherm experiments, Fe<sub>3</sub>O<sub>4</sub>/Graphene hybrids and controls showed better results the higher the graphene to drug concentration ratio (**Figure 3**), presenting a linear behavior and thus validating the analysis method. When the graphitic hybrid concentration was fixed at 1 g/L (**Figure 3A,B**) it was observed a saturated trend for both of the studied drugs, suggesting a limit for the uptake. The absorption values are similar for both of the drugs (IBP in gray and DCF in blue) although for the first one adsorption values are slightly lower. The counterpart experiment, where the concentration of the studied drugs is maintained at EC<sub>50</sub> (100 mg/L in the case of IBP and 68 mg/L in the case of DCF) also showed a linear behavior (**Figure 3C,D**). These experiments allowed finding the operating working range of the hybrid which was defined to be 1 g/L of hybrid at EC<sub>50</sub> concentration for further experiments. The drastic decrease of performance at higher drug concentrations was foreseeable; graphene flakes tend to aggregate and even restack to form graphite when used in bulk-quantities during adsorption operations due to strong interplanar interactions. [54]

On one hand, surface modifications of graphene nanosheets, such as graphene oxidation, prevent aggregation and increase the effective surface area, thus, making them more attractive than pristine graphene. On the other hand, GO has weak binding affinity for anionic compounds due to strong electrostatic repulsion between them. In its purest form, graphene is impermeable, thus, exposed graphitic surface of the synthesized hybrid allows electrostatic interactions, via H-bonds, between Graphene Fe<sub>3</sub>O<sub>4</sub> NCs and the studied drugs. [32] This adsorption process has been proved to occur in the first 80min of exposure.

In **Figure 3**, control experiments where bare graphene was exposed to the drugs are shown. These controls showed better results than the Fe<sub>3</sub>O<sub>4</sub>/Graphene hybrid in all of the cases. This was hypothesized to happen because graphene is a better absorber than

oxide particles, so part of the available surface would be lost when occupied by Fe<sub>3</sub>O<sub>4</sub> NCs.

In the same line of thought, the occupation of adsorption sites by the NCs and its effect on the loss of adsorption was tested by:

- i) *Discarding drug degradation by Fe<sub>3</sub>O<sub>4</sub> NCs:* Comparing the 222 nm UV-Vis signal of IBP and its temporary products at 262 nm after the exposition which maintain a signal ratio  $\lambda_{222\text{nm}}/\lambda_{262\text{nm}} \approx 25$  (**Figure 5**) and, thus, demonstrate the adsorption of the drug as a whole entity instead of the degradation of the 222 nm ibuprofen feature to the 262 nm signature of the temporary products, which would indicate a Fenton-like reaction of the drug with the Fe<sub>3</sub>O<sub>4</sub> NCs [53], [55]

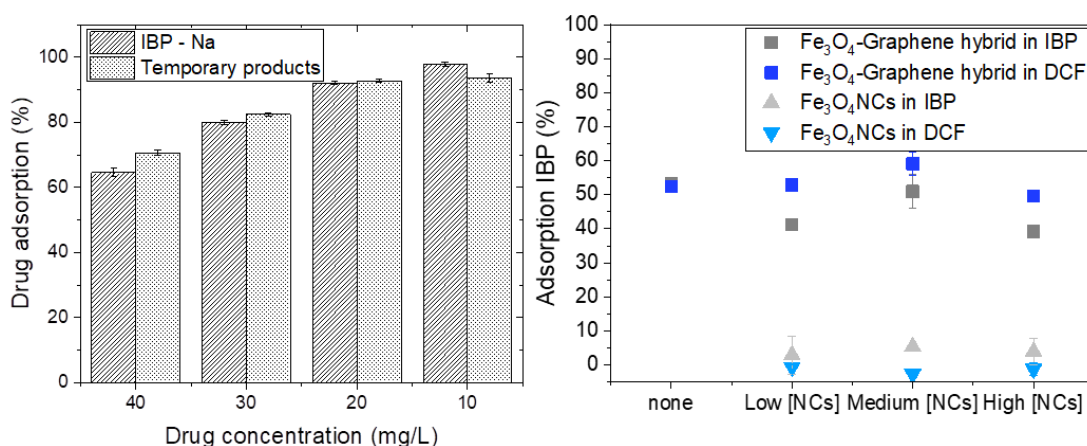


**Figure 5.** Left: plot showing the difference between the 222 nm peak characteristic of IBP-Na and the 262 nm signature from the temporary products from the dose-response experiment. Right: Representation of the drug adsorption onto the Fe<sub>3</sub>O<sub>4</sub>/Graphene hybrid prepared with different Fe<sub>3</sub>O<sub>4</sub> NCs concentration, Fe<sub>3</sub>O<sub>4</sub> NCs controls in a lighter colour, when exposed to 68 mg/L and 100 mg/L of DCF and IBP respectively.

- ii) *Assessing the impact of Fe<sub>3</sub>O<sub>4</sub> NCs density on the adsorption of the sample:* Isolated and clean Fe<sub>3</sub>O<sub>4</sub> NCs were exposed to the media showing no adsorption of the drugs. Drug abatement was tested by preparing Graphene/Fe<sub>3</sub>O<sub>4</sub> NCs samples with different NCs densities (0,  $3.2 \cdot 10^{14}$ ,  $3.2 \cdot 10^{15}$ ,

3.2·10<sup>16</sup> NCs/mg graphene) and the corresponding amount of isolated NCs. A designed 1 g/L suspension of hybrid was exposed to the before mentioned 68 mg/L and 100 mg/L for DCF and IBP respectively solutions under the same exposition parameters.

It is then concluded that the Fe<sub>3</sub>O<sub>4</sub> NCs presence on the graphene surface does not significantly change the adsorption of the drug onto the surface, alterations between adsorption depending on the NCs density are, therefore, explained to be due to experimental error from incrustation of the hybrid on the walls of the dialysis bag and/or material losses during the process of purification.

### **3.3.3. Fe<sub>3</sub>O<sub>4</sub>/Graphene oxide hybrids as an adsorbent for pharmaceutical wastewater**

Since Fe<sub>3</sub>O<sub>4</sub>/Graphene samples rapidly sediment at the bottom of the storage vials showing little to none colloidal behavior due to the aggregation (stacking) of the graphene flakes, same experiments as the ones described above were performed using graphene oxide (GO) synthesized via a modified Hummer's method in the laboratory [49] and characterized by UV-Vis, FT-IR and Electron Microscopy (**Figure 6**). Oxidation under acidic conditions at room temperature was carried for 6 days, an aliquot was taken on the 3<sup>rd</sup> day of the experiment. Samples were thoroughly washed until the pH of the solution was of 5 and concentration of the sample normalized at 1 g/L after drying in an oven at 70 °C overnight.

Both the Fe<sub>3</sub>O<sub>4</sub>/GO hybrid and the controls showed a notable worsening of the adsorption when exposed to IBP and better results in the case of DCF (**Figure 6D**), a trend could be observed in regards of this performance decline depending on the oxidation state of graphene: the longer oxidation, the worse were the results for IBP adsorption and the better for DCF adsorption. This is most probably due to the

apolar/polar character of the species. Graphene most likely interacts via  $\pi$ - $\pi$  with the benzoic ring of both species while, in the case of graphene oxide, at the expenses of said benzoic rings, intermolecular forces are introduced to the system such as hydrogen bridges. These new interactions would explain the improvement of results in the case of DCF, which has free charge in its structure (from the Cl<sup>-</sup> and the NH<sup>+</sup>) while results from IBP with only a polar group are clearly worse.

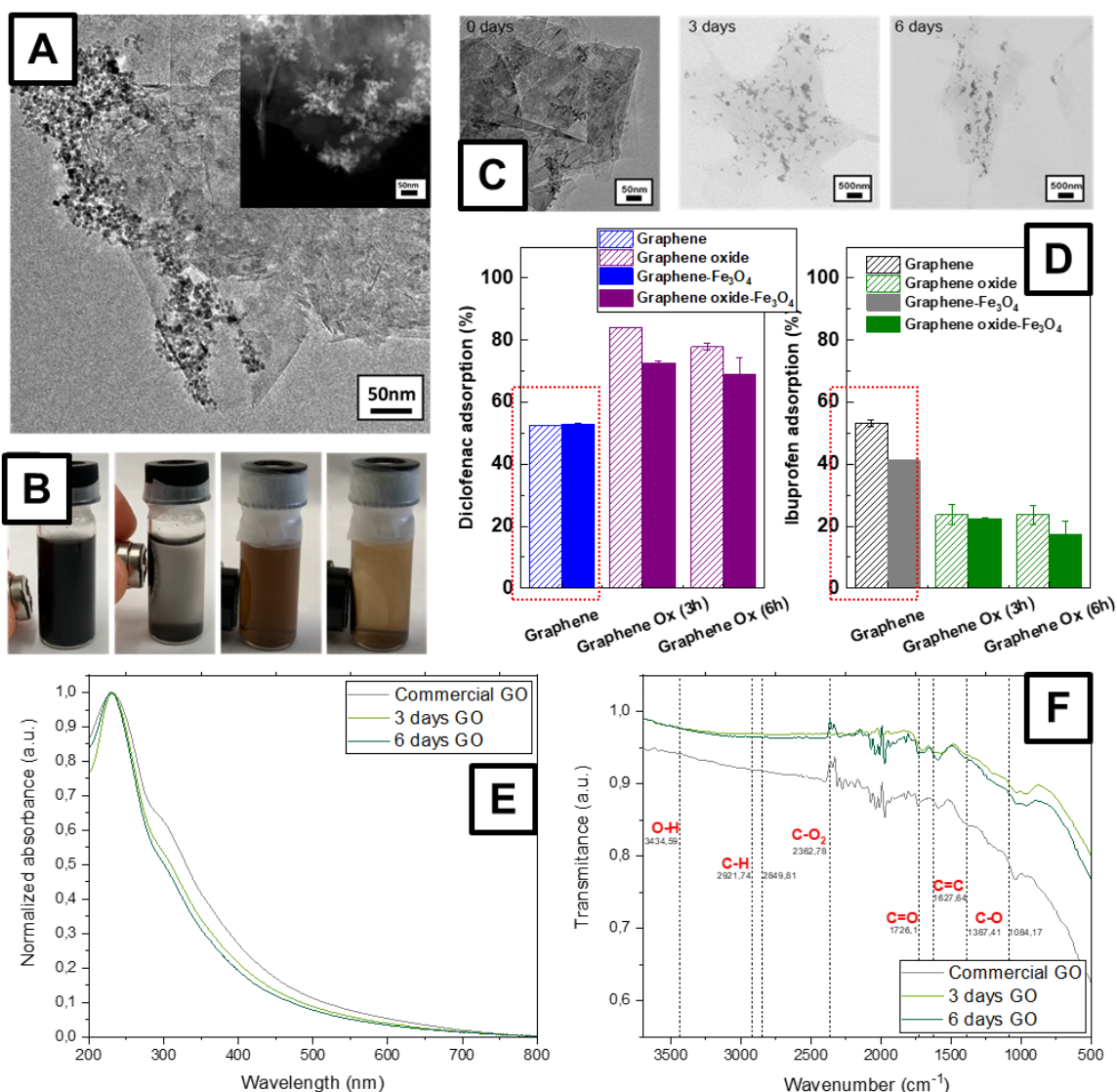


**Figure 6.** A) TEM Microscopy of the Fe<sub>3</sub>O<sub>4</sub>/Graphene hybrid, B) magnetic response of the Fe<sub>3</sub>O<sub>4</sub>/Graphene and Fe<sub>3</sub>O<sub>4</sub>/Graphene Oxide hybrid, C) TEM Microscopy of the Fe<sub>3</sub>O<sub>4</sub>/Graphene oxidized hybrids, D) drug adsorption corresponding to the Fe<sub>3</sub>O<sub>4</sub>/Graphene oxidized hybrids, F) FT-IR of the used GO.

### **3.3.4. Fe<sub>3</sub>O<sub>4</sub>-TiO<sub>2</sub>/Graphene hybrids for the recyclability of the remediation system**

Another surface modification involving a multi component hybrid (**Figure 7**) that allowed the photocatalytic degradation of the captured pharmaceuticals was developed. In that case, TiO<sub>2</sub> NCs were added to the hybrid. TiO<sub>2</sub> NCs were synthesized by adapting an isopropoxide precipitation method which is well described in the literature. [56] Samples were exposed to the usual EC<sub>50</sub> concentration of the studied drugs (100 mg/L and 68 mg/mL for the IBP and the DCF respectively) at 1 g/L of hybrid. The adsorbed drugs have been tried to be degraded before a second exposition has been performed, looking for hybrid recyclability. Firstly, data from a first exposition was taken from the supernatant resulting after 24 h of incubation. Secondly, same samples were then exposed to 1 mM and 100 mM H<sub>2</sub>O<sub>2</sub> solutions which emulated the Reactive Oxygen Species (ROS) that would be generated from a photocatalysis experiment to assess the recyclability of the hybrid provided from the degradation of the captured species. On the one hand, the hybrid showed recyclability in the case of DCF (**Figure 7C**, blue), which consistently adsorbed around 25% of the sample again when allowed to oxidize in presence of the hydrogen peroxide. Hydrogen peroxide is proposed in the literature as the responsible of the degradation of DCF when in its hydroxyl form in a Fenton-like reaction when in presence of Fe<sup>2+</sup> species. [57], [58] On the other hand, in this second exposition intake of the IBP performance decreased from approximately 70% of adsorption in the first exposition to almost zero in the second one (**Figure 7C**, grey). This suggests the space onto the graphitic surface has been occupied already and thus, unavailable for the peroxide to oxidize the already adsorbed drug probably due to the existing equilibrium in between the drug and its secondary products, and the energetically difficult pathway for the species to degrade which also generates byproducts of highly polar character.[53], [55] Nevertheless, when the

samples were exposed to a higher  $H_2O_2$  concentration, IBP showed recyclability too, especially with the  $TiO_2$  containing hybrid (**Figure 7C**, grey). This indicates a successful and complete degradation of both IBP and IBP byproducts, the equilibrium of which did not allow for the reaction to evolve in previous experiments. Control

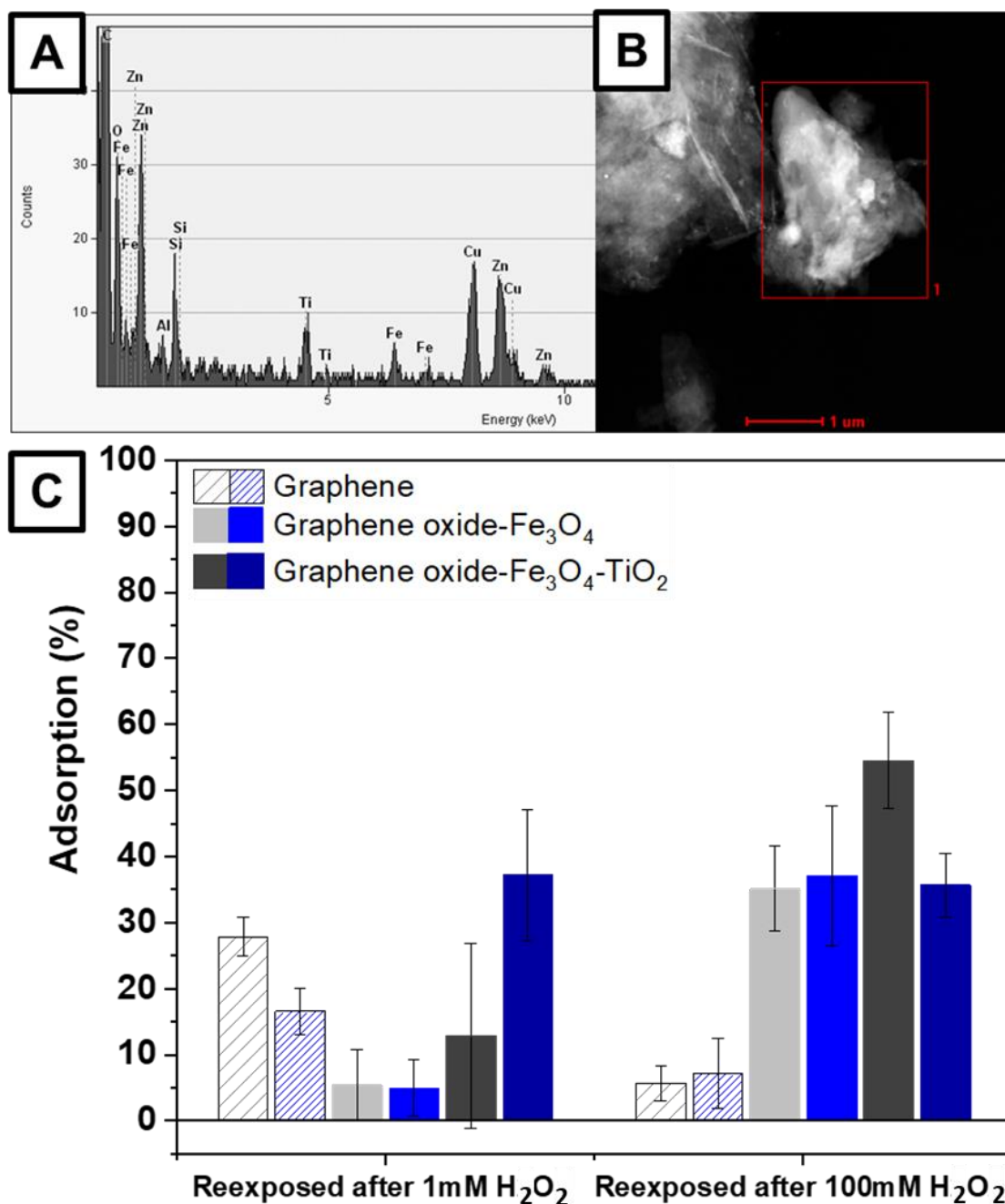


**Figure 7.** A) EELS spectra of the  $Fe_3O_4$ - $TiO_2$ /Graphene hybrid, B) STEM HAADF microscopy of the sample and, C) Concentration of the studied drugs (DCF in blue and IBP in grey) after different hybrid configurations have been exposed to  $EC_{50}$  solutions and  $H_2O_2$  concentrations (increasing with colour intensity).

experiments were resuspended in H<sub>2</sub>O instead of H<sub>2</sub>O<sub>2</sub> and did not show any desorption of the drugs among time.

### 3.4. CONCLUSIONS AND PERSPECTIVES

In conclusion, in this work we have reported a complete characterization and deep understanding for the synthesis graphene-based magnetic hybrid and the design for its application removing of emerging pollutants –IBP and DCF– when they are present at low concentrations such as the ones we can find in nature. Modifications of the Fe<sub>3</sub>O<sub>4</sub>/Graphene hybrid have been made, allowing us to understand i) the role of the functional groups at the surface and the polarity of the adsorbed species in the case of the Graphene Oxide and ii) the synergy that can offer a multi-modal hybrid in the case of the Fe<sub>3</sub>O<sub>4</sub>-TiO<sub>2</sub>/Graphene hybrid. All of this modifications have been useful also as a validation of the decoration method proposed.

Future work should be focused on the understanding of the specificity of the method, assessment of the drug adsorption in more realistic conditions and the recyclability of the hybrid when re-exposed to the drugs several times.

### 3.5. REFERENCES

- [1] M. A. Shannon, P. W. Bohn, M. Elimelech, J. G. Georgiadis, B. J. Mariñas, and A. M. Mayes, “Science and technology for water purification in the coming decades,” *Nature*, vol. 452, no. 7185. Nature Publishing Group, pp. 301–310, 20-Mar-2008.
- [2] P. E. Stackelberg, E. T. Furlong, M. T. Meyer, S. D. Zaugg, A. K. Henderson, and D. B. Reissman, “Persistence of pharmaceutical compounds and other organic wastewater contaminants in a conventional drinking-water-treatment plant,” *Sci. Total Environ.*, vol. 329, no. 1–3, pp. 99–113, Aug. 2004.
- [3] C. G. Daughton and T. A. Ternes, “Pharmaceuticals and personal care products in the environment: Agents of subtle change?,” *Environmental Health Perspectives*, vol. 107, no. SUPPL. 6. Public Health Services, US Dept of Health and Human Services, pp. 907–938, 1999.

- [4] M. Taheran, M. Naghdi, S. K. Brar, M. Verma, and R. Y. Surampalli, “Emerging contaminants: Here today, there tomorrow!,” *Environmental Nanotechnology, Monitoring and Management*, vol. 10. Elsevier B.V., pp. 122–126, 01-Dec-2018.
- [5] R. M. May, “Thresholds and breakpoints in ecosystems with a multiplicity of stable states,” *Nature*, vol. 269, no. 5628. Nature Publishing Group, pp. 471–477, 01-Oct-1977.
- [6] C. S. Holling, “Resilience and Stability of Ecological Systems,” *Annu. Rev. Ecol. Syst.*, vol. 4, no. 1, pp. 1–23, Nov. 1973.
- [7] P. C. Mahoney and M. J. Bishop, “Assessing risk of estuarine ecosystem collapse,” *Ocean and Coastal Management*, vol. 140. Elsevier Ltd, pp. 46–58, 01-May-2017.
- [8] A. Marshall, H. Schulte to Bühne, L. Bland, and N. Pettoelli, “Assessing ecosystem collapse risk in ecosystems dominated by foundation species: The case of fringe mangroves,” *Ecol. Indic.*, vol. 91, pp. 128–137, Aug. 2018.
- [9] D. Das, R. J. Cuthbert, R. D. Jakati, and V. Prakash, “Diclofenac is toxic to the Himalayan Vulture *Gyps himalayensis*,” *Bird Conserv. Int.*, vol. 21, no. 1, pp. 72–75, Mar. 2011.
- [10] A. A. Cunningham *et al.*, “Indian vultures: Victims of an infectious disease epidemic?,” *Anim. Conserv.*, vol. 6, no. 3, pp. 189–197, Aug. 2003.
- [11] J. Lee, K. Ji, Y. Lim Kho, P. Kim, and K. Choi, “Chronic exposure to diclofenac on two freshwater cladocerans and Japanese medaka,” *Ecotoxicol. Environ. Saf.*, vol. 74, no. 5, pp. 1216–1225, Jul. 2011.
- [12] S. Han *et al.*, “Endocrine disruption and consequences of chronic exposure to ibuprofen in Japanese medaka (*Oryzias latipes*) and freshwater cladocerans *Daphnia magna* and *Moina macrocopa*,” *Aquat. Toxicol.*, vol. 98, no. 3, pp. 256–264, Jul. 2010.
- [13] I. Sirés and E. Brillas, “Remediation of water pollution caused by pharmaceutical residues based on electrochemical separation and degradation technologies: A review,” *Environment International*, vol. 40, no. 1. Elsevier Ltd, pp. 212–229, 01-Apr-2012.
- [14] R. Wise, “Antimicrobial resistance: priorities for action,” *J. Antimicrob. Chemother.*, vol. 49, no. 4, pp. 585–586, Apr. 2002.
- [15] O. A. H. Jones, N. Voulvoulis, and J. N. Lester, “Human pharmaceuticals in wastewater treatment processes,” *Critical Reviews in Environmental Science and Technology*, vol. 35, no. 4. Taylor & Francis Group, pp. 401–427, 2005.
- [16] M. Patel, R. Kumar, K. Kishor, T. Mlsna, C. U. Pittman, and D. Mohan,



- “Pharmaceuticals of emerging concern in aquatic systems: Chemistry, occurrence, effects, and removal methods,” *Chemical Reviews*, vol. 119, no. 6. American Chemical Society, pp. 3510–3673, 27-Mar-2019.
- [17] K. Kümmerer, “Drugs in the environment: Emission of drugs, diagnostic aids and disinfectants into wastewater by hospitals in relation to other sources - A review,” *Chemosphere*, vol. 45, no. 6–7, pp. 957–969, Nov. 2001.
- [18] K. Kümmerer, “Pharmaceuticals in the Environment – A Brief Summary,” in *Pharmaceuticals in the Environment*, Springer Berlin Heidelberg, 2008, pp. 3–21.
- [19] M. D. Hernando, M. Mezcua, A. R. Fernández-Alba, and D. Barceló, “Environmental risk assessment of pharmaceutical residues in wastewater effluents, surface waters and sediments,” *Talanta*, vol. 69, no. 2, pp. 334–342, Apr. 2006.
- [20] A. Ginebreda, I. Muñoz, M. L. de Alda, R. Brix, J. López-Doval, and D. Barceló, “Environmental risk assessment of pharmaceuticals in rivers: Relationships between hazard indexes and aquatic macroinvertebrate diversity indexes in the Llobregat River (NE Spain),” *Environ. Int.*, vol. 36, no. 2, pp. 153–162, Feb. 2010.
- [21] E. Godfrey, W. W. Woessner, and M. J. Benotti, “Pharmaceuticals in on-site sewage effluent and ground water, Western Montana,” *Ground Water*, vol. 45, no. 3, pp. 263–271, May 2007.
- [22] L. H. Heckmann *et al.*, “Chronic toxicity of ibuprofen to *Daphnia magna*: Effects on life history traits and population dynamics,” *Toxicol. Lett.*, vol. 172, no. 3, pp. 137–145, Aug. 2007.
- [23] J. Du, C. F. Mei, G. G. Ying, and M. Y. Xu, “Toxicity Thresholds for Diclofenac, Acetaminophen and Ibuprofen in the Water Flea *Daphnia magna*,” *Bull. Environ. Contam. Toxicol.*, vol. 97, no. 1, pp. 84–90, Jul. 2016.
- [24] M. Parolini and A. Binelli, “Sub-lethal effects induced by a mixture of three non-steroidal anti-inflammatory drugs (NSAIDs) on the freshwater bivalve *Dreissena polymorpha*,” *Ecotoxicology*, vol. 21, no. 2, pp. 379–392, Mar. 2012.
- [25] J. Żur, A. Piński, A. Marchlewicz, K. Hupert-Kocurek, D. Wojcieszynska, and U. Guzik, “Organic micropollutants paracetamol and ibuprofen—toxicity, biodegradation, and genetic background of their utilization by bacteria,” *Environmental Science and Pollution Research*, vol. 25, no. 22. Springer Verlag, pp. 21498–21524, 01-Aug-2018.
- [26] M. Cleuvers, “Mixture toxicity of the anti-inflammatory drugs diclofenac, ibuprofen, naproxen, and acetylsalicylic acid,” *Ecotoxicol. Environ. Saf.*, vol. 59, no. 3, pp. 309–

- 315, Nov. 2004.
- [27] P. De Voogt, M. L. Janex-Habibi, F. Sacher, L. Puijker, and M. Mons, “Development of a common priority list of pharmaceuticals relevant for the water cycle,” *Water Sci. Technol.*, vol. 59, no. 1, pp. 39–46, Jan. 2009.
- [28] J. L. Santos, I. Aparicio, and E. Alonso, “Occurrence and risk assessment of pharmaceutically active compounds in wastewater treatment plants. A case study: Seville city (Spain),” *Environ. Int.*, vol. 33, no. 4, pp. 596–601, May 2007.
- [29] L. A. Al-Khateeb, S. Almotiry, and M. A. Salam, “Adsorption of pharmaceutical pollutants onto graphene nanoplatelets,” *Chem. Eng. J.*, vol. 248, pp. 191–199, Jul. 2014.
- [30] P. E. Stackelberg, E. T. Furlong, M. T. Meyer, S. D. Zaugg, A. K. Henderson, and D. B. Reissman, “Persistence of pharmaceutical compounds and other organic wastewater contaminants in a conventional drinking-water-treatment plant,” *Sci. Total Environ.*, vol. 329, no. 1–3, pp. 99–113, Aug. 2004.
- [31] Y. Zhou *et al.*, “Chiral pharmaceuticals: Environment sources, potential human health impacts, remediation technologies and future perspective,” *Environment International*, vol. 121. Elsevier Ltd, pp. 523–537, 01-Dec-2018.
- [32] A. Khan *et al.*, “The role of graphene oxide and graphene oxide-based nanomaterials in the removal of pharmaceuticals from aqueous media: a review.”
- [33] W. F. Jardim, S. G. Moraes, and M. M. K. Takiyama, “Photocatalytic degradation of aromatic chlorinated compounds using TiO<sub>2</sub>: Toxicity of intermediates,” *Water Res.*, vol. 31, no. 7, pp. 1728–1732, Jul. 1997.
- [34] L. Rizzo, “Bioassays as a tool for evaluating advanced oxidation processes in water and wastewater treatment,” *Water Research*, vol. 45, no. 15. Elsevier Ltd, pp. 4311–4340, 01-Oct-2011.
- [35] G. Caviglioli, P. Valeria, P. Brunella, C. Sergio, A. Attilia, and B. Gaetano, “Identification of degradation products of Ibuprofen arising from oxidative and thermal treatments,” *J. Pharm. Biomed. Anal.*, vol. 30, no. 3, pp. 499–509, Sep. 2002.
- [36] I. Ali and V. K. Gupta, “Advances in water treatment by adsorption technology,” *Nat. Protoc.*, vol. 1, no. 6, pp. 2661–2667, Jan. 2007.
- [37] M. Gavrilescu, K. Demnerová, J. Aamand, S. Agathos, and F. Fava, “Emerging pollutants in the environment: present and future challenges in biomonitoring, ecological risks and bioremediation,” *N. Biotechnol.*, vol. 32, no. 1, pp. 147–156, Jan. 2015.

- [38] V. Chandra, J. Park, Y. Chun, J. W. Lee, I.-C. Hwang, and K. S. Kim, “Water-Dispersible Magnetite-Reduced Graphene Oxide Composites for Arsenic Removal,” *ACS Nano*, vol. 4, no. 7, pp. 3979–3986, Jul. 2010.
- [39] H. Sun, L. Cao, and L. Lu, “Magnetite/Reduced Graphene Oxide Nanocomposites: One Step Solvothermal Synthesis and Use as a Novel Platform for Removal of Dye Pollutants,” *Nano Res*, vol. 4, no. 6, pp. 550–562, 2011.
- [40] S. M. Maliyekkal *et al.*, “Graphene: A reusable substrate for unprecedented adsorption of pesticides,” *Small*, vol. 9, no. 2, pp. 273–283, Jan. 2013.
- [41] Y. Zhu *et al.*, “Graphene and graphene oxide: Synthesis, properties, and applications,” *Adv. Mater.*, vol. 22, no. 35, pp. 3906–3924, Sep. 2010.
- [42] F. D. Guerra, M. F. Attia, D. C. Whitehead, and F. Alexis, “Nanotechnology for environmental remediation: Materials and applications,” *Molecules*, vol. 23, no. 7. MDPI AG, p. 1760, 18-Jul-2018.
- [43] Y. Li, J. Chu, J. Qi, and X. Li, “An easy and novel approach for the decoration of graphene oxide by Fe<sub>3</sub>O<sub>4</sub> nanoparticles,” *Appl. Surf. Sci.*, vol. 257, no. 14, pp. 6059–6062, May 2011.
- [44] J. Z. He, X. X. Wang, Y. L. Zhang, and M. S. Cao, “Small magnetic nanoparticles decorating reduced graphene oxides to tune the electromagnetic attenuation capacity,” *J. Mater. Chem. C*, vol. 4, no. 29, pp. 7130–7140, 2016.
- [45] V. Georgakilas *et al.*, “Noncovalent Functionalization of Graphene and Graphene Oxide for Energy Materials, Biosensing, Catalytic, and Biomedical Applications,” *Chem. Rev.*, vol. 116, no. 9, pp. 5464–5519, 2016.
- [46] E. Casals *et al.*, “Programmed Iron Oxide Nanoparticles Disintegration in Anaerobic Digesters Boosts Biogas Production,” *Small*, vol. 10, no. 14, pp. 2801–2808, Jul. 2014.
- [47] R. Massart, “Preparation of Aqueous Magnetic Liquids in Alkaline and Acidic Media,” *IEEE Transactions on Magnetics*, vol. 17, no. 2. pp. 1247–1248, 1981.
- [48] A. Pottier, S. Cassaignon, C. Chanéac, F. Villain, E. Tronc, and J. P. Jolivet, “Size tailoring of TiO<sub>2</sub>anatase nanoparticles in aqueous medium and synthesis of nanocomposites. Characterization by Raman spectroscopy,” *J. Mater. Chem.*, vol. 13, pp. 877–882, 2003.
- [49] K. O. Olumurewa, B. Olofinjana, O. Fasakin, M. A. Eleruja, and E. O. B. Ajayi, “Characterization of High Yield Graphene Oxide Synthesized by Simplified Hummers

- Method,” *Graphene*, vol. 06, no. 04, pp. 85–98, Oct. 2017.
- [50] M. I. Dar and S. A. Shivashankar, “Single crystalline magnetite, maghemite, and hematite nanoparticles with rich coercivity,” *RSC Adv.*, vol. 4, no. 8, pp. 4105–4113, Dec. 2014.
- [51] K. A. Levis, M. E. Lane, and O. I. Corrigan, “Effect of buffer media composition on the solubility and effective permeability coefficient of ibuprofen,” *Int. J. Pharm.*, vol. 253, no. 1–2, pp. 49–59, Mar. 2003.
- [52] M. E. Palomo, M. P. Ballesteros, and P. Frutos, “Analysis of diclofenac sodium and derivatives,” *J. Pharm. Biomed. Anal.*, vol. 21, no. 1, pp. 83–94, Oct. 1999.
- [53] J. Choina, H. Kosslick, C. Fischer, G. U. Flechsig, L. Frunza, and A. Schulz, “Photocatalytic decomposition of pharmaceutical ibuprofen pollutions in water over titania catalyst,” *Appl. Catal. B Environ.*, vol. 129, pp. 589–598, Jan. 2013.
- [54] J. S. Cheng, J. Du, and W. Zhu, “Facile synthesis of three-dimensional chitosan-graphene mesostructures for reactive black 5 removal,” *Carbohydr. Polym.*, vol. 88, no. 1, pp. 61–67, Mar. 2012.
- [55] F. Hua Li *et al.*, “Photodegradation of Ibuprofen Under UV-Vis Irradiation: Mechanism and Toxicity of Photolysis Products.”
- [56] A. Pottier, S. Cassaignon, C. Chanéac, F. Villain, E. Tronc, and J. P. Jolivet, “Size tailoring of TiO<sub>2</sub> anatase nanoparticles in aqueous medium and synthesis of nanocomposites. Characterization by Raman spectroscopy,” *J. Mater. Chem.*, vol. 13, no. 4, pp. 877–882, Apr. 2003.
- [57] R. Banaschik, H. Jablonowski, P. J. Bednarski, and J. F. Kolb, “Degradation and intermediates of diclofenac as instructive example for decomposition of recalcitrant pharmaceuticals by hydroxyl radicals generated with pulsed corona plasma in water,” *J. Hazard. Mater.*, vol. 342, pp. 651–660, Jan. 2018.
- [58] Y. Y. Jiang *et al.*, “Degradation of diclofenac sodium using Fenton-like technology based on nano-calcium peroxide,” *Sci. Total Environ.*, vol. 773, p. 144801, Jun. 2021.



## 4. GENERAL CONCLUSIONS

All of the nanostructures described in this work have been prepared in the laboratory. For doing so, colloidal solutions of a wide array of NCs have been prepared via aqueous and non-aqueous methods following previously described synthesis routes explained in CHAPTER 1.

In **CHAPTER 1** a general approach for the decoration of CNSs is explained. All of the described compounds have been characterised to determine their morphology, size and composition by using different techniques such as UV-Vis spectroscopy, electron microscopy (SEM, TEM, HR-TEM, HAADF-STEM microscopy), EDX elemental mapping composition analysis, EELS chemical composition analysis, XRD and XPS. The nature of both surfaces is explored in order to tune and explain the phenomena. Carbon nanostructures exhibit a hydrophobic behavior whilst nanoparticles are traditionally stabilized using surfactants that avoid their aggregation or dissolution. A controlled depletion of the surfactant allows for the nanoparticle to meet with the CNS before aggregation, allowing for a powerful tool to use in order to achieve a carbon-nanoparticle structure with better control of the properties.

In **CHAPTER 2** a first application of the developed hybrids is studied in the frame of water splitting. A hybrid photocatalyst made of TiO<sub>2</sub> NCs as light absorber, Ru-tda molecular water oxidation catalyst SWCNTs as linkers and electron transfer

platforms is presented and characterized. The system presents a remarkable behavior at neutral pH, with an AQY of 0.9% and a TON of 229 upon illumination. Interestingly, the hybrid remains non-degraded after the electrochemical testing, proving its robustness. The reported results are the seed of a broad and interesting line of research that could lead to a new family of hybrid catalysts based on a building-block strategy to produce clean and renewable fuels.

In **CHAPTER 3** the application of a Fe<sub>3</sub>O<sub>4</sub> NCs/graphene hybrid is tackled for the remediation of waters removing pharmaceutical pollutants. A complete characterization and deep understanding for the synthesis graphene-based magnetic hybrid and its application removing of emerging pollutants –IBP and DCF– when they are present at low concentrations such as the ones we can find in the environment is reported. The system has been modified by i) oxidation of graphene and ii) addition of TiO<sub>2</sub> NCs that would allow for the photocatalysis of the captured drugs and, thus, the recyclability of the hybrid. These modifications allowed to understand i) the role of the functional groups at the surface and the polarity of the adsorbed species in the case of the Graphene Oxide and ii) the synergy that can offer a multi-modal hybrid in the case of the Fe<sub>3</sub>O<sub>4</sub>-TiO<sub>2</sub>/Graphene hybrid.

# APPENDIX I. CHARACTERIZATION TECHNIQUES

**UV–Vis Spectroscopy:** UV–Visible spectra were acquired with a Cary 60 spectrophotometer. A dilution of 1:10 in volume of as-synthesized NC solution in Milli-Q Water was placed in a quartz cuvette and spectral analysis was recorded in the range 200–800 nm at room temperature.

**Ultrasounds:** Ultrasound bath (Branson 2510) was used at 25 °C for 1 h in order to observe any changes to the noble metal NCs – Graphene hybrid.

**Transmission Electron Microscopy (TEM):** **CHAPTER 1** The morphology of the hybrids described in **CHAPTER 1**, SWCNT/TiO<sub>2</sub>-NCs and Ru-tda/SWCNT/TiO<sub>2</sub>-NCs hybrids described in **CHAPTER 2**, and Fe<sub>3</sub>O<sub>4</sub>/Graphene hybrids described in **CHAPTER 3** were visualized using FEI Magellan 400L XHR SEM, in transmission mode operated at 20 kV. Morphology of the NCs described in **CHAPTER 1**, SWCNT/TiO<sub>2</sub>-NCs and Ru-tda/SWCNT/TiO<sub>2</sub>-NCs hybrids described in **CHAPTER 2**, and Fe<sub>3</sub>O<sub>4</sub>NCs described in **CHAPTER 3** was observed using a FEI Tecnai G2 F20 HR(S)TEM operated at 200kV in Bright Field mode. EDX of the samples were performed on an EDAX super ultra-thin window (SUTW) X-ray detector coupled to the Tecnai G2 F20 microscope. The morphology of the TiO<sub>2</sub> NCs described in **CHAPTER 2** was visualized using a JEM 1210, JEOL microscope in transmission mode operated at 120 k. A droplet (10 μL) of the sample was drop casted onto a piece



of ultrathin carbon-coated 200-mesh copper grid (Ted-pella, Inc.) and left to dry in air. TEM images were used for the size distribution measurements. For each sample, the size of a significant number of crystals was measured and the average size and standard deviation obtained. For hybrid morphological characterization the same drop casting process was performed with previous 5-minute ultrasonication of a 1:5 dilution of the samples

**Image analysis:** The program *Nano2* runs in command, by informing of the background (bright field, dark field), the scale (1 nm/pixel), the expected diameter range (2,100nm), the eccentricity of the particles (>75%) and the gray range (automatic).

**X-ray Photoelectron Spectroscopy (XPS)** was performed on a SPECS system equipped with a monochromatic Al source operating at 300 W and a Phoibos 150 analyser. The pass energy of the hemispherical analyser was set at 20 eV and the energy step of high-resolution spectra was set at 0.05 eV. Binding energy (BE) values were referred to the C 1 s peak at 285.0 eV. Data processing was performed with the Casa XPS software.

## APPENDIX II. LIST OF CONTRIBUTIONS

### SCIENTIFIC ARTICLES

M. Ventosa, **J. Oliveras**, N. G. Bastús, C. Gimbert-Suriñach, V. Puentes, and A. Llobet, “Nanocrystal–Molecular Hybrids for the Photocatalytic Oxidation of Water,” *ACS Appl. Energy Mater.*, Sep. 2020. (*equal contribution*)

L. Marcon, **J. Oliveras**, and V. F. Puentes, “In situ nanoremediation of soils and groundwaters from the nanoparticle’s standpoint: A review,” *Science of the Total Environment*, vol. 791. Elsevier B.V., p. 148324, 15-Oct-2021.

### ORAL CONTRIBUTIONS

**September 2020:** Oral contribution to JPhD2020 organised by ICMAB ‘Facile, fast and high reproducible method for nanocrystal decoration of carbon nanostructures’

**July 2021:** Speaker at NanoGe iNCNC: Synthesis and application study of Fe<sub>3</sub>O<sub>4</sub>/Graphene hybrid for water remediation.

**April 2021:** Speaker at News in Nanocrystals seminar: Presenting Nanocrystal–Molecular Hybrids for the Photocatalytic Oxidation of Water: a modular approach.

**December 2021:** Speaker at the first Severo Ochoa Workshop on Environment presenting: Synthesis and application study of Fe<sub>3</sub>O<sub>4</sub>/Graphene hybrid for water remediation.

## POSTER CONTRIBUTIONS

**May 2019:** Attendance to Nanospain Conference and presentation of the Poster ‘Facile, fast and highly reproducible method for Nanocrystals coupling to Carbon Nanotubes’.

**July 2021:** Attendance to Exciting nanostructures: Characterizing advanced confined Systems and presentation of a poster: Towards a general strategy for the functionalization of carbon nanostructures by inorganic nanocrystals and related applications.

## SCIENTIFIC DISSEMINATION AND OTHER CONTRIBUTIONS

Organizer of the Scientific Imaging Contest at ICN2 ‘Art Meets Nano’.

**June 2021:** Poster jury at BIST Symposium on Microscopy, Nanoscopy and Imaging Sciences.

**March 2021:** Poster jury at II SCN<sup>2</sup> Dresselhaus prize.

**Feb 2019, Feb 2020, Feb 2021:** Volunteer guide and teacher to the ‘Bojos per la Física’ (Crazy for Physics), outreach activities as a host. Performance of *in situ* nanoparticle synthesis experiments for/by high school visitors.

**October 2019:** 3rd biennial prize of scientific photography dedicated to Nanochemistry, 3rd position award at IUNAN.



